UNIVERSITY OF CALIFORNIA
RIVERSIDE

Understanding the Electrode Electrolyte Interphase for Metal Sulfur Batteries

A Dissertation submitted in partial satisfaction
of the requirements for the degree of

Doctor of Philosophy

in

Materials Science and Engineering

by

Yifan Zhao

September 2021

Dissertation Committee:
Dr. Juchen Guo, Chairperson
Dr. Bryan Wong
Dr. Lorenzo Mangolini

The Dissertation of Yifan Zhao is approved:

Committee Chairperson

University of California, Riverside

ACKNOWLEDGMENTS

Firstly, I would like to thank my advisor Juchen Guo for his professional guidance, strong supporting, encouragement and motivation during my PhD life. When I was failed in experiment, he was always there being ready to share his hands, leading and getting me out from troubles with his expertise, no matter how late the time was. When I was freak out in my life, he would always be a good listener and made me feel better with his optimism. When I made mistake, no matter how small it was, he would point out and corrected me with his insight. I am deeply grateful for everything he had offered for my research and life. Without his mentoring throughout my doctoral study, I won`t be able to complete my PhD.

Additionally, I would like to thank the members of my dissertation committee, Dr. Bryan Wong and Dr. Lorenzo Mangolini, for their advice, comments and suggestions throughout my research.

I would also like to appreciate those helped me or collaborated with me in my PhD study: Anton Tomich for his contribution in carbonrane electrolyte synthesis. Chengyin Fu for his patient training in experiment skills, And my lab mate Jian Zhang, Jiayan Shi and Xiaoyu Wen for their selfless support and help. I am highly appreciated for all the help I received from you all.

Lastly, I would like to thank my parents, my wife and all my family members as well as my three cats. With my parents and my parents in law, I don`t need to be afraid for losing anything. They will always be my harbor of my heart. I had a lot of words to express my

gratitude to my wife, Ms. Chi Zhang, I owe you too much that I would have to pay back with all my life. I love you.

Thank you to everyone who had share their hands or smiles to me during my life. Those made my life meaningful. And thanks to all the hard experiences I had. Those shaped me to be a better person.

ABSTRACT OF THE DISSERTATION

Understanding the Electrode Electrolyte Interphase for Metal Sulfur Batteries

by

Yifan Zhao

Doctor of Philosophy, Graduate Program in Materials Science and Engineering
University of California, Riverside, September 2021
Dr. Juchen Guo, Chairperson

The demand for rechargeable batteries has rapidly grown due to the increasing gap between limit amount of fossil fuel and rapid growth of energy consumption. Rechargeable battery which known as electrochemical energy storage device was a major focus for academic and industrial research. Sulfur (S) has been regarded as one of the most promising candidates for high specific energy cathode materials due to its high abundance, low toxicity, high theoretical specific capacity, and low density. Owing to the high theoretical specific capacity and low redox potential, lithium (Li) is the most promising anode material which raises most research attention. Researcher also interested in magnesium (Mg) metal anode due to its high natural abundance, good safety and high theoretical volumetric energy.

The cathode electrolyte interfacial process in Li-S batteries under lean electrolyte condition was studied with the most widely used electrolyte The interfacial processes on

the sulfur cathode under the lean electrolyte condition was probed using operando electrochemical impedance spectroscopy (EIS) and galvanostatic intermittent titration technique (GITT). The operando EIS reveals a significant and rapid increase in charge transfer resistance during the transition from high-order polysulfides to low-order ones under a low E/S ratio, which is induced by a kinetic bottleneck at the interphase due to Li-ion mass transfer limitation. The GITT results confirm the kinetic bottleneck by revealing a large discharge overpotential during the transition phase. The understanding of Li-S reactions under lean electrolyte condition is then applied to a carboranyl ionic liquid electrolyte system. Such novel ionic electrolyte was first synthesized and reported in this paper with good chemically and electrochemically stability with Li anode and S cathode as well as polysulfide. High specific energy Li-S battery can be achieved via sparingly dissolving pathway during discharging in carboranyl ionic liquid electrolyte. Mg-S batteries in magnesium monocarborane ($Mg(CB_{11}H_{12})_2$) in tetraglyme (G4) electrolyte was first studied by our group. Understanding of cathode electrolyte interface reveal that sulfur is unstable under oxidation in the $Mg(CB_{11}H_{12})_2$ electrolyte. With the X-ray Photoelectron Spectroscopy (XPS) data of pristine sulfur cathode after charging, we propose a novel explanation of the overcharge behavior for Mg-S.

Table of Contents

List of Figures

List of Tables

Chapter 1: Introduction

1.1 Rechargeable batteries overview

With the rapid growth in energy demands and the decreasing traditional energy source like petroleum and natural gas, clean energy including solar energy, wind energy or nuclear energy are good alternative energy sources. These different formats of energies need to be converted to electrical energy and stored for commercial using. Hence high energy density energy storage devices are urgently desired in storage and distribution of these clean energies. Rechargeable batteries are the electrochemical devices which can convert and store the electrical energy to chemical energy during charging and release the chemical energy to electrical energy during discharging. Thanks to the effort made by researcher and scientist in past century, rechargeable batteries are now widely using in mobile phones, laptops, electrical vehicles and large-scale grid energy storage. Many terms are used to describe the rechargeable battery technologies. Coulombic efficiency describes the efficiency when charge transferred during charging and discharging. It is usually express as the ratio of discharge capacity over charge capacity. A good coulombic efficiency often means longer cycle life. [1] Specific energy (or gravimetric energy density) or energy density (or volumetric energy density) is the amount of energy stored per unit weight or volume. The higher specific energy or energy density is, the wider range rechargeable batteries can apply. C rate is describing battery discharging and charging rate. A rate of nC means fully discharge or charge the cells in 1/n hour. Capacity is the total electric charge transfer in an electrochemical reaction. Specific capacity is the electric charge transfer per mass of the electrode material in an electrochemical reaction.

A rechargeable battery has three major components, the electronic conducting anode and cathode and ionic conducting electrolyte. During battery operation, redox reactions take place at the electrodes. Electrons transfer between cathode and anode in the external circuit, and ions transfer through electrolyte to ensure electroneutrality. Specifically, anode materials are oxidized during discharging process, and electrons transport through external circuit to cathode, which is reduced. During charging, such process is reversed. Reversibility is the main difference between rechargeable battery (secondary battery) and primary battery. In 1860, French scientist Gaston Plante invented the first practical version of a rechargeable battery based on lead-acid chemistry.[2] Lead acid battery is a wide spread technology which has been studied for a century. However, due to the heavy pollution and low specific energy (40Wh kg^{-1}), the matured lead acid technology can not meet nowadays requirement. Li-ion technology are invented three decades ago[3]. A typical Li-ion battery with graphite anode and lithium transition metal oxide layered materials as cathode is illustrated in **Figure 1.1**. Less than 200 Wh kg^{-1} specific energy can be achieved by the state of the art Li-ion batteries. Nowadays, most of the mobile phones, laptops and electrical vehicles are powered by such Li-ion batteries with this lithium ion intercalation chemistry. When comparing with graphite, metal anode have much higher specific capacity (3860 mAh g^{-1} for Li, 2205 mAh g^{-1} for Mg, and 372 mAh g^{-1} for graphite) and higher volumetric capacity (2061 mAh cm^{-3} for Li, 3832 mAh cm^{-3} for Mg, and 837 mAh cm^{-3} for graphite). Beside this, high redox potential and high abundance also arises researchers` interests. Sulfur as important cathode candidate for next generation rechargeable batteries can meet the rapid increase requirements of high

specific energy batteries, due to its high abundance, low toxicity, high theoretical specific capacity, low density. Technology paring sulfur cathode and metal anode will definitely lead to promising rechargeable batteries.

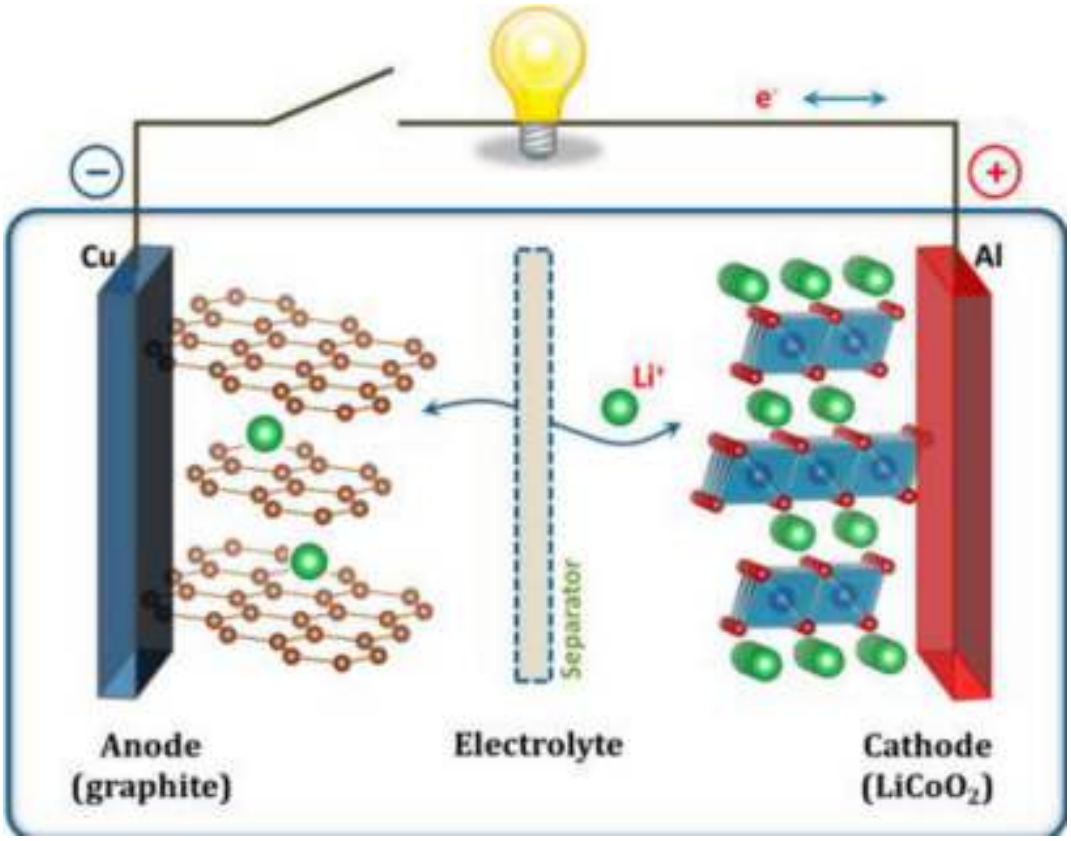

Figure 1.1 Schematic of the Li-ion battery ($LiCoO_2$ || graphite).[4] Reprinted with permission from ref. 4. Copyright 2013 American Chemical Society

1.2 Lithium-Sulfur batteries

1.2.1 Overview

The concept of lithium-sulfur (Li-S) battery was developed in 1960s.[5] In 1962, Herbert patented a battery with Li alloy as the anode and sulfur as the cathode. Aliphatic saturated amines are used as electrolyte. [6] Several years later, organic solvents were used as electrolyte solvent for Li-S system. A typical Li-S battery consists of a sulfur-based cathode, a lithium metal anode, and an organic lithium salt solution as the electrolyte shown in **Figure 1.2 a**.[7] With the founding of ethereal solvents, [8] carbon based sulfur cathode[9] and other resurrected research efforts in the past two decade, in-depth understanding and technologic know-how of Li-S technology have been accumulated thus leading to tremendous improvement of battery performance.[10-13] Owing to the high specific capacity (1675 mA h g^{-1} for S and 3860 mA h g^{-1} for Li), low density (2.07 g cm^{-3} for S and 0.59 g cm^{-3} for Li), good working potential (around 2.1V), high theoretical specific energy (2458 Wh kg^{-1} comparing to around 500 Wh kg^{-1} for Li-ion batteries) and large abundance, low cost and good environment compatibility of S, Li-S battery has been regarded as one of the most promising candidate for the next generation rechargeable batteries. However, wide deployment of Li-S batteries is still hindered by a few challenges such as non-ideal specific energy and short cycle life. These challenges are dictated by the interplay of the Li anode, sulfur cathode and electrolyte in the battery. The redox chemistry of sulfur in the cathode is a solid-liquid-solid reaction starting with an insulating cyclo-S_8 (electronic conductivity at 5×10^{-30} S cm^{-1} at 25°C) reduced to soluble high order polysulfide S_8^{2-} then subsequently lower order polysulfides such as

S_6^{2-} and S_4^{2-} and eventually reduced to insoluble Li_2S_2 and Li_2S which is also insulating (electronic conductivity at 1×10^{-13} S cm^{-1} at 25°C) as shown in **Figure 1.2b**.[14]

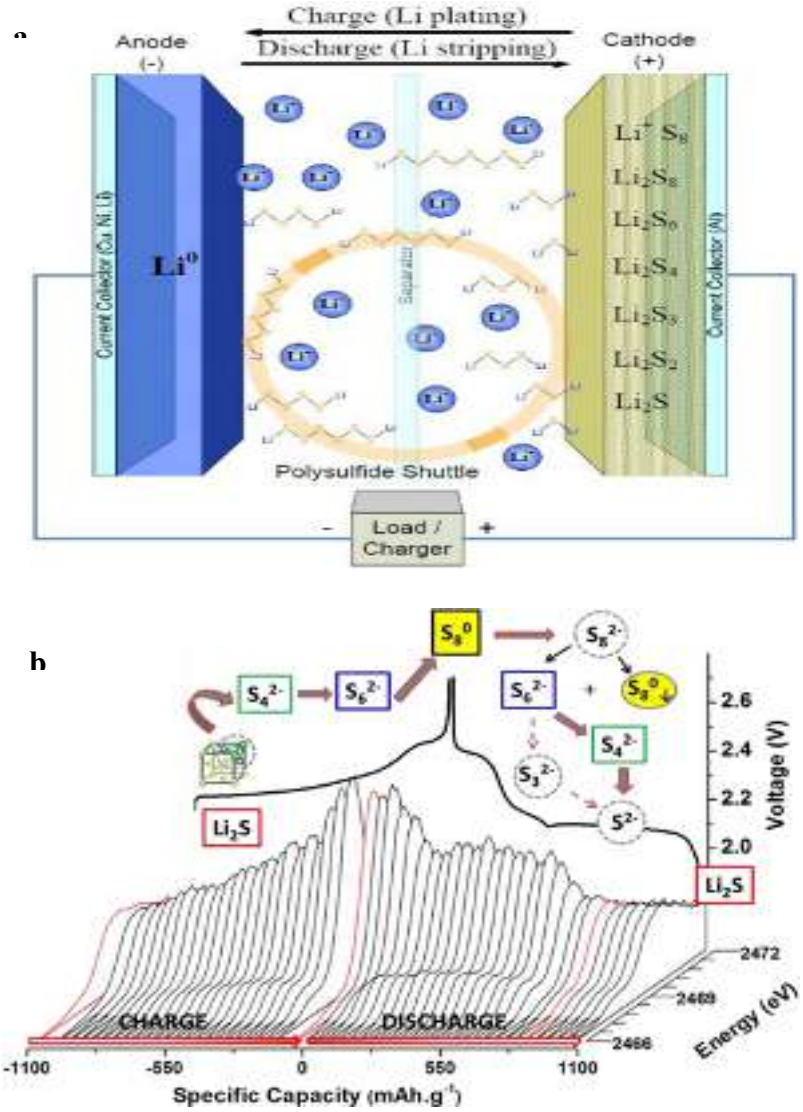

Figure 1.2 (a) Schematic configuration of Li-S battery based on organic liquid electrolyte.[7] Reprinted with permission from ref. 7. Copyright 2015 Li, Li, Zhang and Lin.(b)Sulfur Speciation in Li–S Batteries**.**[14] Reprinted with permission from ref. 14. Copyright 2013 American Chemical Society.

The intrinsic nature of sulfur and sulfides requires sulfur to be loaded into a conductive framework to make cathode electronic conductive. S content and S areal loading as well as the S utilization have to be well considered by researchers. The conductive frame, no matter how light it is, is not electrochemically active which means it will be the dead weight in Li-S and hinder the advantage of low density. Around 80% volume change during charging and discharging may destroy the meticulous designed host material structure in cycling, due to the density difference between charged product S (2.07 g cm^{-3}) and discharged product Li_2S (1.66 g cm^{-3}). Other factors such as easy preparing and low cost also need to be considered. To find a better sulfur host material, a lot of well-designed sulfur hosts were invented by researchers in the past decade.[9, 15-20] Li metal is the best choice as anode material because of its highest theoretical capacity (3860 mAh g^{-1}) and lowest electrochemical potential (–3.04 V versus the standard hydrogen electrode (SHE)) which indicate that Li anode can deliver the highest theoretical specific energy among all the anode material candidates. However, safety issue and cyclability problem hinder the wide commercialization of Li anode. Intrinsic dendritic growth of Li metal leads to internal short circuit and cause thermal runaway and other safety hazard issues. [21-23] Due to the high chemical and electrochemical activity, Li reacts with electrolyte and form solid electrolyte interphase (SEI).[24] The formation of SEI consumes both Li and electrolyte. The dendrite growth also produces “dead” Li which means the Li is covered by passivated insulating surface species. Both the formation of SEI and “dead” Li lead to low coulombic efficiency, short cycle life and low energy density. Due to the solid- liquid- solid pathway, the solvent selected for the electrolyte in

Li-S battery must have good polysulfide solubility. Comparing to the commonly used carbonate solvent in Li-ion batteries, ethereal electrolyte especially the mixture of 1,3-dioxolane (DOL) and 1,2-dimethoxyethane (DME) with volume ratio 1:1 is the most commonly used in Li-S batteries research. Because carbonate solvents have a nucleophilic reaction with polysulfides causing active material loss and electrolyte depletion.[25] On the other hand, ethereal electrolytes have good polysulfide solubility and good compatibility with Li anode as well as sulfur species in cathode. The redox chemistry of sulfur in the cathode is starting with a cyclo-S_8 reduced to soluble high order polysulfide S_8^{2-} then subsequently lower order polysulfides such as S_6^{2-} and S_4^{2-} and eventually reduced to insoluble Li_2S_2 and Li_2S. The solution phase Li-S electrochemical reaction is necessary for functioning Li-S batteries. However, such solution phase also caused some challenges. During the charging process, the dissolved high order polysulfides cross the separator driven by concentration gradient and react with Li metal anode chemically to form lower order polysulfides, which can diffuse back to the cathode being oxidized again. The electrochemical oxidation and chemical reduction for shuttled polysulfides is called shuttle effect. Such solution phase caused shuttle effect leads to loss of both active sulfur cathode materials and Li anode materials and intricate liquid phase electrochemical processes. The dissolved polysulfides redistribute in cathode frame via precipitation, disproportionation, and comproportionating during charge and discharge process. Owing to the well-designed cathode structure impaired by the sulfur species redistribution and shuttle effect, Li-S cyclability is significantly worse than commercialized Li-ion batteries. Beside the issues mentioned above, the requirement of

low mass ratio of electrolyte to sulfur also cause some challenges. It is necessary to have high areal loading of sulfur with high specific capacity. However, high specific energy of the battery without implementing low E/S mass ratio is impossible. To understand the Li-S batteries under lean electrolyte condition, calculated specific energy of a 5Ah Li-S pouch cell at different Li excess level as a function of the E/S ratio is illustrated in **Figure 1.3a.** The parameters of this Li-S pouch cell, based on the realistic values obtained in our laboratory, are listed in **Table 1.1**. It is clear from Figure 1.3a that implementing low E/S ratio is really the key to achieve specific energy close to or even higher that 500 Wh kg^{-1}, as long as Li anode does not excess to a great extent. **Figure 1.3b** displays the mass percentage of the components in the Li-S pouch cell under three E/S ratios (1, 5, and 10) with 100% Li excess, which is equivalent to a Li foil anode with 70 μm thickness. (Commercial 750 μm Li foil is equivalent to 1400% excess.) The electrolyte takes more than 60 wt.% of the cell when E/S mass ratio is higher than 5. It is suggested that an E/S ratio at least lower than 3 is mandatory to realize Li-S batteries with specific energy significantly higher that of the current lithium-ion batteries. It is worth noting that E/S=3 in the calculated 5Ah Li-S pouch cell is approximately equal to 2.7 g of electrolyte per Ah, which is close to the electrolyte to capacity ratio in the typical lithium-ion batteries.

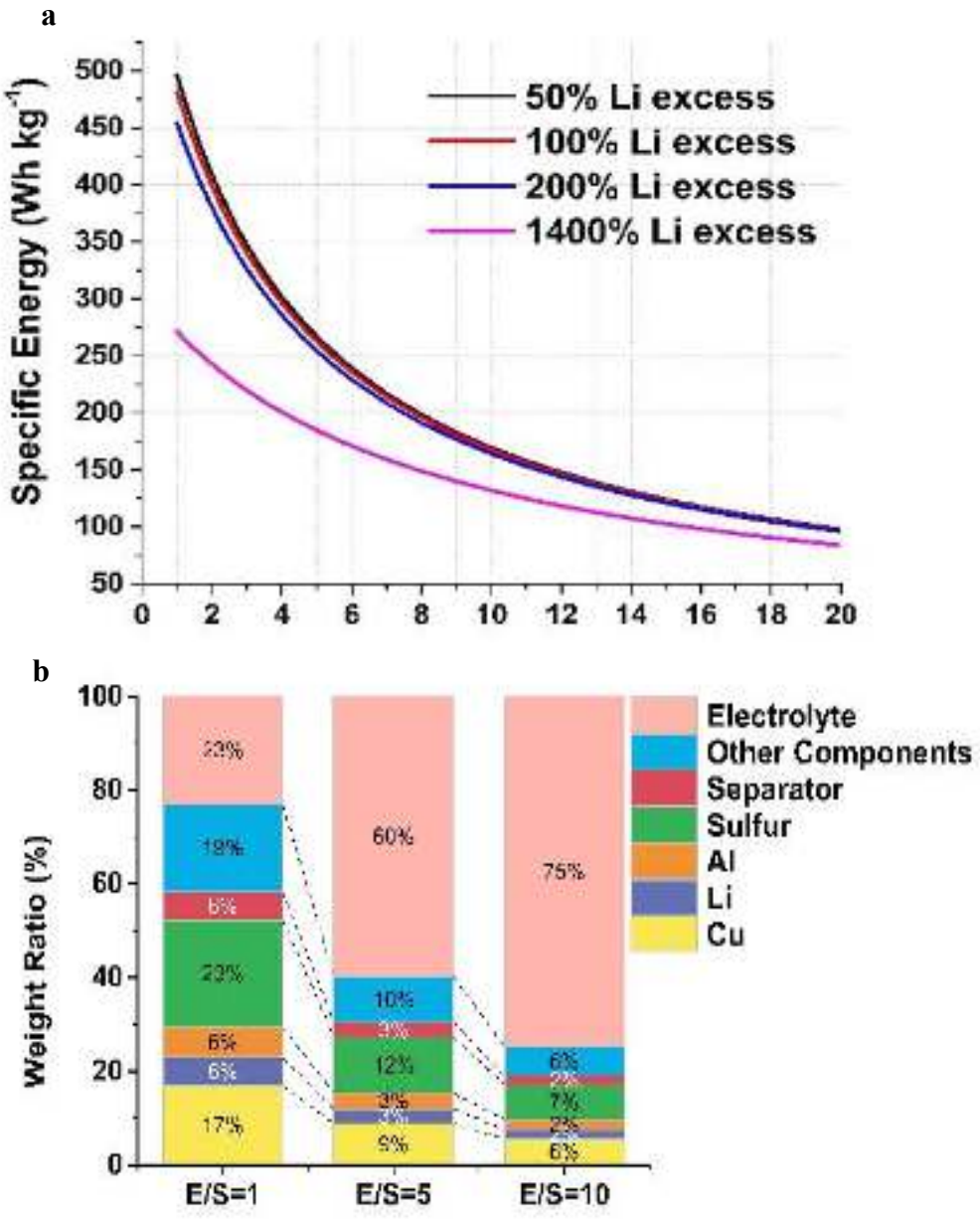

Figure 1.3 (a) The specific energy of a 5Ah Li-S pouch cell as a function of E/S mass ratio with different Li excess; (b) weight percentage of the components of the 5Ah Li-S cell (with 100% Li excess) under various E/S ratios.

Table 1.1 Parameters of a realistic Li-S pouch cell.

Cell Capacity & Nominal Voltage		**5 Ah & 2.1 V**
Cell Dimensions		**6 cm x 4 cm x (0.76 to 2.15) cm**
Structure	Double side Li anode:	16 layers
	Double side sulfur cathode:	15 layers
	Single side sulfur cathode:	2 layers
Cathode Components	12 μm Al current collector:	Areal density: 3.2 mg cm^{-2}
	Sulfur/Carbon/Binder ratio:	64/26/10 wt.%
	Sulfur areal loading:	6 mg cm^{-2}
	Sulfur specific capacity:	1100 mAh g^{-1} at 35 mA g^{-1}
Electrolyte Components	25 μm Polypropylene separator:	Areal density: 1.4 mg cm^{-2}
	1 M LiTFSI in DOL/DME:	Variable mass (E/S ratio)
Anode Components	6 μm Cu current collector:	Areal density: 5.4 mg cm^{-2}
	Li anode:	Variable thickness (Li excess)
Other Components	115 μm pouch cell casing foil:	Areal density: 18 mg cm^{-2}
	Kapton tape:	Mass: 30 mg
	Current collector tabs:	Mass: 140 mg

1.2.2 State of the Art of Low E/S ratio studies

In the past few years, there has been an increasing number of investigations paying attention to E/S ratio as summarized in **Table 1.2**. From a practical perspective, at least in coin cells used by academic laboratories, lowering the E/S ratio can be straightforwardly achieved by increasing the areal loading of sulfur, i.e., increasing the absolute amount of electrolyte in the cell. The most common strategy to achieve high areal loading of sulfur is to utilize carbon-based porous current collectors including carbon cloth, carbon fiber paper and carbon nanotube paper. [16, 26, 27]However, these "free-standing" carbon current collectors may lead to difficulty in scalable electrode manufacturing and cell assembly. They may also result to overheating (due to inferior electronic conductivity comparing to Al) thus causing safety hazards during operation of the Li-S batteries at practical scale. Therefore, our focus will be on the investigations using conventional Al current collector. Several attempts were made on S-cathodes improvement to gain ultrahigh sulfur area loading by employing high porous carbon materials [28-30], layer-by layer construction [27]or foam type current collectors [26, 31, 32]. Several issues are challenging the ultrahigh sulfur loading cathodes. 1) Owing to the insulating feature of S_8 and Li_2S, the ultrahigh sulfur loading cathodes are difficult to get high active material utilization, and high current density. 2) Large-area uniform coatings onto traditional current collector without pinholes and cracks are another a big challenge for ultrahigh sulfur area loading cathodes using nanoparticles [33]. 3)For freestanding cathodes, ultrahigh sulfur loading led to higher local current on battery tab during cycling which may generate heat and cause danger. 4)With the increment of sulfur loading, the thickness of cathode will also increase leading

to a lower volumetric energy density [34].5) In the meanwhile, the cost of fabricating cathodes also need to be considered when comparing with the state-of-art Li-ion batteries. 6) The total numbers of electrons participating in charge/discharge reaction in thick S cathode is increased which means more Li metal will be involved during each stripping/deposition process, more insulating productions will be produced and more volume expansion there will be in sulfur cathode [35]. After limited cycling, the passivation of Li anode and deposition of Li_2S cause large cell impedance and overpotential which terminates the battery electrochemical reaction. And the well-designed cathode structure may crack.

Table 1.2. Recent Li-S battery investigations with low E/S mass ratio.

E/S mass ratio [a]	S areal loading (mg cm^{-2})	Sulfur wt.% [b]	S specific capacity (mAh g^{-1})	Approach
4.7 [28]	13.0	45.9	778 at C/40	Using porous carbon cloth as current collector
8.4 [27]	17.3	54.0	1150 at C/20	Multilayer CNT-S paper as current collector
3.3 [36]	10.24	42.4	720 at C/85	Activated carbon fiber cloth as current collector
3.9 [32]	21.2	74.0	1100 at C/10	Hollow carbon fiber foam as current collector
5.0 [37]	13.5	75.0	1052 at C/20	Carbon fiber current collector derived from electro spun polyacrylonitrile-ZIF fibers
3.9 [38]	14.9	53.1	1000 at C/50	Electrode composed of g-C_3N_4 and N-graphene with crosslinked binder on carbon paper
4.8 [39]	11.3	68.2	579.7 at C/5	Sulfur in free standing HKUST-1/CNT current collector
4.4[40]	6.0	36.4	830 at C/30	molybdenum phosphide electrocatalysis with carbon paper current collector
7.5 [26]	61.4	80.0 [c]	912 at C/10	Using free standing porous carbon current collector derived from cotton
5.5 [41]	46.0	70.0 [c]	926 at C/10	Free standing porous carbon current collector derived from cotton and graphene
4.4 [16]	13.0	75.0 [c]	535 at C/10	Free standing carbon paper current collector and polysulfide catholyte
4.3 [16]	17.0	80.0 [c]	473 at C/10	
1.7 [42]	9.0	51.2	1014 at C/20	S embedded with hollow carbon nanospheres on Al current collector

6.2 [30]	2.0	26.4	1053 at C/2	CaO templated CVD growth of graphene as S host on Al current collector
3.3 [43]	4.0	42.3	1100 at C/10	Controlling porosity of IKB/S cathode on Al current collector (0.15 M Li_2S_6 additive)
1.9 [43]			800 [d]	
4.4 [44]	10.2	52.3	1010 at C/10	N-doped porous carbon with polymodal size distribution as S host (Al current collector)
4.4 [45]	11.1	62.4	1010 at C/30	PANI-treat acetylene black@CTAB/ABS+CNT_S as S host (Al current collector)
7.2 [46]	8.0	44.7	600 at C/10	black phosphorus quantum dot electrocatalyzed polysulfides adsorption/conversion by (Al current collector)
4.4 [46]	13.2	68.0 [c]	909 at C/10	
3.5 [47]	2.9	35.5	1131 at C/10	CoS_2 electrocatalyzed polysulfides adsorption/conversion (Al current collector)
5.2 [48]	4.8	44.3	1007 at C/10	Ni_3FeN electrocatalyzed polysulfides adsorption/conversion (Al current collector)
7.7 [49]	5.5	50.7	1200 at C/30	Ionomer binder with quaternary ammonium cations (Al current collector)
4.0 [50]	4.0	42.6	1200 at C/20	PEO-LiTFSI gel polymer as binder for S-CNTs composite (Al current collector)
5.5 [51]	3.0	40.6	900 at C/10	Using NH_4TFSI as electrolyte additive to promote short chain polysulfides dissociation (Al current collector)
5.5 [52]	1.2	21.4	1150 at C/30	Using sparingly solvating ACN_2LiTFSI-TTE electrolyte at 55°C (Al current collector)

5.5 [13]	4.0	35.2	1319 at C/30	Dimethyl disulfide as electrolyte additive (Al current collector)
7.2 [53]	4.0	34.8	1250 at C/10	1,2-(1,1,2,2-tertafluoroethoxy)ethane as co-solvent in electrolyte (Al current collector)
3.3[54]	2.5	34.9	1524 at C/50	High dielectric constant TMU-based electrolyte to promote sulfide radical (Al current collector)
5.5 [55]	2.0	29.5	1300 at C/20	LiTFSI saturated G2 electrolyte (G2:LiTFSI=0.8:1) at 55 °C (Al current collector)

[a] Most of the studies reported E/S ratio in mL/g, thus we assume a density of 1.1 g mL^{-1}, which is based on 1M LiTFSI in DOL/DME.

[b] Sulfur content in the entire electrode including either a 12 μm Al current collector or the porous carbon current collector used in the corresponding study, unless otherwise noted.

[c] Sulfur content from the studies using catholyte.

[d] C rate unknown.

Tuning the cathode by using electrocatalysis rather than ultrahigh sulfur loading under lean electrolyte condition is achieved. Sluggish kinetics of sulfur species is the main challenge under lean electrolyte condition. With over-saturated the long chain soluble lithium polysulfide dissolved into the limited amount of electrolyte, the viscosity and ionic conductivity of electrolyte changed dramatically. Molybdenum phosphide(MoP) nanoparticles [40]and black phosphorus quantum dots(BPQD) [46]show the catalytic effect on facilitating the charge/discharge sluggish kinetics. Since the porous cathode has to take

some amount of electrolyte, tuning the porosity is also a method to operate Li-S system under lean electrolyte condition [43]. Higher volumetric energy density can also be achieved by reducing the cathode porosity. Never the less, the slow electrolyte infiltration and penetration suppress the sulfur utilization and kinetics is hard to avoid. And the large volume change will destroy the dense cathode.

The requirements for the electrolyte solvents are quite rigid. Since the polysulfide will irreversibly react with carbonate and esters in several reduction steps, the organic carbonates and esters are not suitable for Li-S system. Ethers and glymes are most common electrolyte solvents. The binary mixture of DOL and DME (volume ratio 1:1) is the most adopted solvent for Li-S system due to its high lithium polysulfide solubility, low viscosity, high dielectric permittivity, high ionic conductivity. 1 M lithium bis(trifluoromethanesulfonyl)imide (LiTFSI) used as lithium salt and ~0.2 M lithium nitrate ($LiNO_3$) added as electrolyte additive to suppress the negative effect of polysulfide shuttle process. However, such successful solvent can no longer meet the requirement of high energy density. The moderate lithium polysulfide solubility (~6 M with respect to sulfur) means the minimum E/S ratio that enables the full dissolution of lithium polysulfide is ~5$mL g_s^{-1}$ [56]. An extra amount of electrolyte about 10-20 μl is needed in wetting cathode, lithium anode and separator in coil cell with a diameter around 1cm [35]. The side reaction with lithium metal in stripping/deposition process cause solvent gradual depletion [24]. The solvent evaporation also limits its usage in future high energy density Li-S system. Another approach to achieve low E/S ratio is to change the electrolyte formulas. NH_4TFSI [57]were applied in the DOL/DME electrolyte as an additive to

enhances the dissociation of Li_2S and reduces the Li_2S large particles accumulation enables the Li-S battery. Wang`s group introduce dimethyl disulfide (DMDS)[13] and dimethyl trisulfide (DMTS) [58] as a co-solvent which generate a new discharge pathway of polysulfide. The formation of Lithium organo-sulfides boost the cell performance. The Fluorinated Ether 1,2-(1,1,2,2-tetrafluoroethoxy)ethane (TFEE) is used together with 1,3-dioxolane (DOL) as electrolyte solvent[59].

Except changing the electrolyte formula based on the popular using DOL/DME system, the new concept of sparingly solvating electrolyte was developed in past few years. The traditional Li-S system operate on solution-mediated, precipitation-dissolution chemistry. The sparingly solvating electrolyte create a new operation pathway with controlled species migration and diffusion [60]. The concepts of high salt concentration electrolyte [61] and fluorinated ether dilute [62] were combined by Nazar`s group [52, 63]An extreme low E/S ratio of 1.6 mL/g was reported with almost 100% Coulombic Efficiency. The novel "nonsolvent" sparingly solvating electrolyte delivers a quasi-solid-state reaction and minimal polysulfide shuttling. However, the sulfur loading and working temperature limit the practical usage. Such quasi-solid-state mechanism under lean electrolyte condition is also discovered by Wang and coworkers.[40] They tailored reaction pathway by employing activated carbon fiber cloth as micropore confinement. Even though the 60 °C working temperature and low discharge current density 0.2 mA cm^{-2} (~C/80) reveal that the quasi-solid discharge reaction pathway is far from the conventional use. Such strategy provides a new approach for cathode and electrolyte design under lean electrolyte condition.

Several novel binders were discovered to trap polysulfide and improve the cell performance. But only few of them operate under the lean electrolyte condition. A multidimensional water-soluble polymer with a quaternary ammonium cation, polycation β-cyclodextrin polymer (β-CDp-N^+)[49], was demonstrated as an effective binder. Chen and coworkers developed a soft PEO_{10}LiTFSI polymer swellable gel as a reservoir for Li-ion conducting, electrode wetting, electrolyte and polysulfide trapping. Such method implies that the role of binders is not only binding, but also storing the electrolyte. In their approach, E/S ratio as low as 3.3 mL/g can be achieved without using ultrahigh sulfur loading.[50] However, the Li_2S accumulation still limit the cycle life.

Rapid development of advanced Li-S battery has been achieved in the past 5 to 10 years. Lowering the E/S ratio attracts more attention in recent years. Many attempts were made on engineering cathode, binder and electrolyte to achieve Li-S battery working under the lean electrolyte condition. However, none of them are working perfectly to some degree.

1.3 Magnesium-sulfur batteries

1.3.1 Overview

Mg-S battery technology as an alternative for next generation rechargeable batteries, was first reported by Toyota Motor Corp. research group in 2011.[64] Mg-S batteries is working based on the redox reaction between Mg and sulfur, which is similar to Li-S. Mg metal is oxidized to Mg^{2+} ion and releasing two electrons while sulfur gains the electrons through the external circuit and is reduced to high order long chain polysulfide, then lower order short chain polysulfide then finally MgS during discharging. During charging, Mg^{2+} ion is reduced and deposited onto the Mg anode while MgS is oxidized to elemental sulfur on cathode. As an alternative to Li metal anode, Mg metal has a low electrochemical potential (-2.356 V vs SHE) and highest volumetric capacity among the Group I and II metals. Mg-S battery has received increasing research interests due to its advantages : high theoretical volumetric capacity (3832 mAh cm^{-3} vs 2062 mAh cm^{-3} for Li-S)[65] due to the divalent nature of Mg and high abundance (Mg is the 5th most abundant metal element on earth and S is the 10th most common element in the universe). However, the availability of Mg-S batteries electrolyte is actually the main obstacle which limits the development of Mg-S system.

1.3.2 Mg-S electrolyte

Due to the short history of Mg-S battery development, Mg-S systems still suffer from limitation of electrolyte systems. The suitable electrolytes should have high ionic conductivity, good stability with Mg and sulfur both chemically and electrochemically, good electrochemical stable voltage window for sulfur redox reaction and Mg stripping

and deposition. Even though a lot of electrolyte researches have been carried out for Mg-ion batteries, most of them are nucleophilic electrolytes which are not suitable with sulfur cathodes. [66-68] The electrolyte studies for Mg-S can be divided into two kinds: chloride containing and chloride free as listed in **Table 1.3**. A common strategy for chloride containing Mg-S electrolyte is to combine a Mg complex contained nonnucleophilic base such as Hauser base–derived magnesium hexamethyldisilazide chloride (HMDSMgCl)[69], $(HMDS)_2Mg$ [70] , magnesium bis(diisopropylamide) [71] with boron or aluminum contained Lewis acid.[72] Some improvements were made by using additives such as ionic liquid (IL) N-methyl-N-butyl-piperidinium TFSI ($PP_{14}TFSI$)[73] or LiTFSI.[74, 75] Other electrolyte system such as organic magnesium boron-based electrolyte,[76] and trifluoromethanesulfonate-based electrolyte[77] . Despite how good the Mg-S is performing in these chloride containing electrolyte system, these electrolytes are leading to corrosion due to the chlorides in the cation.[78] The chloride free, non-corrosive, nonnucleophilic electrolytes is the main research object for Mg-S batteries. Simple salt, $Mg(TFSI)_2$, was first investigated by Ha and his group in 2013.[79] However, the poor reductive stability of the $TFSI^-$ anions will lead to the decomposition of $TFSI^-$ anions and passivate Mg anode. [80] Many additives such as $MgCl_2$ [81], LiTFSI[75] ,iodine [82] and ionic liquid[83] are introduced to modify $Mg(TFSI)_2$ electrolyte system. However, more in-depth understanding of the chemistry in electrodes and electrolyte interphase are still needed. Another success try in Mg-S chloride free electrolytes is the fluorinated magnesium alkoxyborate–based electrolyte ($Mg[B(HFIP)_4]_2$),[84-86] which is good candidate for Mg-S chloride free electrolytes.

Table 1.3 Available electrolyte systems for use in Mg-S batteries.[65]
Reprinted with permission from ref. 61. Copyright 2019 John Wiley and Sons

Type	salt cation	salt anion	additives	solvents
Nucleophilic	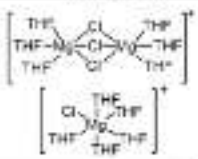	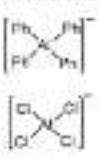	LiCl	 THF
Non-nucleophilic	 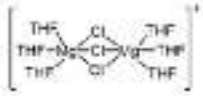  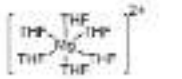  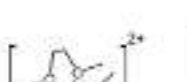 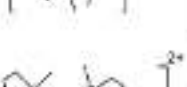 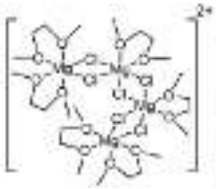	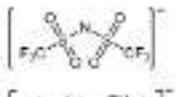 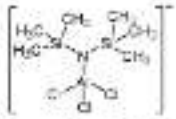 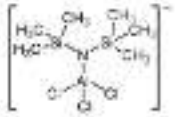 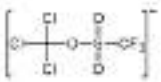 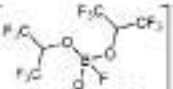  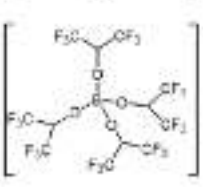	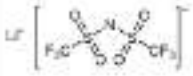 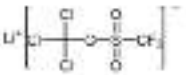 LiCl	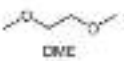 DME 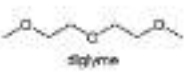 diglyme 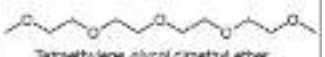 Tetraethylene glycol dimethyl ether

1.4 Research objectives

With the two metal-sulfur batteries (Li-S and Mg-S) introduced above in this chapter, the studies for electrode electrolyte interphase for both Li-S and Mg-S are important. Studying the cathode electrolyte interphase for Li-S under the lean electrolyte condition can reveal the origin of the low performance of Li-S under lean electrolyte condition which is now the main obstacle for high specific energy Li-S. Investigating the cathode electrolyte interphase for Mg-S can promote the understanding of the electrochemical mechanism undergoing in Mg-S and facilitate the discovery of suitable electrolyte systems for Mg-S batteries. The following chapters in this thesis will focus on understating the cathode electrolyte interphase for Li-S batteries under the lean electrolyte condition, apply the understanding to a Li-S system to a novel carboranyl ionic liquid system under lean electrolyte condition and study the cathode electrolyte interphase for Mg-S batteries.

Reference

1. Xiao, J.; Li, Q.; Bi, Y.; Cai, M.; Dunn, B.; Glossmann, T.; Liu, J.; Osaka, T.; Sugiura, R.; Wu, B.; Yang, J.; Zhang, J.-G.; Whittingham, M. S., Understanding and applying coulombic efficiency in lithium metal batteries. *Nature Energy* **2020,** *5* (8), 561-568.

2. Kurzweil, P., Gaston Planté and his invention of the lead–acid battery—The genesis of the first practical rechargeable battery. *Journal of Power Sources* **2010,** *195* (14), 4424-4434.

3. Reddy, M. V.; Mauger, A.; Julien, C. M.; Paolella, A.; Zaghib, K., Brief History of Early Lithium-Battery Development. *Materials (Basel)* **2020,** *13* (8).

4. Goodenough, J. B.; Park, K. S., The Li-ion rechargeable battery: a perspective. *J Am Chem Soc* **2013,** *135* (4), 1167-76.

5. J. R. Birk , R. K. S., Chemical Investigations of Lithium-Sulfur Cells. *Advances in Chemistry* **1975**.

6. Ulam, D. H. a. J. Electric Dry Cells And Stroage Batteries. 1962.

7. Li, G.; Li, Z.; Zhang, B.; Lin, Z., Developments of Electrolyte Systems for Lithiumâ€“Sulfur Batteries: A Review. *Frontiers in Energy Research* **2015,** *3*.

8. E. Peled, Y. S., A. Gorenshtein, and Y. Lavi, Lithium-Sulfur Battery: Evaluation of Dioxolane-Based Electrolytes. *J. Electrochem. Soc.* **1989,** *136*.

9. Ji, X.; Lee, K. T.; Nazar, L. F., A highly ordered nanostructured carbon-sulphur cathode for lithium-sulphur batteries. *Nat Mater* **2009,** *8* (6), 500-6.

10. Kopera, J. Sion Power's Lithium-Sulfur Batteries Power High Altitude Pseudo-Satellite Flight. https://www.businesswire.com/news/home/20140922005174/en/Sion-Power%E2%80%99s-Lithium-Sulfur-Batteries-Power-High-Altitude-Pseudo-Satellite-Flight (accessed April 28).

11. Crittenden, M. With Ultralight Lithium-Sulfur Batteries, Electric Airplanes Could Finally Take Off. https://spectrum.ieee.org/aerospace/aviation/with-ultralight-lithiumsulfur-batteries-electric-airplanes-could-finally-take-off.

12. Zhao, C.; Xu, G. L.; Yu, Z.; Zhang, L.; Hwang, I.; Mo, Y. X.; Ren, Y.; Cheng, L.; Sun, C. J.; Ren, Y.; Zuo, X.; Li, J. T.; Sun, S. G.; Amine, K.; Zhao, T., A high-energy and long-cycling lithium-sulfur pouch cell via a macroporous catalytic cathode with double-end binding sites. *Nat Nanotechnol* **2021,** *16* (2), 166-173.

13. Chen, S.; Gao, Y.; Yu, Z.; Gordin, M. L.; Song, J.; Wang, D., High capacity of lithium-sulfur batteries at low electrolyte/sulfur ratio enabled by an organosulfide containing electrolyte. *Nano Energy* **2017,** *31*, 418-423.

14. Cuisinier, M.; Cabelguen, P.-E.; Evers, S.; He, G.; Kolbeck, M.; Garsuch, A.; Bolin, T.; Balasubramanian, M.; Nazar, L. F., Sulfur Speciation in Li–S Batteries Determined by Operando X-ray Absorption Spectroscopy. *The Journal of Physical Chemistry Letters* **2013,** *4* (19), 3227-3232.

15. Lv, D.; Zheng, J.; Li, Q.; Xie, X.; Ferrara, S.; Nie, Z.; Mehdi, L. B.; Browning, N. D.; Zhang, J.-G.; Graff, G. L.; Liu, J.; Xiao, J., High Energy Density Lithium-Sulfur Batteries: Challenges of Thick Sulfur Cathodes. *Advanced Energy Materials* **2015,** *5* (16).

16. Chung, S. H.; Manthiram, A., Designing Lithium-Sulfur Batteries with High-Loading Cathodes at a Lean Electrolyte Condition. *ACS Appl Mater Interfaces* **2018,** *10* (50), 43749-43759.

17. Wang, M.; Fan, L.; Sun, X.; Guan, B.; Jiang, B.; Wu, X.; Tian, D.; Sun, K.; Qiu, Y.; Yin, X.; Zhang, Y.; Zhang, N., Nitrogen-Doped CoSe2 as a Bifunctional Catalyst for High Areal Capacity and Lean Electrolyte of Li–S Battery. *ACS Energy Letters* **2020,** *5* (9), 3041-3050.

18. Luo, C.; Hu, E.; Gaskell, K. J.; Fan, X.; Gao, T.; Cui, C.; Ghose, S.; Yang, X. Q.; Wang, C., A chemically stabilized sulfur cathode for lean electrolyte lithium sulfur batteries. *Proc Natl Acad Sci U S A* **2020,** *117* (26), 14712-14720.

19. Guo, J.; Yang, Z.; Yu, Y.; Abruna, H. D.; Archer, L. A., Lithium-sulfur battery cathode enabled by lithium-nitrile interaction. *J Am Chem Soc* **2013,** *135* (2), 763-7.

20. Fu, C.; Oviedo, M. B.; Zhu, Y.; von Wald Cresce, A.; Xu, K.; Li, G.; Itkis, M. E.; Haddon, R. C.; Chi, M.; Han, Y.; Wong, B. M.; Guo, J., Confined Lithium-Sulfur Reactions in Narrow-Diameter Carbon Nanotubes Reveal Enhanced Electrochemical Reactivity. *ACS Nano* **2018,** *12* (10), 9775-9784.

21. Xu, W.; Wang, J.; Ding, F.; Chen, X.; Nasybulin, E.; Zhang, Y.; Zhang, J.-G., Lithium metal anodes for rechargeable batteries. *Energy Environ. Sci.* **2014,** *7* (2), 513-537.

22. Lin, D.; Liu, Y.; Cui, Y., Reviving the lithium metal anode for high-energy batteries. *Nat Nanotechnol* **2017,** *12* (3), 194-206.

23. Liu, J.; Bao, Z.; Cui, Y.; Dufek, E. J.; Goodenough, J. B.; Khalifah, P.; Li, Q.; Liaw, B. Y.; Liu, P.; Manthiram, A.; Meng, Y. S.; Subramanian, V. R.; Toney, M. F.; Viswanathan, V. V.; Whittingham, M. S.; Xiao, J.; Xu, W.; Yang, J.; Yang, X.-Q.; Zhang, J.-G., Pathways for practical high-energy long-cycling lithium metal batteries. *Nature Energy* **2019,** *4* (3), 180-186.

24. Zhang, S. S., Liquid electrolyte lithium/sulfur battery: Fundamental chemistry, problems, and solutions. *Journal of Power Sources* **2013,** *231*, 153-162.

25. Li, L.; Wang, L.; Liu, R., Effect of Ether-Based and Carbonate-Based Electrolytes on the Electrochemical Performance of Li–S Batteries. *Arabian Journal for Science and Engineering* **2019,** *44* (7), 6361-6371.

26. Chung, S. H.; Chang, C. H.; Manthiram, A., A Carbon-Cotton Cathode with Ultrahigh-Loading Capability for Statically and Dynamically Stable Lithium-Sulfur Batteries. *ACS Nano* **2016,** *10* (11), 10462-10470.

27. Yuan, Z.; Peng, H.-J.; Huang, J.-Q.; Liu, X.-Y.; Wang, D.-W.; Cheng, X.-B.; Zhang, Q., Hierarchical Free-Standing Carbon-Nanotube Paper Electrodes with Ultrahigh Sulfur-Loading for Lithium-Sulfur Batteries. *Advanced Functional Materials* **2014,** *24* (39), 6105-6112.

28. Sheng S. Zhang, D. T. T., A proof-of-concept lithium/sulfur liquid battery with exceptionally high capacity density. *Journal of Power Sources* **2012,** *211*, 169-172.

29. Zhang, S. S., Does the sulfur cathode require good mixing for a liquid electrolyte lithium/sulfur cell. *Electrochemistry Communications* **2013,** *31*, 10-12.

30. Tang, C.; Li, B.-Q.; Zhang, Q.; Zhu, L.; Wang, H.-F.; Shi, J.-L.; Wei, F., CaO-Templated Growth of Hierarchical Porous Graphene for High-Power Lithium-Sulfur Battery Applications. *Advanced Functional Materials* **2016,** *26* (4), 577-585.

31. Ma, L.; Wei, S.; Zhuang, H. L.; Hendrickson, K. E.; Hennig, R. G.; Archer, L. A., Hybrid cathode architectures for lithium batteries based on TiS2 and sulfur. *Journal of Materials Chemistry A* **2015,** *3* (39), 19857-19866.

32. Fang, R.; Zhao, S.; Hou, P.; Cheng, M.; Wang, S.; Cheng, H. M.; Liu, C.; Li, F., 3D Interconnected Electrode Materials with Ultrahigh Areal Sulfur Loading for Li-S Batteries. *Adv Mater* **2016,** *28* (17), 3374-82.

33. Xiao, J., Understanding the Lithium Sulfur Battery System at Relevant Scales. *Advanced Energy Materials* **2015,** *5* (16).

34. Hagen, M.; Hanselmann, D.; Ahlbrecht, K.; Maça, R.; Gerber, D.; Tübke, J., Lithium-Sulfur Cells: The Gap between the State-of-the-Art and the Requirements for High Energy Battery Cells. *Advanced Energy Materials* **2015,** *5* (16).

35. Guo, W.; Fu, Y., A Perspective on Energy Densities of Rechargeable Li-S Batteries and Alternative Sulfur-Based Cathode Materials. *Energy & Environmental Materials* **2018,** *1* (1), 20-27.

36. Wang, H.; Adams, B. D.; Pan, H.; Zhang, L.; Han, K. S.; Estevez, L.; Lu, D.; Jia, H.; Feng, J.; Guo, J.; Zavadil, K. R.; Shao, Y.; Zhang, J.-G., Tailored Reaction Route by Micropore Confinement for Li-S Batteries Operating under Lean Electrolyte Conditions. *Advanced Energy Materials* **2018,** *8* (21).

37. Li, G.; Lei, W.; Luo, D.; Deng, Y.; Deng, Z.; Wang, D.; Yu, A.; Chen, Z., Stringed "tube on cube" nanohybrids as compact cathode matrix for high-loading and lean-electrolyte lithium–sulfur batteries. *Energy & Environmental Science* **2018,** *11* (9), 2372-2381.

38. Pang, Q.; Liang, X.; Kwok, C. Y.; Kulisch, J.; Nazar, L. F., A Comprehensive Approach toward Stable Lithium–Sulfur Batteries with High Volumetric Energy Density. *Advanced Energy Materials* **2016,** *7* (6).

39. Mao, Y.; Li, G.; Guo, Y.; Li, Z.; Liang, C.; Peng, X.; Lin, Z., Foldable interpenetrated metal-organic frameworks/carbon nanotubes thin film for lithium-sulfur batteries. *Nat Commun* **2017,** *8*, 14628.

40. Yang, Y.; Zhong, Y.; Shi, Q.; Wang, Z.; Sun, K.; Wang, H., Electrocatalysis in Lithium Sulfur Batteries under Lean Electrolyte Conditions. *Angew Chem Int Ed Engl* **2018,** *57* (47), 15549-15552.

41. Chung, S. H.; Manthiram, A., Rational Design of Statically and Dynamically Stable Lithium-Sulfur Batteries with High Sulfur Loading and Low Electrolyte/Sulfur Ratio. *Adv Mater* **2018,** *30* (6).

42. Osada, N.; Bucur, C. B.; Aso, H.; Muldoon, J., The design of nanostructured sulfur cathodes using layer by layer assembly. *Energy & Environmental Science* **2016,** *9* (5), 1668-1673.

43. Lu, D.; Li, Q.; Liu, J.; Zheng, J.; Wang, Y.; Ferrara, S.; Xiao, J.; Zhang, J. G.; Liu, J., Enabling High-Energy-Density Cathode for Lithium-Sulfur Batteries. *ACS Appl Mater Interfaces* **2018,** *10* (27), 23094-23102.

44. Li, M.; Zhang, Y.; Hassan, F.; Ahn, W.; Wang, X.; Liu, W. W.; Jiang, G.; Chen, Z., Compact high volumetric and areal capacity lithium sulfur batteries through

rock salt induced nano-architectured sulfur hosts. *J. Mater. Chem. A* **2017,** *5* (40), 21435-21441.

45. Zeng, F.; Wang, A.; Wang, W.; Jin, Z.; Yang, Y.-S., Strategies of constructing stable and high sulfur loading cathodes based on the blade-casting technique. *Journal of Materials Chemistry A* **2017,** *5* (25), 12879-12888.

46. Xu, Z. L.; Lin, S.; Onofrio, N.; Zhou, L.; Shi, F.; Lu, W.; Kang, K.; Zhang, Q.; Lau, S. P., Exceptional catalytic effects of black phosphorus quantum dots in shuttling-free lithium sulfur batteries. *Nat Commun* **2018,** *9* (1), 4164.

47. Yuan, Z.; Peng, H. J.; Hou, T. Z.; Huang, J. Q.; Chen, C. M.; Wang, D. W.; Cheng, X. B.; Wei, F.; Zhang, Q., Powering Lithium-Sulfur Battery Performance by Propelling Polysulfide Redox at Sulfiphilic Hosts. *Nano Lett* **2016,** *16* (1), 519-27.

48. Zhao, M.; Peng, H. J.; Zhang, Z. W.; Li, B. Q.; Chen, X.; Xie, J.; Chen, X.; Wei, J. Y.; Zhang, Q.; Huang, J. Q., Activating Inert Metallic Compounds for High-Rate Lithium-Sulfur Batteries Through In Situ Etching of Extrinsic Metal. *Angew Chem Int Ed Engl* **2019,** *58* (12), 3779-3783.

49. Zeng, F.; Wang, W.; Wang, A.; Yuan, K.; Jin, Z.; Yang, Y. S., Multidimensional Polycation beta-Cyclodextrin Polymer as an Effective Aqueous Binder for High Sulfur Loading Cathode in Lithium-Sulfur Batteries. *ACS Appl Mater Interfaces* **2015,** *7* (47), 26257-65.

50. Chen, J.; Henderson, W. A.; Pan, H.; Perdue, B. R.; Cao, R.; Hu, J. Z.; Wan, C.; Han, K. S.; Mueller, K. T.; Zhang, J. G.; Shao, Y.; Liu, J., Improving Lithium-Sulfur Battery Performance under Lean Electrolyte through Nanoscale Confinement in Soft Swellable Gels. *Nano Lett* **2017,** *17* (5), 3061-3067.

51. Pan, H.; Han, K. S.; Engelhard, M. H.; Cao, R.; Chen, J.; Zhang, J.-G.; Mueller, K. T.; Shao, Y.; Liu, J., Addressing Passivation in Lithium-Sulfur Battery Under Lean Electrolyte Condition. *Advanced Functional Materials* **2018,** *28* (38).

52. Lee, C. W.; Pang, Q.; Ha, S.; Cheng, L.; Han, S. D.; Zavadil, K. R.; Gallagher, K. G.; Nazar, L. F.; Balasubramanian, M., Directing the Lithium-Sulfur Reaction Pathway via Sparingly Solvating Electrolytes for High Energy Density Batteries. *ACS Cent Sci* **2017,** *3* (6), 605-613.

53. Drvarič Talian, S.; Jeschke, S.; Vizintin, A.; Pirnat, K.; Arčon, I.; Aquilanti, G.; Johansson, P.; Dominko, R., Fluorinated Ether Based Electrolyte for High-Energy Lithium–Sulfur Batteries: Li+ Solvation Role Behind Reduced Polysulfide Solubility. *Chemistry of Materials* **2017,** *29* (23), 10037-10044.

54. Zhang, G.; Peng, H. J.; Zhao, C. Z.; Chen, X.; Zhao, L. D.; Li, P.; Huang, J. Q.; Zhang, Q., The Radical Pathway Based on a Lithium-Metal-Compatible High-Dielectric Electrolyte for Lithium-Sulfur Batteries. *Angew Chem Int Ed Engl* **2018,** *57* (51), 16732-16736.

55. Pang, Q.; Shyamsunder, A.; Narayanan, B.; Kwok, C. Y.; Curtiss, L. A.; Nazar, L. F., Tuning the electrolyte network structure to invoke quasi-solid state sulfur conversion and suppress lithium dendrite formation in Li–S batteries. *Nature Energy* **2018,** *3* (9), 783-791.

56. Shen, C.; Xie, J.; Zhang, M.; Andrei, P.; Hendrickson, M.; Plichta, E. J.; Zheng, J. P., Understanding the role of lithium polysulfide solubility in limiting lithium-sulfur cell capacity. *Electrochimica Acta* **2017,** *248*, 90-97.

57. Pan, H.; Han, K. S.; Vijayakumar, M.; Xiao, J.; Cao, R.; Chen, J.; Zhang, J.; Mueller, K. T.; Shao, Y.; Liu, J., Ammonium Additives to Dissolve Lithium Sulfide through Hydrogen Binding for High-Energy Lithium-Sulfur Batteries. *ACS Appl Mater Interfaces* **2017,** *9* (5), 4290-4295.

58. Chen, S.; Wang, D.; Zhao, Y.; Wang, D., Superior Performance of a Lithium-Sulfur Battery Enabled by a Dimethyl Trisulfide Containing Electrolyte. *Small Methods* **2018,** *2* (6).

59. Chivers, T.; Elder, P. J., Ubiquitous trisulfur radical anion: fundamentals and applications in materials science, electrochemistry, analytical chemistry and geochemistry. *Chem Soc Rev* **2013,** *42* (14), 5996-6005.

60. Cheng, L.; Curtiss, L. A.; Zavadil, K. R.; Gewirth, A. A.; Shao, Y.; Gallagher, K. G., Sparingly Solvating Electrolytes for High Energy Density Lithium–Sulfur Batteries. *ACS Energy Letters* **2016,** *1* (3), 503-509.

61. Suo, L.; Hu, Y. S.; Li, H.; Armand, M.; Chen, L., A new class of Solvent-in-Salt electrolyte for high-energy rechargeable metallic lithium batteries. *Nat Commun* **2013,** *4*, 1481.

62. Dokko, K.; Tachikawa, N.; Yamauchi, K.; Tsuchiya, M.; Yamazaki, A.; Takashima, E.; Park, J.-W.; Ueno, K.; Seki, S.; Serizawa, N.; Watanabe, M., Solvate Ionic Liquid Electrolyte for Li–S Batteries. *Journal of The Electrochemical Society* **2013,** *160* (8), A1304-A1310.

63. Cuisinier, M.; Cabelguen, P. E.; Adams, B. D.; Garsuch, A.; Balasubramanian, M.; Nazar, L. F., Unique behaviour of nonsolvents for polysulphides in lithium–sulphur batteries. *Energy Environ. Sci.* **2014,** *7* (8), 2697-2705.

64. Kim, H. S.; Arthur, T. S.; Allred, G. D.; Zajicek, J.; Newman, J. G.; Rodnyansky, A. E.; Oliver, A. G.; Boggess, W. C.; Muldoon, J., Structure and compatibility of a magnesium electrolyte with a sulphur cathode. *Nat Commun* **2011,** *2*, 427.

65. Wang, P.; Buchmeiser, M. R., Rechargeable Magnesium–Sulfur Battery Technology: State of the Art and Key Challenges. *Advanced Functional Materials* **2019,** *29* (49).

66. Du, H.; Zhang, Z.; He, J.; Cui, Z.; Chai, J.; Ma, J.; Yang, Z.; Huang, C.; Cui, G., A Delicately Designed Sulfide Graphdiyne Compatible Cathode for High-Performance Lithium/Magnesium-Sulfur Batteries. *Small* **2017,** *13* (44).

67. Wang, W.; Yuan, H.; NuLi, Y.; Zhou, J.; Yang, J.; Wang, J., Sulfur@microporous Carbon Cathode with a High Sulfur Content for Magnesium–Sulfur Batteries with Nucleophilic Electrolytes. *The Journal of Physical Chemistry C* **2018,** *122* (46), 26764-26776.

68. Zeng, L.; Wang, N.; Yang, J.; Wang, J.; NuLi, Y., Application of a Sulfur Cathode in Nucleophilic Electrolytes for Magnesium/Sulfur Batteries. *Journal of The Electrochemical Society* **2017,** *164* (12), A2504-A2512.

69. C. Liebenow, Z. Y., P. Lobitz, The electrodeposition of magnesium using solutions
of organomagnesium halides, amidomagnesium halides and magnesium organoborates. *Electrochemical Communications* **2000,** *2*, 641-645.

70. Xu, Y.; Li, W.; Zhou, G.; Pan, Z.; Zhang, Y., A non-nucleophilic mono-Mg2+ electrolyte for rechargeable Mg/S battery. *Energy Storage Materials* **2018,** *14*, 253-257.

71. Zhao, X.; Yang, Y.; NuLi, Y.; Li, D.; Wang, Y.; Xiang, X., A new class of electrolytes based on magnesium bis(diisopropyl)amide for magnesium-sulfur batteries. *Chem Commun (Camb)* **2019,** *55* (43), 6086-6089.

72. Wanfei Li, S. C., Jian Wang,Yongcai Qiu, Zhaozhao Zheng,Hongzhen Lin, SanjayNanda, Qian Ma, YanXu, Fangmin Ye,Meinan Liu, Lisha Zhou, and Yuegang Zhang, Synthesis,Crystal Structure,and Electrochemical Properties of aSimple Magnesium Electrolyte for Magnesium/Sulfur Batteries. *Angew Chem Int Ed Engl* **2016,** *55*, 6406-6410.

73. Zhao-Karger, Z.; Zhao, X.; Wang, D.; Diemant, T.; Behm, R. J.; Fichtner, M., Performance Improvement of Magnesium Sulfur Batteries with Modified Non-Nucleophilic Electrolytes. *Advanced Energy Materials* **2015,** *5* (3).

74. Zhou, X.; Tian, J.; Hu, J.; Li, C., High Rate Magnesium-Sulfur Battery with Improved Cyclability Based on Metal-Organic Framework Derivative Carbon Host. *Adv Mater* **2018,** *30* (7).

75. Gao, T.; Noked, M.; Pearse, A. J.; Gillette, E.; Fan, X.; Zhu, Y.; Luo, C.; Suo, L.; Schroeder, M. A.; Xu, K.; Lee, S. B.; Rubloff, G. W.; Wang, C., Enhancing the reversibility of Mg/S battery chemistry through Li(+) mediation. *J Am Chem Soc* **2015,** *137* (38), 12388-93.

76. Du, A.; Zhang, Z.; Qu, H.; Cui, Z.; Qiao, L.; Wang, L.; Chai, J.; Lu, T.; Dong, S.; Dong, T.; Xu, H.; Zhou, X.; Cui, G., An efficient organic magnesium borate-based electrolyte with non-nucleophilic characteristics for magnesium–sulfur battery. *Energy & Environmental Science* **2017,** *10* (12), 2616-2625.

77. Yang, Y.; Wang, W.; Nuli, Y.; Yang, J.; Wang, J., High Active Magnesium Trifluoromethanesulfonate-Based Electrolytes for Magnesium-Sulfur Batteries. *ACS Appl Mater Interfaces* **2019,** *11* (9), 9062-9072.

78. Muldoon, J.; Bucur, C. B.; Oliver, A. G.; Zajicek, J.; Allred, G. D.; Boggess, W. C., Corrosion of magnesium electrolytes: chlorides – the culprit. *Energy Environ. Sci.* **2013,** *6* (2), 482-487.

79. Ha, S. Y.; Lee, Y. W.; Woo, S. W.; Koo, B.; Kim, J. S.; Cho, J.; Lee, K. T.; Choi, N. S., Magnesium(II) bis(trifluoromethane sulfonyl) imide-based electrolytes with wide electrochemical windows for rechargeable magnesium batteries. *ACS Appl Mater Interfaces* **2014,** *6* (6), 4063-73.

80. Gao, T.; Ji, X.; Hou, S.; Fan, X.; Li, X.; Yang, C.; Han, F.; Wang, F.; Jiang, J.; Xu, K.; Wang, C., Thermodynamics and Kinetics of Sulfur Cathode during Discharge in MgTFSI2 -DME Electrolyte. *Adv Mater* **2018,** *30* (3).

81. Gao, T.; Hou, S.; Wang, F.; Ma, Z.; Li, X.; Xu, K.; Wang, C., Reversible S(0) /MgSx Redox Chemistry in a MgTFSI2 /MgCl2 /DME Electrolyte for Rechargeable Mg/S Batteries. *Angew Chem Int Ed Engl* **2017,** *56* (43), 13526-13530.

82. Li, X.; Gao, T.; Han, F.; Ma, Z.; Fan, X.; Hou, S.; Eidson, N.; Li, W.; Wang, C., Reducing Mg Anode Overpotential via Ion Conductive Surface Layer Formation by Iodine Additive. *Advanced Energy Materials* **2018,** *8* (7).

83. Ma, Z.; Forsyth, M.; MacFarlane, D. R.; Kar, M., Ionic liquid/tetraglyme hybrid Mg[TFSI]2 electrolytes for rechargeable Mg batteries. *Green Energy & Environment* **2019,** *4* (2), 146-153.

84. Zhao-Karger, Z.; Liu, R.; Dai, W.; Li, Z.; Diemant, T.; Vinayan, B. P.; Bonatto Minella, C.; Yu, X.; Manthiram, A.; Behm, R. J.; Ruben, M.; Fichtner, M., Toward Highly Reversible Magnesium–Sulfur Batteries with Efficient and Practical Mg[B(hfip)4]2Electrolyte. *ACS Energy Letters* **2018,** *3* (8), 2005-2013.

85. Zhao-Karger, Z.; Gil Bardaji, M. E.; Fuhr, O.; Fichtner, M., A new class of non-corrosive, highly efficient electrolytes for rechargeable magnesium batteries. *Journal of Materials Chemistry A* **2017,** *5* (22), 10815-10820.

86. Zhang, Z.; Cui, Z.; Qiao, L.; Guan, J.; Xu, H.; Wang, X.; Hu, P.; Du, H.; Li, S.; Zhou, X.; Dong, S.; Liu, Z.; Cui, G.; Chen, L., Novel Design Concepts of Efficient Mg-Ion Electrolytes toward High-Performance Magnesium-Selenium and Magnesium-Sulfur Batteries. *Advanced Energy Materials* **2017,** *7* (11).

Chapter 2: Cathode-Electrolyte Interfacial Processes in Lithium||Sulfur Batteries under Lean Electrolyte Condition

2.1 Abstract

The implementation of a low electrolyte/sulfur (E/S) ratio is essential to achieving high specific energy for lithium||sulfur (Li||S) batteries. In reality, however, the lean electrolyte condition result in low achievable capacity and inferior cyclability. In this study, we probe the interfacial processes on the sulfur cathode under the lean electrolyte condition using operando electrochemical impedance spectroscopy (EIS) and galvanostatic intermittent titration technique (GITT). The operando EIS reveals a significant and rapid increase in charge transfer resistance during the transition from high-order polysulfides to low-order ones under a low E/S ratio, which is induced by a kinetic bottleneck at the interphase due to Li-ion mass transfer limitation. The GITT results confirm the kinetic bottleneck by revealing a large discharge overpotential during the transition phase. We further demonstrate that improving the adsorption of dissolved high-order polysulfides, a key step in the interfacial processes, can alleviate the kinetic limitation, thus enhancing the achievable capacity under the lean electrolyte condition.

2.2 Introduction

Lithium||sulfur (Li||S) batteries have been considered one of the most promising rechargeable battery technologies since their inception in the 1960s.[1, 2] Owing to resurrected research efforts in the past two decades, tremendous knowledge on Li||S

batteries has been gained and promising prototypes have been demonstrated.[3-5] However, the widespread deployment of Li||S batteries remains hindered by their low specific energy and short cycle life, which are dictated by the complex interplay of the sulfur cathode, electrolyte, and Li anode. Among all the important parameters of the Li||S battery, a low electrolyte/sulfur (E/S) mass ratio (the "lean electrolyte" condition) is the most crucial requirement for the achievement of high specific energy.[5-20] To demonstrate the performance of realistic Li||S batteries, we assembled 0.9 Ah Li||S pouch cells as pictured in **Figure 2.1a**. The key parameters of these pouch cells are listed in **Table 2.1**. Two E/S mass ratios at 5.29 and 2.79 were used, resulting in specific capacities of 229 and 300 Wh kg^{-1}, respectively. **Figure 2.1b** shows the specific energy of the pouch cells as a function of E/S ratio based on the parameters in Table 2.1. It is worth noting that with the current cathode capacity (1027 mAh g^{-1} sulfur capacity, 6 mg cm^{-2} sulfur loading, and 64 wt.% sulfur in cathode) and Li loading (200% in excess), a Li||S battery with 400 Wh kg^{-1} specific energy requires an E/S ratio of 1, which is a very tall order. The representative discharge-charge curves and the cycle stability of Li||S pouch cells with these two E/S ratios are shown in **Figures 2.1c** to **2.1e**. By comparison, it is clear that the pouch cell with E/S ratio at 2.79 suffers inferior cycle stability, C rate, and coulombic efficiency (CE) despite its high initial specific energy. In this study, we attempt to probe the cathode-electrolyte interfacial processes in Li||S batteries under the lean electrolyte condition and provide our perspective on how to address the challenges induced by low E/S ratios.

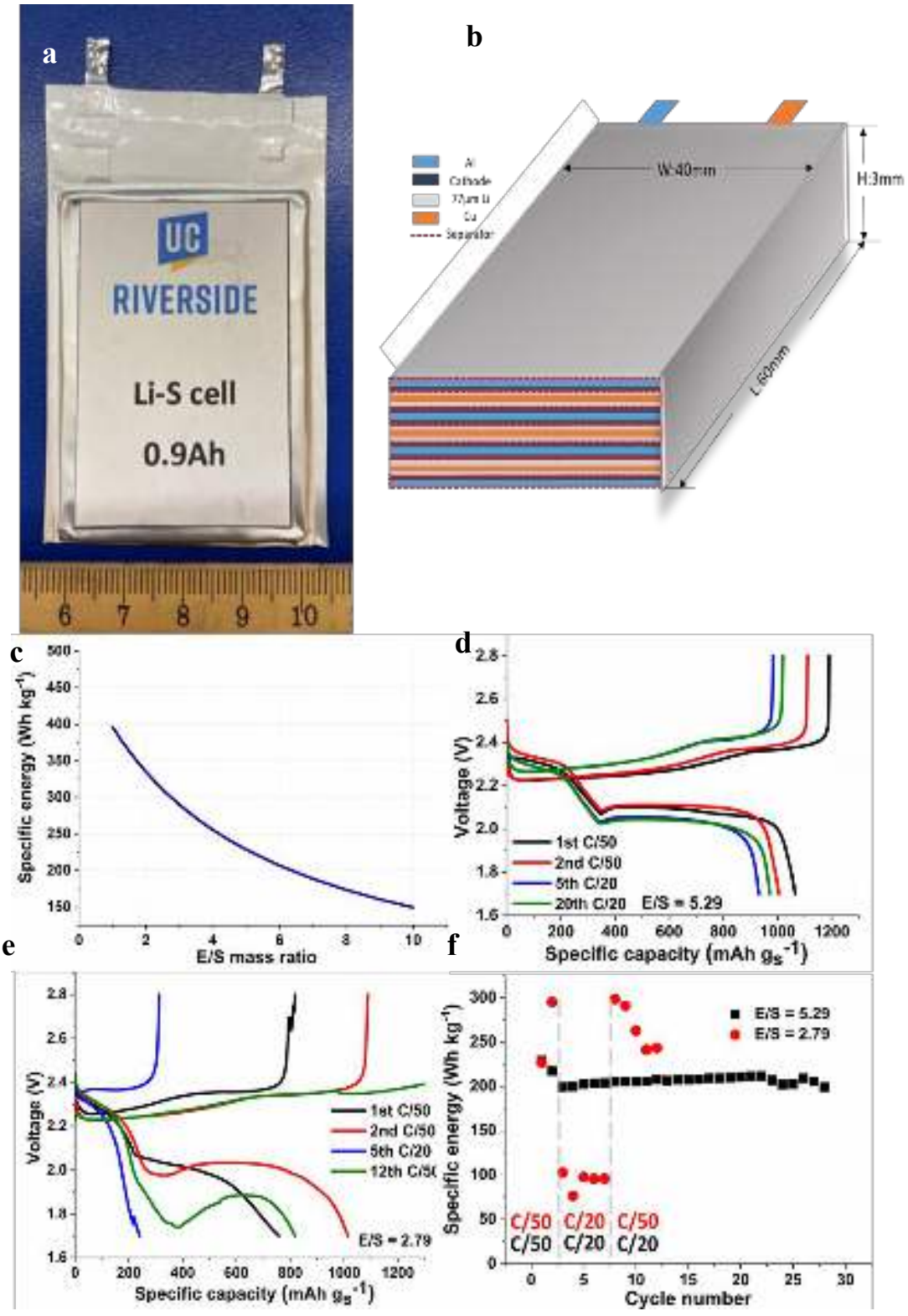
a
UC
RIVERSIDE
Li-S cell
0.9Ah
b
Al
Cathode
Cu
Separator
W:40mm
H:3mm
L:60mm
c
Specific energy (Wh kg-1)
E/S mass ratio
d
Voltage (V)
1st C/50
2nd C/50
5th C/20
20th C/20
E/S = 5.29
Specific capacity (mAh gS-1)
e
Voltage (V)
1st C/50
2nd C/50
5th C/20
12th C/50
E/S = 2.79
Specific capacity (mAh gS-1)
f
Specific energy (Wh kg-1)
E/S = 5.29
E/S = 2.79
C/50 C/20 C/50
C/50 C/20 C/20
Cycle number

Figure 2.1. (a) Digital photo of a 0.9 Ah Li||S pouch cell; (b)Schematic image of a Li||S pouch cell with internal components (c) Li||S specific energy as a function of E/S ratio based on the cell parameters in Table 1; Representative discharge-charge curves with (d) E/S = 5.29 and (e) E/S = 2.79 at C/50 (0.21 mA cm^{-2}) and C/20 (0.53 mA cm^{-2}); and (f) Cycle stability of the pouch cells at different E/S ratios.

Table 2.1. Parameters of demonstrated realistic Li||S pouch cells.

Cell Capacity		0.9 Ah
Cell Dimensions		6 cm × 4 cm × 0.3 cm
Structure	Double-sided Li anode	3 layers
	Double-sided S-C cathode	2 layers
	Single-sided S-C cathode	2 layers
Cathode	Sulfur/carbon/binder ratio:	64/26/10 wt.%
	Sulfur areal loading on Al foil:	6 mg cm^{-2}
	Sulfur specific capacity:	1027 mAh g^{-1} at 35 mA g^{-1} (0.21 mA cm^{-2})
Electrolyte	0.2 M LiTFSI in DOL/DME with 1.5 wt.% of $LiNO_3$	1) 4.57 g (E/S mass ratio = 5.29) 2) 2.41 g (E/S mass ratio = 2.79)
Anode	Li metal film on Cu foil	70 μm (200% Li excess)

2.3 Experimental section

2.3.1Materials Preparation and Cell Assembly

In this study, integrated ketjen black (IKB) was used as the sulfur host; its synthesis method was adopted from a previous study by Lv et al.[21] Briefly, ketjen black was mixed with citric acid in an aqueous suspension, following which ethylene glycol was added. The mixture was heated at 130°C for 6 hours under agitation. The obtained solid product was then carbonized under argon at 400°C for 6 hours and 800°C for another 10 hours to produce IKB. The sulfur-carbon (S-C) composite was prepared by mixing 80 wt.% sulfur (Sigma Aldrich) with 20 wt.% IKB, followed by a heating process at 155°C for 10 hours.

The cathode slurry was prepared by mixing 80 wt.% S-C composite, 10 wt.% binder, 5 wt.% multi-walled carbon nanotubes (Sigma Aldrich), and 5 wt.% carbon nanofibers (Carbon Nanotube Plus) in N-Methyl-2-pyrrolidone. The solid content of the slurry was 22 wt.%. Two polymer binders, polyvinylpyrrolidone (PVP) and poly(diallyldimethyl ammonium triflate) (PDAT), were used in this study. The slurry was coated onto Al foil and the electrode was dried in a vacuum oven at 50°C for 12 hours. The double-sided cathode was prepared by coating slurry on the other side of the Al foil after the preparation of a single-side cathode. The sulfur loading was approximately 6 mg cm^{-2} per side in all cathodes used in this study. The electrolyte was composed of 0.2 M lithium bis-(trifluoromethanesulfonyl)imide (LiTFSI) in a mixture of 1,2-dioxolane and dimethoxyethane (DOL/DME with 50/50 vol. ratio) with 1.5 wt.% lithium nitrate ($LiNO_3$). The LiTFSI and $LiNO_3$ were vacuum dried for 12 hours at 80°C. The DOL and DME were dried over molecular sieves with water content less than 10 ppm, measured through Karl Fischer titration. Both coin cells (2032 type) and pouch cells in this study were assembled in an argon-filled glovebox with Celgard® 2400 separator. Commercial 750-um Li foil (Alfa Aesar) was used as the anode in coin cells. The Li anode in the pouch cells was prepared using a method reported by our group. [22] A clean Li nugget was first obtained by cutting the surface of a Li rod (99.8% Strem Chemicals). The obtained nugget was then sandwiched between two pieces of laminated aluminum film (MTI Corporation) and compressed with a mechanical roller to yield the Li foil with thickness of 70 μm. A layer of the obtained 70-μm Li foil was then compressed onto each side of a piece of Cu foil. Prior to cell assembly, the cathodes were soaked in the electrolyte

overnight. The amount of adsorbed electrolyte was measured as the difference of the mass before and after electrolyte soaking, and different E/S ratios were achieved by adding additional electrolyte to the cells accordingly. The actual E/S ratios (i.e., amount of electrolyte) in the cells were determined through subtraction of the mass of all dry components in a cell from the total mass of the assembled cell.

2.3.2 Electrochemical Characterizations

The pouch cells were cycled between 1.7 and 2.8 V versus Li/Li^+ at C/50 and C/20 at room temperature. For the operando electrochemical impedance spectroscopy (EIS) experiments, galvanostatic discharge was performed using coin cells between 1.7 and 2.8 V versus Li/Li^+ under a current of 16 mA g^{-1} using an Arbin battery test station. Operando EIS was measured hourly during cell discharging using a Gamry Interface 1000 with a sinusoidal perturbation voltage of 5 mV RMS. The frequency range for the potentiostatic EIS was set with an initial frequency of 10^6 Hz and a final frequency of 50 Hz to ensure that the EIS measurement could be completed within 1 minute to minimize the interference to the discharge process. Galvanostatic intermittent titration technique (GITT) discharge was performed with a 10-minute current pulse at 40 mA g^{-1} (C/40) followed by a 40-minute resting period. The GITT discharge was completed when the 0.5 V cut-off potential was reached during the titration. Electrolyte without $LiNO_3$ was used in the GITT experiments to avoid the potential decomposition of $LiNO_3$ under low cathodic potentials.[23-25]

2.4 Results and discussion

The evolution of the electrochemical resistances during discharge may shed some light on the interfacial processes under different E/S ratios. The Nyquist plots from the operando EIS measurements were fitted with the equivalent circuit as displayed in **Figure 2.2**. The high-frequency intersection with the real axis is attributed to the combination of the electrode ohmic resistance and the electrolyte ionic resistance ($R_{\Omega+el}$); the first semi-circle in the Nyquist plot is assigned to the interphase impedance represented by the interphase resistance (R_{int}) and a constant phase element (CPE) in parallel. R_{int} is the analog of the solid electrolyte interphase resistance at the anode. It is the measurement of the ionic conductivity in the vicinity of the cathode-electrolyte interface (i.e., the interphase), which changes with the evolution of the interphase composition. The second semi-circle is due to the charge transfer impedance of the electrochemical reduction of the active species in the cathode represented by the charge transfer resistance (R_{ct}) and a CPE in parallel.

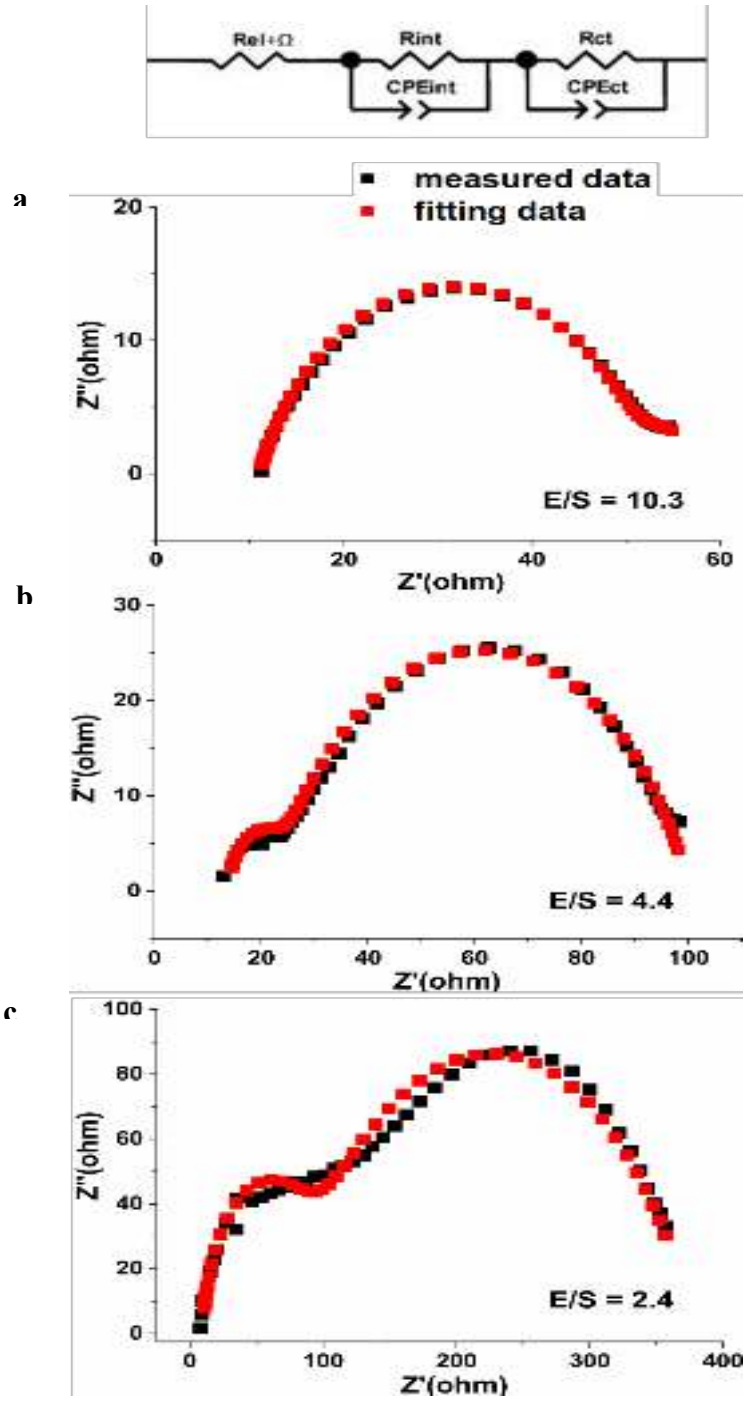

Figure 2.2. Representative Nyquist plots with data fitting based on the displayed equivalent circuit: the 20th EIS measurement under E/S ratio of (a) 10.3, (b) 4.4, and (c) 2.4.

The evolution of the electrochemical resistances during discharge alongside the potential profiles are displayed in **Figure 2.3**. Three E/S mass ratios including 10.3, 4.4, and 2.4 were used in the discharge. It is noticeable that the discharge under higher E/S ratios (10.3 and 4.4) can achieve high specific capacity of sulfur (>1000 mAh g^{-1}) with the typical two-plateau discharge profile. On the other hand, the discharge under an E/S ratio of 2.4 terminates at the first plateau, reaching the lower cutoff voltage with very low capacity at 200 mAh g^{-1}. As Figures 3a to 3c show, the changes of $R_{\Omega+el}$ under all three E/S ratios are minimal and demonstrate an identical trend: It first increases as the discharge begins, which likely reflects the increasing ohmic resistance at the Li anode due to passivation by polysulfides. After reaching a peak in the middle of the first plateau, $R_{\Omega+el}$ starts to decrease and leveling off till the end of the discharge. This behavior can be attributed to the continuous dissolution of high-order polysulfides, which increases the ion concentration in the electrolyte.

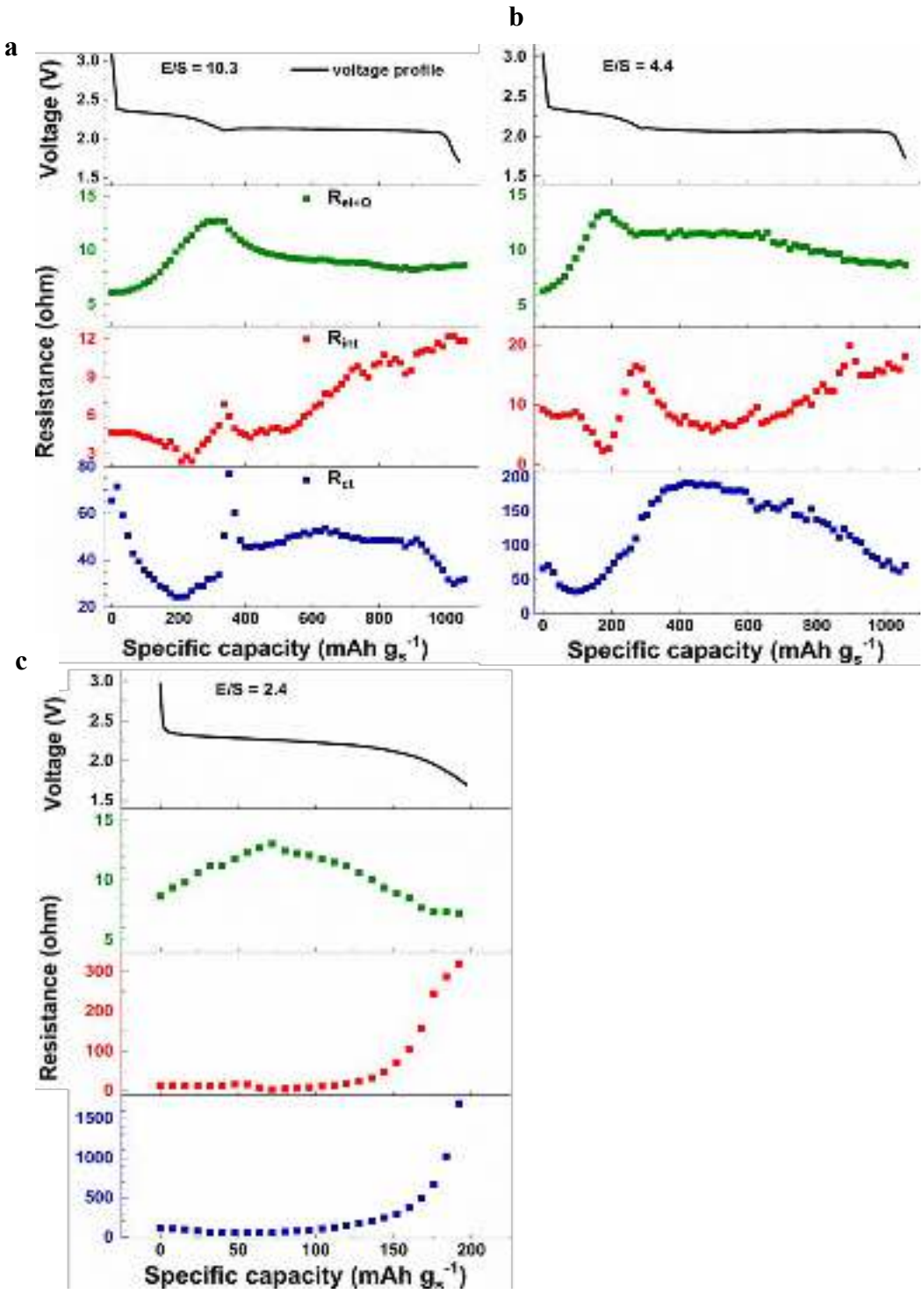

Figure 2.3. Discharge voltage profiles of Li||S cells alongside the simultaneous electrochemical resistance under E/S ratio at (a) 10.3, (b) 4.4, and (c) 2.4

The evolution of the interphase resistance can be analyzed through the different discharge plateaus. When the discharge process starts, R_{int} first remains stable and then gradually decreases. After reaching the lowest point in the middle of the first plateau, it starts to rapidly increase to a peak point, which coincides with the end of the first plateau. The peak value of R_{int} under the low E/S ratio of 2.4 reaches 320 ohms, which is an order of magnitude higher than those under higher E/S ratios (10.3 and 4.4). These observations reflect the chemical and physical phenomena at the cathode-electrolyte interface during discharge. When discharge begins, sulfur is first reduced to high-order polysulfides that are rapidly dissolved away from the cathode due to the high concentration gradient at the interface. This dissolution of high-order polysulfides induces the initial decrease of the interphase resistance. While the discharging proceeds, the rate of dissolution decreases due to the increase of polysulfide concentration in the electrolyte (i.e., lower concentration gradient). As a result, the high-order polysulfides start to accumulate at the cathode-electrolyte interface, thus increasing interphase resistance. The lean electrolyte condition (E/S ratio at 2.4) accelerates the polysulfide accumulation at the interface due to the higher concentration than that of the electrolyte with higher E/S ratios. As such, the interphase resistance reaches 320 ohms at the end of the first plateau, which is the transition point of the discharge process from the "liquid phase" (i.e., high-order polysulfides dominating) to the "solid phase" (i.e., low-order polysulfides dominating).[26, 27] While the discharge process with E/S ratio of 2.4 terminates at the transition point, the discharges with higher E/S ratios proceed with decreasing R_{int} at the beginning of the second plateau due to the downstream reduction of interphase high-order polysulfides.

The R_{int} then starts to gradually increase until the end of the second plateau due to an increase of lithium sulfide (Li_2S) generated in the interphase. The evolution of the charge transfer resistance R_{ct} in the first plateau is fully consistent with that of the interphase resistance R_{int}. Regardless of the E/S ratio, R_{ct} first decreases at the beginning of the discharge due to the improved reduction kinetics enabled by the high-order polysulfides' dissolution (i.e., reduced R_{int}). After reaching the lowest point in the middle of the first plateau, R_{ct} rapidly increases alongside the simultaneously increasing R_{int}. The matching trends of R_{int} and R_{ct} indicate that the change transfer resistance is positively correlated to the interphase resistance, which represents the degree of difficulty with which Li-ions are transferred across the interphase. Similarly to R_{int}, the magnitude of R_{ct} increases with decreasing E/S ratio; at the transition point, the peak R_{ct} values with E/S ratios of 10.3 and 4.4 are 73 and 192 ohms, respectively. In stark contrast, the charge transfer resistance with an E/S ratio of 2.4 reaches 1691 ohms. Such a high R_{ct} is the direct cause of the early termination of the discharge and likely results from the large Li-ion mass transfer limitation at the interface.[28-30]

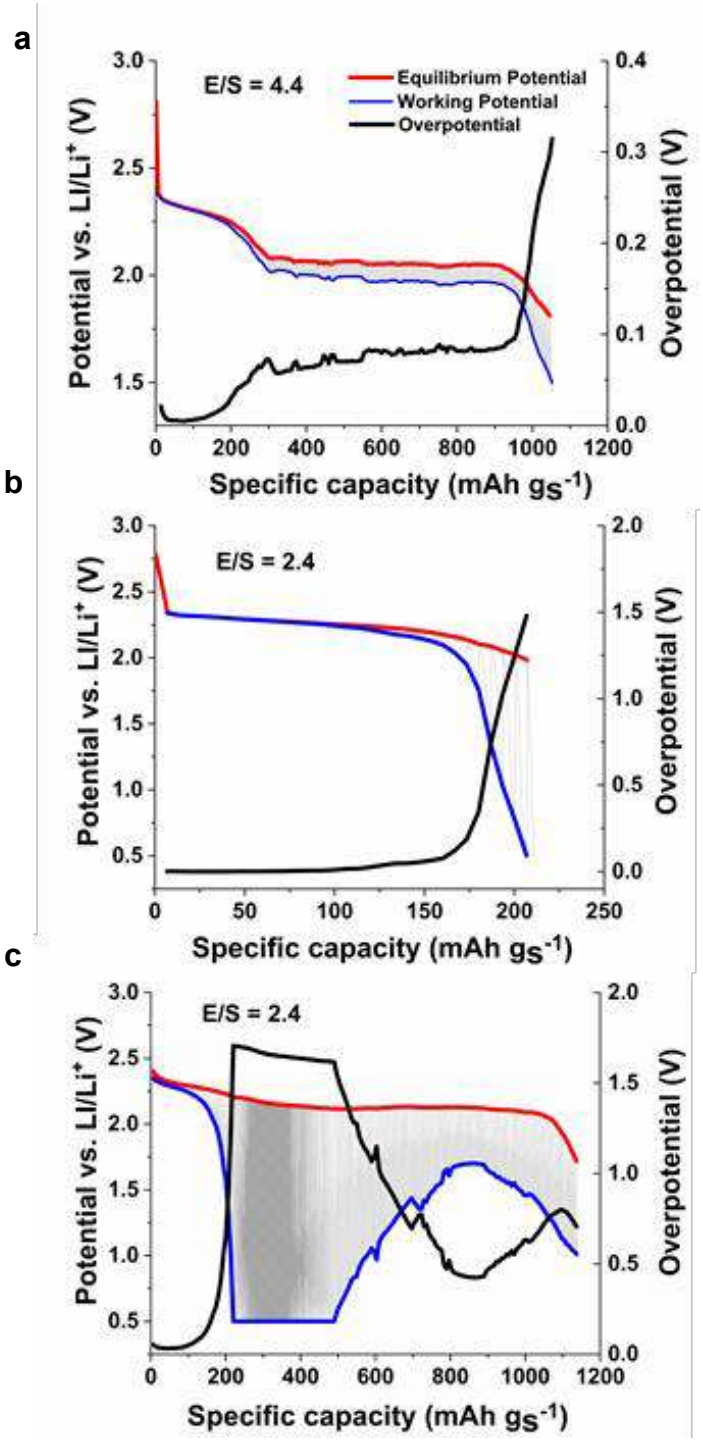

Figure 2.4. GITT results of discharge of Li-S battery with E/S ratio of (a) 4.4 and (b) 2.4; (c) result from modified GITT experiment under E/S ratio of 2.4.

The overpotentials of the discharge process with different E/S ratios were revealed with the GITT experiments as shown in **Figure 2.4** with two E/S ratios at 4.4 (**Figure 2.4a**) and 2.4 (**Figures 2.4b** and **2.4c**). The red curve is the near-equilibrium discharge potential profile, the blue curve is the working potential profile, and the black curve is the overpotential (the difference between working and near-equilibrium potentials). The overpotential with E/S ratio of 4.4 is low, although there is a clear increase toward the transition point as shown in Figure 4a. The increase of overpotential at the transition becomes much steeper with E/S ratio at 2.4 as displayed in Figure 4b; the GITT discharge is stopped when the working potential reaches the cutoff potential at 0.5 V while the near-equilibrium discharge potential is at 2 V vs. Li/Li^+. The large overpotential under the low E/S ratio clearly indicates that this "liquid-to-solid" transition is the kinetic bottleneck. The result from a modified GITT experiment displayed in Figure 4c provides additional evidence. In the modified GITT discharge, we allow the experiment to continue after the working potential reaches the cutoff potential at 0.5 V. In another words, we force the discharge with short current pulses despite the large overpotential. The near-equilibrium discharge in Figure 4c demonstrates the typical two-plateau potential profile, but the transition region experiences large overpotential over a long period equivalent to 300 mAh g^{-1} capacity. Once the transition period ends, the discharge overpotential drastically decreases and high capacity is achieved.

The GITT and the operando EIS results unambiguously prove that the low specific energy under the lean electrolyte condition is due to the inferior discharge kinetics during the transition period from high-order to low-order polysulfides. The discharge

mechanism during the first plateau (high-order polysulfide region) is proposed in **Scheme 1** to describe the key process parameters. The first elementary step of the discharge is the electrochemical reduction (i.e., charge transfer) of sulfur to high-order polysulfides (represented by S_8^{2-} anion), followed by instantaneous dissolution to form the dissolved S_8^{2-}(sol) anions. S_8^{2-}(sol) can diffuse into the electrolyte, driven by the concentration gradient. Under the lean electrolyte condition, the dissolved S_8^{2-}(sol) can rapidly saturate the electrolyte and limit mass transfer at the interface for the upstream sulfur reduction. Meanwhile, the S_8^{2-}(sol) anions must be adsorbed on the electrode to form adsorbed S_8^{2-}(ads) anions to be further reduced to lower-order polysulfides during the transition. Based on the proposed discharge process, improving the adsorption and/or the reduction kinetics of S_8^{2-} anions can alleviate the charge transfer kinetic bottleneck.

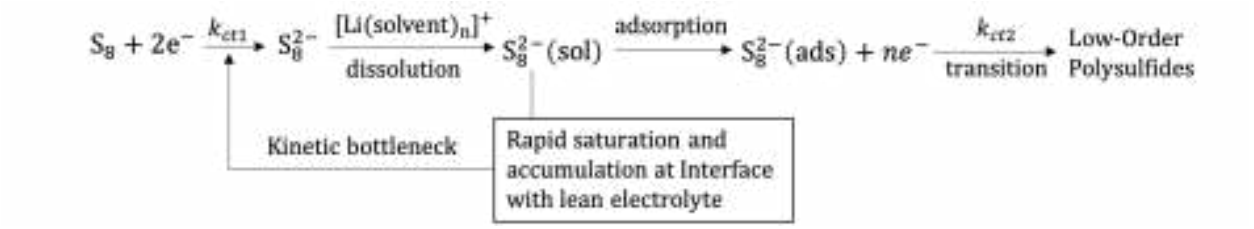

Scheme 1. Kinetic steps during the discharge transition from high-order polysulfides to low-order polysulfides.

To validate the hypothesis that improving the adsorption of high-order polysulfide anions can improve the charge transfer kinetics,[31-33] we replaced the PVP binder with PDAT, which is an ionomer with a positively charged backbone. PDAT has been previously shown to be an effective adsorbent for polysulfides.[34] With PDAT binder, the

electrochemical resistances during discharge with E/S ratios of 4.4 and 2.4 were measured with the operando EIS. As displayed in **Figure 2.5a**, the electrochemical resistances under an E/S ratio of 4.4 demonstrate a similar trend to the ones in Figure 3b. However, the magnitude of the charge transfer resistance with the PDAT binder is reduced to half of that measured when using the PVP binder. **Figure 2.5b** displays the discharge potential profile under an E/S ratio of 2.4 alongside the simultaneous electrochemical resistances from using the PDAT binder. Compared to Figure 3c, the most significant difference is that PDAT enables the second plateau of the discharge with high specific capacity at 1100 mAh g^{-1} by overcoming the high charge transfer resistance. The GITT discharge under an E/S ratio of 2.4 in **Figure 2.5c** also demonstrates the effectiveness of PDAT binder to alleviate the kinetic bottleneck under the lean electrolyte condition. Compared to Figures 4b and 4c, the PDAT binder under an E/S ratio of 2.4 enables high capacity with significantly reduced overpotential in the transition region.

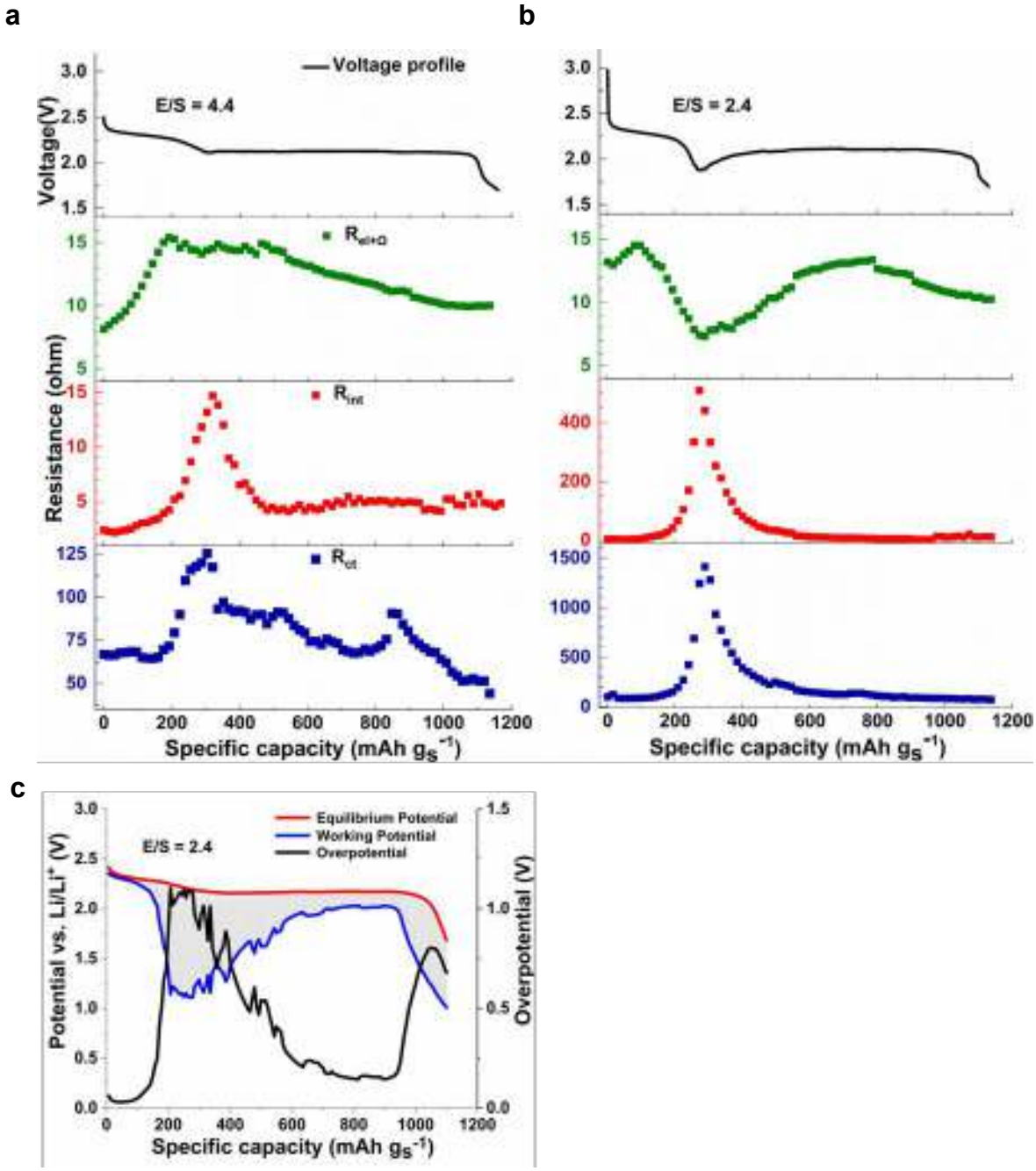

Figure 2.5. Discharge voltage profiles of Li||S cells alongside the simultaneous electrochemical resistances under E/S ratio of (a) 4.4 and (b) 2.4 using PDAT binder; (c) GITT discharge of Li||S cell under E/S ratio of 2.4 using PDAT binder

2.5 Conclusions

In this study we probe the interfacial process during the discharge of a sulfur-carbon cathode under the lean electrolyte condition. Our operando EIS and GITT experiments indicate that the cause of low achievable specific energy of Li||S batteries with low E/S ratios is the kinetic bottleneck occurring during the transition from high-order to low-order polysulfides. Such a bottleneck is induced by high mass transfer limitations due to rapid accumulation of polysulfides at the electrode-electrolyte interface. We also demonstrate that improving the adsorption of high-order polysulfides can effectively alleviate this kinetic limitation. In future work, we will investigate and develop comprehensive strategies to implement low E/S ratios while retaining high specific energy and cycle stability in the Li||S batteries based on the revealed interfacial processes.

References

1. Steunenberg, J. R. B. a. R. K., Chemical Investigations of Lithium-Sulfur Cells. *Advances in Chemistry* **1975**.

2. Rauh, R. D. A., K. M.; Pearson, G. F.; Surprenant, J. K., A Lithium Dissolved Sulfur Battery with an OrganicElectrolyte. *J. Electrochem. Soc.* **1979,** *126*, 523-527.

3. Crittenden, M. With Ultralight Lithium-Sulfur Batteries, Electric Airplanes Could Finally Take Off. https://spectrum.ieee.org/aerospace/aviation/with-ultralight-lithiumsulfur-batteries-electric-airplanes-could-finally-take-off.

4. Zhao, C.; Xu, G. L.; Yu, Z.; Zhang, L.; Hwang, I.; Mo, Y. X.; Ren, Y.; Cheng, L.; Sun, C. J.; Ren, Y.; Zuo, X.; Li, J. T.; Sun, S. G.; Amine, K.; Zhao, T., A high-energy and long-cycling lithium-sulfur pouch cell via a macroporous catalytic cathode with double-end binding sites. *Nat Nanotechnol* **2021,** *16* (2), 166-173.

5. Shi, L.; Bak, S.-M.; Shadike, Z.; Wang, C.; Niu, C.; Northrup, P.; Lee, H.; Baranovskiy, A. Y.; Anderson, C. S.; Qin, J.; Feng, S.; Ren, X.; Liu, D.; Yang, X.-Q.; Gao, F.; Lu, D.; Xiao, J.; Liu, J., Reaction heterogeneity in practical high-energy lithium–sulfur pouch cells. *Energy & Environmental Science* **2020,** *13* (10), 3620-3632.

6. Bhargav, A.; He, J.; Gupta, A.; Manthiram, A., Lithium-Sulfur Batteries: Attaining the Critical Metrics. *Joule* **2020,** *4* (2), 285-291.

7. Chung, S.-H.; Manthiram, A., Designing Lithium-Sulfur Cells with Practically Necessary Parameters. *Joule* **2018,** *2* (4), 710-724.

8. Dörfler, S.; Althues, H.; Härtel, P.; Abendroth, T.; Schumm, B.; Kaskel, S., Challenges and Key Parameters of Lithium-Sulfur Batteries on Pouch Cell Level. *Joule* **2020,** *4* (3), 539-554.

9. Shi, H.; Qin, J.; Lu, P.; Dong, C.; He, J.; Chou, X.; Das, P.; Wang, J.; Zhang, L.; Wu, Z. S., Interfacial Engineering of Bifunctional Niobium (V)-Based Heterostructure Nanosheet Toward High Efficiency Lean-Electrolyte Lithium–Sulfur Full Batteries. *Advanced Functional Materials* **2021**.

10. Wang, H.; Shao, Y.; Pan, H.; Feng, X.; Chen, Y.; Liu, Y.-S.; Walter, E. D.; Engelhard, M. H.; Han, K. S.; Deng, T.; Ren, G.; Lu, D.; Lu, X.; Xu, W.; Wang, C.; Feng, J.; Mueller, K. T.; Guo, J.; Zavadil, K. R.; Zhang, J.-G., A lithium-sulfur battery with a solution-mediated pathway operating under lean electrolyte conditions. *Nano Energy* **2020,** *76*.

11. Shin, W.; Zhu, L.; Jiang, H.; Stickle, W. F.; Fang, C.; Liu, C.; Lu, J.; Ji, X., Fluorinated co-solvent promises Li-S batteries under lean-electrolyte conditions. *Materials Today* **2020,** *40*, 63-71.

12. Nanda, S.; Bhargav, A.; Manthiram, A., Anode-free, Lean-Electrolyte Lithium-Sulfur Batteries Enabled by Tellurium-Stabilized Lithium Deposition. *Joule* **2020,** *4* (5), 1121-1135.

13. Zhang, G.; Peng, H. J.; Zhao, C. Z.; Chen, X.; Zhao, L. D.; Li, P.; Huang, J. Q.; Zhang, Q., The Radical Pathway Based on a Lithium-Metal-Compatible High-Dielectric Electrolyte for Lithium-Sulfur Batteries. *Angew Chem Int Ed Engl* **2018,** *57* (51), 16732-16736.

14. Li, G.; Lei, W.; Luo, D.; Deng, Y.; Deng, Z.; Wang, D.; Yu, A.; Chen, Z., Stringed "tube on cube" nanohybrids as compact cathode matrix for high-loading and lean-electrolyte lithium–sulfur batteries. *Energy & Environmental Science* **2018,** *11* (9), 2372-2381.

15. Chung, S. H.; Manthiram, A., Designing Lithium-Sulfur Batteries with High-Loading Cathodes at a Lean Electrolyte Condition. *ACS Appl Mater Interfaces* **2018,** *10* (50), 43749-43759.

16. Chen, S.; Gao, Y.; Yu, Z.; Gordin, M. L.; Song, J.; Wang, D., High capacity of lithium-sulfur batteries at low electrolyte/sulfur ratio enabled by an organosulfide containing electrolyte. *Nano Energy* **2017,** *31*, 418-423.

17. Luo, C.; Hu, E.; Gaskell, K. J.; Fan, X.; Gao, T.; Cui, C.; Ghose, S.; Yang, X. Q.; Wang, C., A chemically stabilized sulfur cathode for lean electrolyte lithium sulfur batteries. *Proc Natl Acad Sci U S A* **2020,** *117* (26), 14712-14720.

18. Liu, J.; Li, S.; Marium, M.; Wang, B.; Ueno, K.; Dokko, K.; Watanabe, M., Towards practical cells: combined use of titanium black as a cathode additive and sparingly solvating electrolyte for high-energy-density lithium–sulfur batteries. *Sustainable Energy & Fuels* **2021,** *5* (6), 1821-1831.

19. Wang, M.; Fan, L.; Sun, X.; Guan, B.; Jiang, B.; Wu, X.; Tian, D.; Sun, K.; Qiu, Y.; Yin, X.; Zhang, Y.; Zhang, N., Nitrogen-Doped CoSe2 as a Bifunctional Catalyst for High Areal Capacity and Lean Electrolyte of Li–S Battery. *ACS Energy Letters* **2020,** *5* (9), 3041-3050.

20. Yang, Y.; Zhong, Y.; Shi, Q.; Wang, Z.; Sun, K.; Wang, H., Electrocatalysis in Lithium Sulfur Batteries under Lean Electrolyte Conditions. *Angew Chem Int Ed Engl* **2018,** *57* (47), 15549-15552.

21. Lv, D.; Zheng, J.; Li, Q.; Xie, X.; Ferrara, S.; Nie, Z.; Mehdi, L. B.; Browning, N. D.; Zhang, J.-G.; Graff, G. L.; Liu, J.; Xiao, J., High Energy Density Lithium-Sulfur Batteries: Challenges of Thick Sulfur Cathodes. *Advanced Energy Materials* **2015,** *5* (16).

22. Zhang, J.; Shi, J.; Wen, X.; Zhao, Y.; Guo, J., Properties of Thin Lithium Metal Electrodes in Carbonate Electrolytes with Realistic Parameters. *ACS Appl Mater Interfaces* **2020,** *12* (29), 32863-32870.

23. Sheng S. Zhang, D. T. T., A proof-of-concept lithium/sulfur liquid battery with exceptionally high capacity density. *Journal of Power Sources* **2012,** *211*, 169-172.

24. Zhang, S. S., Effect of Discharge Cutoff Voltage on Reversibility of Lithium/Sulfur Batteries with LiNO3-Contained Electrolyte. *Journal of The Electrochemical Society* **2012,** *159* (7), A920-A923.

25. Rosenman, A.; Elazari, R.; Salitra, G.; Markevich, E.; Aurbach, D.; Garsuch, A., The Effect of Interactions and Reduction Products of LiNO3, the Anti-Shuttle Agent, in Li-S Battery Systems. *Journal of The Electrochemical Society* **2015,** *162* (3), A470-A473.

26. Peng, H.-J.; Huang, J.-Q.; Cheng, X.-B.; Zhang, Q., Review on High-Loading and High-Energy Lithium-Sulfur Batteries. *Advanced Energy Materials* **2017,** *7* (24).

27. Cuisinier, M.; Cabelguen, P.-E.; Evers, S.; He, G.; Kolbeck, M.; Garsuch, A.; Bolin, T.; Balasubramanian, M.; Nazar, L. F., Sulfur Speciation in Li–S Batteries Determined by Operando X-ray Absorption Spectroscopy. *The Journal of Physical Chemistry Letters* **2013,** *4* (19), 3227-3232.

28. Zhang, T.; Marinescu, M.; Walus, S.; Kovacik, P.; Offer, G. J., What Limits the Rate Capability of Li-S Batteries during Discharge: Charge Transfer or Mass Transfer? *Journal of The Electrochemical Society* **2017,** *165* (1), A6001-A6004.

29. Fan, F. Y.; Chiang, Y.-M., Electrodeposition Kinetics in Li-S Batteries: Effects of Low Electrolyte/Sulfur Ratios and Deposition Surface Composition. *Journal of The Electrochemical Society* **2017,** *164* (4), A917-A922.

30. Fan, F. Y.; Carter, W. C.; Chiang, Y. M., Mechanism and Kinetics of Li2S Precipitation in Lithium-Sulfur Batteries. *Adv Mater* **2015,** *27* (35), 5203-9.

31. Tao, X.; Wang, J.; Liu, C.; Wang, H.; Yao, H.; Zheng, G.; Seh, Z. W.; Cai, Q.; Li, W.; Zhou, G.; Zu, C.; Cui, Y., Balancing surface adsorption and diffusion of

lithium-polysulfides on nonconductive oxides for lithium-sulfur battery design. *Nat Commun* **2016,** *7*, 11203.

32. Wu, D. S.; Shi, F.; Zhou, G.; Zu, C.; Liu, C.; Liu, K.; Liu, Y.; Wang, J.; Peng, Y.; Cui, Y., Quantitative investigation of polysulfide adsorption capability of candidate materials for Li-S batteries. *Energy Storage Materials* **2018,** *13*, 241-246.

33. Li, J.; Qu, Y.; Chen, C.; Zhang, X.; Shao, M., Theoretical investigation on lithium polysulfide adsorption and conversion for high-performance Li-S batteries. *Nanoscale* **2021,** *13* (1), 15-35.

34. Su, H.; Fu, C.; Zhao, Y.; Long, D.; Ling, L.; Wong, B. M.; Lu, J.; Guo, J., Polycation Binders: An Effective Approach toward Lithium Polysulfide Sequestration in Li–S Batteries. *ACS Energy Letters* **2017,** *2* (11), 2591-2597.

Chapter 3: Carboranyl Ionic Liquids: Single Component Electrolytes Towards Stable Lithium Deposition and High Specific Energy Li-S Batteries

3.1 Abstract

As the public pays more and more attention to environmental and energy issues, a lot of efforts have been made in the development of cutting-edge electrochemical energy storage technology. As an important part of rechargeable battery, a stable and functional electrolyte is urgently required to enable high specific energy battery with strong oxidizing or reducing electrodes materials. Ionic liquid-based electrolytes attract more attention due to their excellent thermal stability, negligible volatility and non-flammability. For the first time, we report a novel Carboranyl Ionic Liquids (CIL) -- $[H_9C_4CB_9H_9]^-[Li(THF)_{1.0}]^+$. We demonstrated good chemical and electrochemical stability of CIL in the presence of lithium metal. High specific energy Li-S battery is also prospected in applying CIL via a sparingly dissolving pathway.

3.2 Introduction

Due to the increasing energy demand and diminishing fossil source, the urgent desire for alternative environmentally friendly energy resources such as solar energy, wind energy or tide are increasing rapidly. Beside energy generation, energy storage is also eagerly desired. Rechargeable batteries raise intense research interest as an ideal energy storage device which can convert electricity to chemical potential and store for future use. With the development of materials science, electrode technology is advancing by leaps and bounds. As an important part of the battery, electrolyte plays the key role in enabling

electrochemical performance. Electrolytes are ubiquitous and indispensable in battery. The role of the electrolyte is serving as a medium for transferring ions between cathode and anode. Most electrolytes are liquid state in the service temperature range which consist of salts dissolved in water (aqueous) or organic molecules (non-aqueous). Electrolytes must be inert in a battery both electrochemically and chemically. However, the reality is, the stability often challenged by the strong oxidizing or reducing nature of cathode or anode. With the increasing pursuit for high energy density battery, more oxidizing cathodes and more reducing anodes were applied in batteries as electrodes materials which require a wider stable electrochemical window for electrolyte. Beside chemical and electrochemical stability, electrolyte should also be a good ionic conductor and electronic insulator. Robustness to any thermal or mechanical abuse should also be considered for the requirement of electrolyte.

Room temperature ionic liquid (RTIL) as a new type of liquid electrolyte, are organic salts in liquid state containing charge balanced cations and anions. Because of the safety concerns, RTIL which has large liquid phase range, low vapor pressure, high boiling point, nonflammability and wide electrochemical stable window is an ideal electrolyte material. Several researches are reported in using RTIL as electrolyte for Li-ion batteries or Li-S batteries. [1-5] Typically, these consist of two components: a lithium salt dissolved within an electrochemically stable ionic liquid medium consists of onium cations and bulky and weakly coordinating anions. These components work in tandem to comprise the electrolyte; the ionic liquid medium serving as a non-flammable, safe liquid medium and the lithium salt mediating charge transfer within. Although the thermal stability and

non-flammability of the electrolyte is greatly improved, its transport performance is not as good as that of conventional organic electrolyte. When the lithium salt is dissolved in the aprotic IL, the viscosity of the solution greatly increases, resulting in a decrease in the ionic conductivity as the concentration of the lithium salt increases. In addition, since the aprotic ionic solvent itself is a charged solvent, not only Li^+ but also the cations and anions constituting the ionic liquid are movable under an electric field. This will result in low Li^+ transference number.

In 2010, concept of solvate ionic liquid (SIL) is a new emerging class of ionic liquid (IL) was reported by Watanabe group. [6] Generally, the presence of SIL is due to the diffusion of cationic charge through chelating hard cations in ethereal solvents or Acetonitrile.[7-10] SIL not only shows similar thermal stability, non-flammability and good electrochemical stability but also improve the ion transportation. So far the SIL electrolyte studies only focus on lithium bis(trifluoromethane sulfonyl)imide (LiTFSI) or lithium bis(fluorosulfonyl)imide(LiFSI) with diglyme (G2),triglyme(G3) or tetraglyme(G4) as listed in **Table 3.1**.

Herein, we report a series of lithium salts of the carborane that persist as liquids at room temperature These Carboranyl Ionic Liquids (CILs) consist solely of a CB_9H_9 carborane anion that has been functionalized at the carbon vertex with an alkyl moiety, R-CB_9H_9 (R = H, C_nH_m), as shown in **Figure 3.1 a**.

CILs are distinguished from RTIL of their kind as they are true single component ionic liquid electrolytes – rather than consisting of two components, an imidazolium-based ionic liquid medium and conducting salt, it effectively functions as both.

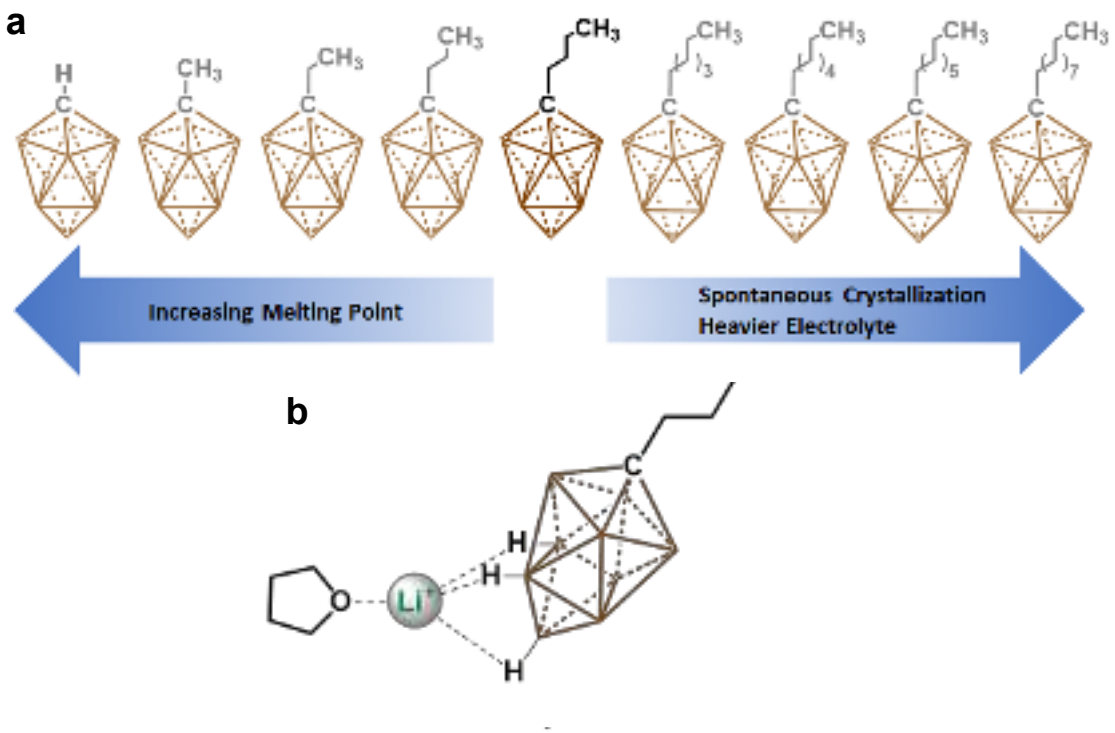

Figure 3.1. (a) Series of lithium salts of the CB_9H_9 carborane with an alkyl moiety R-CB_9H_9 (R = H, CnHm) (b) Structure of CIL $[H_9C_4CB_9H_9]^-[Li(THF)_{1.0}]^+$ with one THF molecules coordinate to the Li cation.

3.3 Experiment Section

General Considerations

Unless otherwise stated all manipulations were carried out using standard Schlenk or glovebox techniques (O2, H2O < 1ppm) under a dinitrogen or argon atmosphere. Solvents tetrahydrofuran (THF), and pentane (C_5H_{10}) were dried on K, Na or CaH_2, and distilled under argon before use. NMR spectra were recorded on Bruker Avance 300 MHz, Varian Inova 300 MHz, Varian Inova 400 MHz, or Varian Inova 500 MHz spectrometers. NMR chemical shifts are reported in parts per million (ppm). 1H NMR

and 13C NMR chemical shifts were referenced to residual solvent. 11B NMR chemical shifts were externally referenced to BF_3OEt_2.

3.3.1 Materials preparation and cell assembly

Carboranyl Ionic Liquid Synthesis

$[HCB_9H_9]^-[HNMe_3]^+$ was synthesized from a modified literature procedure.[25, 26]

Synthesis of $[C_4H_9\text{-}CB_9H_9]^-Cs^+$ from $[HCB_9H_9]^-[HNMe_3]^+$

12.1 grams (67.4 mmol) of $[HCB_9H_9]^-[HNMe_3]^+$ was dried in-vacuo at 150°C prior to the reaction. Working in a glovebox, the quantity of $[HCB_9H_9]^-[HNMe_3]^+$ was fully dissolved in 150 mL THF and stirred until complete dissolution of the compound was achieved. Concurrently, 56.6 mL (141.5 mmol) of 2.5M n-butyl-lithium solution in hexane was concentrated in-vacuo. The n-butyl-lithium was slowly added over the period of an hour to prevent the reaction from bubbling over. Once added, the reaction was left to stir for an additional 30 minutes, and complete conversion to the dianionic carborane species, $[CB_9H_9]^{2-}2Li^+$ was verified by ^{11}B NMR before proceeding. The THF solution was then added dropwise to a 400 mL stirring solution of hexane to precipitate the $[CB_9H_9]^{2-}2Li^+$ as a white solid. The hexane was decanted, and the solid was dried briefly in-vacuo for 5 minutes. Once dry, 7.3 mL (67.5 mmol) BrC_4H_9 and 75 mL THF were added, and the reaction was left to stir overnight. The reaction mixture was then charged in an addition funnel and added dropwise to a stirring 500 mL solution of hexane. 200 mL of water was added resulting in a bi-phasic mixture. 10 grams of CsCl was added to the stirring solution which slowly precipitated a white solid over a period of 10 minutes. The solid

was filtered and allowed to dry. The resulting solid was recrystallized from 500 mL of water yielding 18.4 g of $[H_9C_4CB_9H_9]Cs^+$ as pearlescent crystals.

Synthesis of $[C_4H_9\text{-}CB_9H_9]^-[Li(THF)_{4.0}]^+$ from $[C_4H_9\text{-}CB_9H_9]^-[HNMe_3]^+$

Salt exchange to yield $[H_9C_4CB_9H_9]^-[HNMe_3]^+$ was accomplished by redissolving the crystalline $[H_9C_4CB_9H_9]Cs^+$ in boiling water followed by the addition of $HNMe_3^+Cl^-$ to immediately yield a white precipitate which was collected via vacuum filtration. $[H_9C_4CB_9H_9]^-[HNMe_3]^+$ was dried in-vacuo at 80°C prior to the reaction. Working in a glovebox, 16.0 grams of $[H_9C_4CB_9H_9]^-[HNMe_3]^+$ dissolved in 200 mL THF. To the stirring THF solution, excess LiH was added until gas evolution seized. The solution was left to stir for an additional 6 hours before being filtered 2x through glass microfiber filter. The solution was concentrated in-vacuo at 25°C until $[C_4H_9\text{-}CB_9H_9][Li(THF)_4]^+$ was obtained as a waxy off-white solid.

Synthesis of $[C_4H_9\text{-}CB_9H_9]^-[Li(THF)_{1.0}]^+$ from $[C_4H_9\text{-}CB_9H_9]^-[Li(THF)_{4.0}]^+$

A quantity of $[C_4H_9\text{-}CB_9H_9][Li(THF)_{4.0}]^+$ was heated to 110°C in-vacuo in a 100 mL side arm Schlenk flask. Within the first hour of heating, the white solid gradually melted into a viscous faint-yellow liquid. After 24 hours, liquid was confirmed by ^1H NMR to contain 1 THF molecule via integration relative to the 2H resonance at δ = 3.17 in $CDCl_3$ in **Figure 3.S2**.

^1H NMR (400 MHz, $CDCl_3$, 25°C): δ = 3.85 (m, 4H), 3.17 (t, 2H), 2.0 (pt, 2H), 1.92 (m, 4H), 1.57 (sextet, 2H), 1.03 (t, 3H), 5.25 – 4.25 (bm, 1H, B - H) 2.50 - 0.0 (bm, 8 H, B - H) ppm; $^{11}B\{\delta\ 1H\}$NMR (96 MHz, $CDCl_3$, 25 °C): δ = 25.7, -17.1, -24.9 ppm.

Purification of CIL

200 mL of pentane was added to a quantity of $[C_4H_9\text{-}CB_9H_9]^-[Li(THF)_{4.0}]^+$ and stirred rigorously for 5 minutes. The emulsion was allowed to settle before carefully decanting the pentane layer over a glass microfiber filter into another vessel (this was often done by pipette to avoid potential impurities). Once separated, the pentane supernatant was concentrated in-vacuo to yield a clear, viscous solution at room-temperature. This process was repeated until all of the $[C_4H_9\text{-}CB_9H_9]^-[Li(THF)_{4.0}]^+$ was extracted and filtered. To obtain a quantity of pure $[C_4H_9\text{-}CB_9H_9]^-[Li(THF)_{1.0}]^+$ suitable for this study, care was taken to desolvate the material as described above. The quantity of $[C_4H_9\text{-}CB_9H_9]^-[Li(THF)_{1.0}]^+$ then obtained was redissolved in pentane and filtered through a 0.1 μm PTFE filter. The filtrate was concentrated in-vacuo to yield a clear solution of $[C_4H_9\text{-}CB_9H_9]^-[Li(THF)_{1.0}]^+$ in high purity.

Transference number Experimental section.

^{7}Li diffusion coefficients are measured on 300 MHz NMR spectrometer operating at a magnetic field of 7 T (^{7}Li Larmor frequencies of 300, respectively) with Agilent/Varian DDR console two channel solids configuration equipped with a Doty Z-spec PFG NMR probe. ^{1}H diffusion coefficients are measured on a Bruker 400 MHz Avance III NMR spectrometer operating at a magnetic field of 9.4 T equipped with liquid state NMR probe and Z-gradient coil with a maximum gradient strength of 50 G/cm. The diffusion coefficients were measured by using spin echo or stimulated echo pulse sequence at 25 ^{o}C, 40 ^{o}C and 80 ^{o}C. The signal was accumulated for minimum 16 scans with optimized recycling delay of 2 s. For the ^{7}Li measurements, the gradient strength was varied over the range of 0-900 G/cm for 16 increments. The diffusion time (Δ) and the diffusion pulse

length (δ) were in the range of 0.05-1.2 s and 0.004-0.009 s, respectively, with the longer times used for ^{1}H diffusion. The attenuated signal intensity is plotted against the gradient strength and the diffusion coefficients were calculated by Stejkal-Tanner equation.

$$\frac{I}{I_0} = \exp\left[-(G\gamma\delta)^2\left(\Delta - \frac{\delta}{3}\right)D\right] \quad (1)$$

Where γ is the gyromagnetic ratio, G is the gradient strength and D is the diffusion coefficient.

As shown in **Figure 3.S5**, ^{1}H NMR spectra shows distinct ^{1}H features corresponding to THF and carborane. ^{1}H peaks resonating at 1.9 and 3.8 ppm could be assigned to the THF, and those at 1, 1.6, 2 and 3.2 ppm could be assigned to the butyl chain attached to the carborane. A broad peak centered at 0.8 ppm is the result of protons directly bonded to B atoms. ^{7}Li NMR spectra shows a single sharp peak that could be assigned to the Li^{+} ions. ^{11}B NMR spectra show three ^{11}B peaks revealing the existence of multiple B environments in the carborane unit. The ^{1}H signal intensities of peak 1 (3.8 ppm) and 3 (3.2 ppm) were integrated to calculate the diffusion coefficients of THF and carborane, respectively. The accuracy of diffusion plots is shown in Figure 3.S6, where the signal intensity is plotted against the gradient strength in order to calculate D_{THF}, $D_{carborane}$, D_{Li+}.

Integrated ketjen black (IKB) was used as the sulfur host. The synthesis method was adopted from Lv et al.[11] Briefly, ketjen black was mixed with citric acid in an aqueous suspension, and then ethylene glycol was added. The mixture was heated at 130°C for 6 hours with stirring. The obtained solid product was then carbonized under argon at 400°C

for 6 hours and 800°C for another 10 hours to produce IKB. The sulfur-carbon (S-C) composite was prepared by mixing 80 wt.% sulfur (Sigma Aldrich) with 20 wt.% IKB, followed by a heating process at 155°C for 10 hours. The cathode slurry was prepared by mixing 80 wt.% S-C composite, 10 wt.% binder, 5 wt.% multi-walled carbon nanotubes (Sigma Aldrich), and 5 wt.% carbon nanofibers (Carbon Nanotube Plus) in N-Methyl-2-pyrrolidone. The slurry was coated onto Al foil and the electrode was dried in a vacuum oven at 50°C for 12 hours. The sulfur loading was approximately 6 mg cm^{-2}.

Coin cells (2032 type) were assembled in an argon-filled glovebox with Celgard® 2400 separator. Commercial 750-um Li foil (Alfa Aesar) was used as the anode in Li-S coin cells. The Li metal for Li symmetrical cell and electrolyte soaking experiment was prepared using a method reported by our group. [12] A clean Li nugget was first obtained by cutting the surface of a Li rod (99.8% Strem Chemicals). The obtained clean nugget was then sandwiched between two pieces of laminated aluminum film (MTI Corporation) and compressed with a mechanical roller to yield the Li foil with thickness of 50 μm. A layer of the obtained 50-μm Li foil was then compressed onto one side of a piece of Cu foil (Alfa Aesar). Cu was treated in atmosphere of 5% Hydrogen and 95% Argon at 300°C for 10 hours in glovebox to remove oxide layer before compressed with Li foil.

For Li||Li symmetric cells, two 50-μm Li foil on Cu electrodes with 1.27 cm diameter were used. 15ul CIL electrolyte was applied on both side of separator. For low E/S ratio Li-S cells, the cathodes were soaked in the electrolyte overnight before cell assembly. The amount of adsorbed electrolyte was measured as the difference of the mass before and after electrolyte soaking, and different E/S ratios were achieved by adding additional

electrolyte to the cells accordingly. The actual E/S ratios (i.e., amount of electrolyte) in the cells were determined through subtraction of the mass of all dry components in a cell from the total mass of the assembled cell.

3.3.2 Materials and electrochemical Characterizations:

A scanning electron microscope (SEM, Nova Nano S450, 20 kV) was used to characterize the structure and thickness of the lithium electrode in the symmetrical battery. Place the sample in a glove box filled with argon and wash it thoroughly with hexane to remove residual electrolyte. After washing, the samples were dried for 24 hours at room temperature in glove box before SEM. The sample was placed in a stainless steel tube sealed with a KF flange when transferring. A glove bag with argon purging gas was used to load the sample into the SEM. Li-S coin cells were cycled between 1-2.8V versus Li/Li^+ at C/100 at 50 °C using an Arbin battery test station. Cyclic voltammetry was operated in using a Gamry Interface 1000.

3.4 Result and discussion

3.4.1 Physicochemical Property of CIL

Anions functionalized with a hydrocarbon moiety greater than n = 4 were found to yield room temperature liquids that do not crystallize at sub-zero temperatures. Multiple structural factors were found to be paramount to achieving a lithium salt of the carborane anion that persists in the liquid phase including the 1) alkyl moiety length, 2) coordinated solvent, and 3) the coordination environment around Li^+. The varying length of the hydrocarbon moiety was found to impart a variety physical property to the material. Most

importantly, the unfunctionalized anion was observed to be solid at room temperature. Only with the addition of an alkyl chain (n >= 2) did the material begin to display persistent liquid properties at ambient temperatures. At sub-zero temperatures, anions where n < 4 displayed crystallizations over time at -30°C, whereas anions with longer alkyl moieties crystallized spontaneously at ambient temperatures. The ideal formulation was determined to be $[H_9C_4CB_9H_9]^-$ as it was found to be the lowest molecular weight anion that did not crystallize at sub-zero temperatures over time nor crystallize spontaneously as was observed with anions containing a longer alkyl moiety.

Solvent choice was found to be extremely important to achieving liquid materials. Cyclic ethers -Tetrahydrofuran(THF) were the only solvents found to yield liquids at or below ambient temperatures.

Most intriguingly, the coordination environment around the Li^+ was found to be a significant contributor to the low melting point of the materials. Only Li^+ salts that were not coordinatively saturated by solvent molecules and, consequently, able to interact directly with the B-H vertices of the anion, displayed liquid properties at room temperature. Which makes CIL structurally similar to SIL. However, CIL is slightly different with SIL. The solvated analogues of CIL could be isolated as white powders, while the abovementioned SIL keeps liquid.

The resulting CIL of interest to this work is a carborane anion functionalized with a C_4 alkyl moiety paired with a complex cation $[Li(THF_{1.0})]^+$ rendering it a single component ionic liquid electrolyte. This material persists in the liquid state below -50°C and, despite remaining in this environment for extended periods of time, does not display any

observable crystallization. Considering the multi-nuclear NMR data (**Figure 3.S2**) we propose $[H_9C_4CB_9H_9]^-[Li(THF)_{1.0}]^+$ in **Figure3.1b** as the most likely structure for our material of interest.

The above described CILs have negligible vapor pressure, are less viscous relative to currently known IL and SIL electrolytes alike, and do not combust under direct exposure to flame. Furthermore, these materials have demonstrated chemical stability in the presence of lithium metal and under standard electrochemical cycling conditions.

Table 3.1 Physicochemical properties of solvated ionic liquids

	Conductivity S cm^{-1}	T_{Li^+}	Melting point	Density g mL^{-1}	Lithium Compatibility	Flammability
CIL	3.5×10-4	0.52*	-56°C**	0.923	yes	no
$[Li(ACN)_2]^+TFSI^-$ [7]	9.8×10-4	0.4-0.6	N/A	1.515	no	reduced
$[Li(ACN)_2]^+FSI^-$ [7]	9.7×10-3	0.4-0.6	N/A	1.339	no	reduced
$[Li(G2)_{0.8}]^+TFSI^-$ [10]	2.7×10-4	0.55	N/A	1.53	yes	reduced

* Transference number is determined by NMR with detail shown in .
Differential Scanning Calorimetry data is shown in **Figure 3.S3

3.4.2 Chemical and electrochemical stability with Li metal

For some years now, our collaborative efforts have been aimed at developing high performance ion conducting materials that employ the thermal, chemical, electrochemical, and weakly coordinating properties of carborane anions.[13-15] Thus, we were intrigued at the prospect of implementing a carboranyl ionic liquid material in electrochemical systems based on lithium. We reasoned the inherent reductive stability of the material along with its inflammability should permit safe operation of electrochemical cells that utilize lithium metal as an anode material.

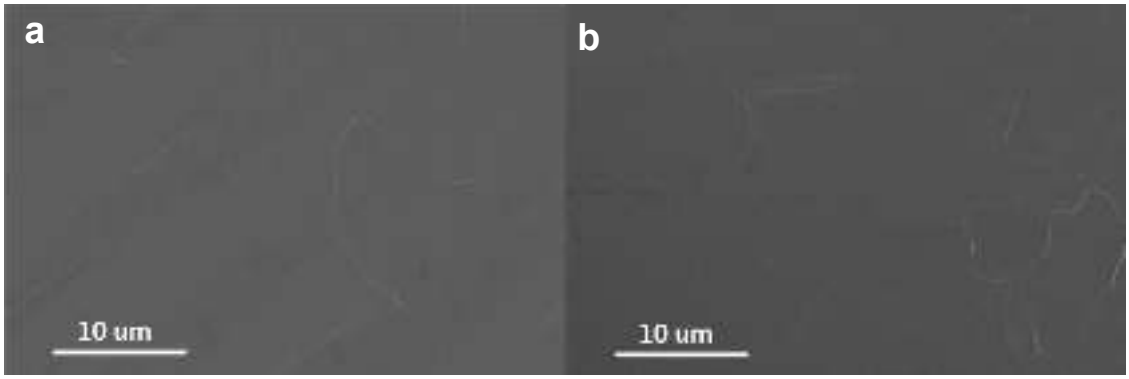

Figure 3.2 (a) SEM image of pristine Li (b) SEM image of Li after soaking in CIL for one month.

Li, due to its high reactive nature, will form a pristine surface film including Li_2CO_3, LiOH and Li_2O as shown in **Figure 3.2a**. Li is inevitable to react will all polar-aprotic solvent and salt anion to form a solid-electrolyte interphase (SEI). The SEI layer is electronically insulating but ionically conducting. When pristine Li soaked into electrolyte, there will be a chemical redox reaction immediately between Li and electrolyte. [16] Given the inherent reductive stability of $[H_9C_4CB_9H_9]^-[Li(THF)_{1.0}]^+$and our prior work with reductively stable anions,[14, 17, 18] we undertook surface characterization studies of the anode in an effort to observe resulting SEI film compositions. Intriguingly, as a testament to the reductively stable components of $[H_9C_4CB_9H_9]^-[Li(THF)_{1.0}]^+$, no chemical decomposition was observed after direct exposure to a lithium metal anode for over a month. evident shown in **Figure 3.2b** with no corrosion on Li surface.

The CIL are termed closo-clusters as they have closed shell electronic structures and complete polyhedral shapes. The molecular orbitals of CIL is composed of both strongly bonding purely σ- and π- type overlaps. Anions are inherently weakly coordinating as the

charge of the cluster is delocalized throughout the three dimensionally aromatic core. Resulting the potential of lowest unoccupied molecular orbital (E_{LUMO}) is larger than the electrochemical potential of Li anode. [14] Tetrahydrofuran (THF) as a cyclic ether also show a good reduction stability.[14, 18] Besides, there is no free THF can be found in CIL, all the THF molecules are strongly coordinated to Li ion to form a solvate, which promote the stability of CIL.

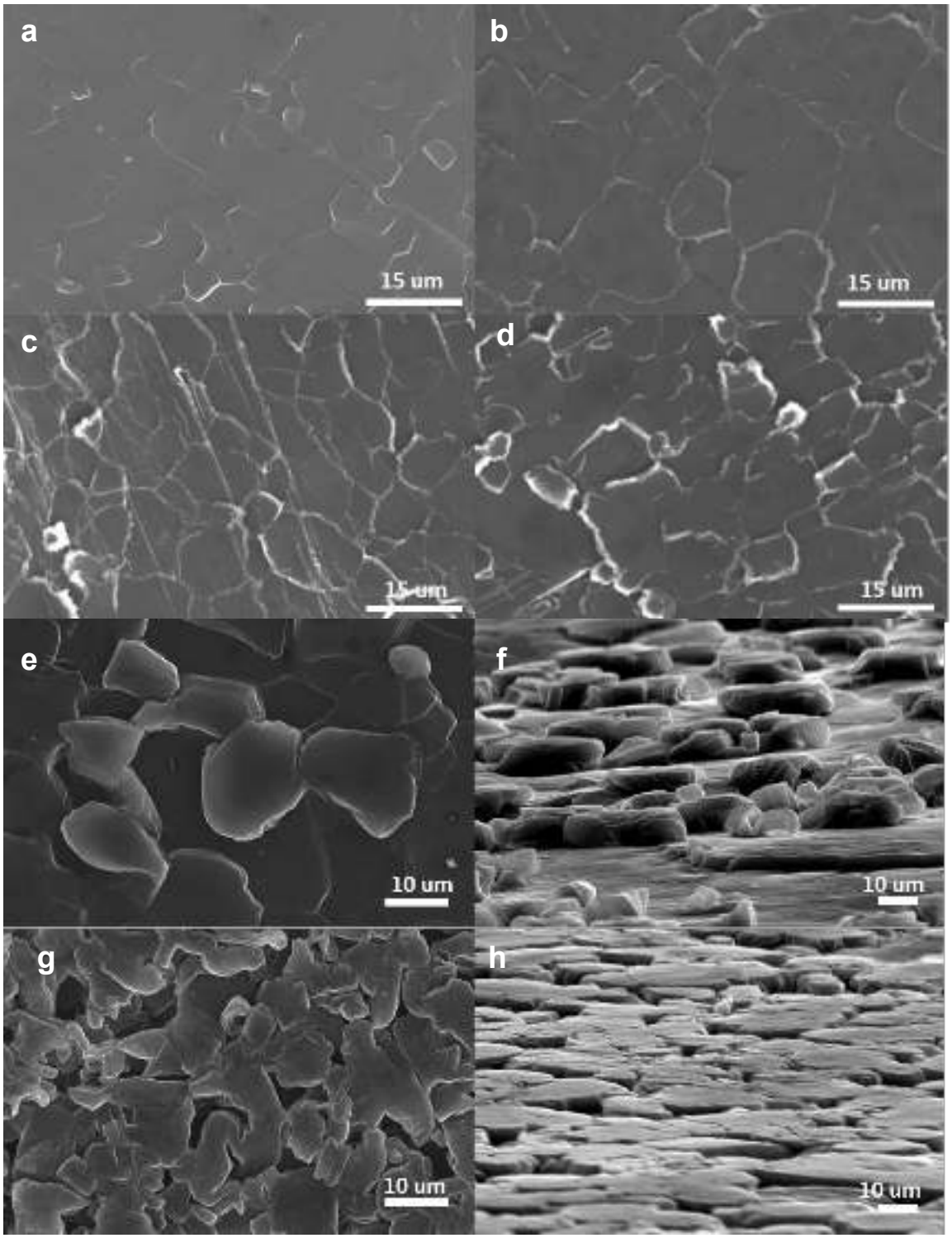

Figure 3.3 SEM image of Li deposition onto Li with current of 0.5mA cm-2 for (a)2 mins (b)4 mins (c) 8 mins (d)12 mins (e)1.5 hours (g)3 hours. SEM tilt image of Li deposition onto Li with current of 0.5mA cm-2 for (f)1.5 hours (h)3 hours**.**

Different from traditional carbonate-based electrolytes or ether-based electrolytes, which will produce Li ion diffusion impediment SEI. The nucleation of Li in CIL system is preferable for obtaining a dendrite free morphology as shown in **Figure 3.3.** A surface nucleating and diffusion model can be used to explain the planar growth morphology of Li in CIL.[19] Refer to the Li deposition kinetic, the solvated Li ion in bulk electrolyte need to break up the solvation sheath and diffuse through SEI film before plating and migrating on SEI/Li interphase. Therefore, SEI can influence Li deposition. Li ion diffusion in SEI will be a rate-determining step. The higher migration energy and lower surface energy of Li ion on SEI rather than on Li means that, the surface diffusion of Li ion on SEI is more sluggish than on Li metal,[20] which further indicates the Li ion exhibits a tendency to deposit toward the nearby areas rather than on a lumped site to form dendrites. [21] The CIL electrolyte gives us a chance to reveal how Li nucleation and growth without SEI. Recent research reveals that the highly concentrated viscoelastic electrolyte such as CIL, can slow localized growth of dendritic structure by interfacial mechanical stresses. It can be regarded as an intermediate state between the liquid and solid-state electrolyte.[22]

The solvated Li ion shed solvent molecules and migrate with short-range solid-state transport through the native oxide layer. Then Li deposits along the grain boundaries of Li surface with a layered pattern as shown in Figure 3.3a. The white line in the figure is the grain boundary of Li. With more Li deposit onto Li, each grain may extend and

squeeze each other and lead to wrinkle and rough surface with tip occurring shown as the white particles in Figure 3.3b, c, and d, which will lead to ununiform local current density and further lead to ununiform Li deposition as shown in Figure 3.3 e. The long-time deposition morphology in Figure 3.3 g show lithium with kinks. However, Li still grows in a flat pattern which is different with Li deposition morphology in conventional electrolyte. Owing to the high stability between CIL and Li as well as the dense dendrite free Li growth, Li metal cycle life is improved in CIL system evident by Li||Li symmetric cell cycling data in **Figure 3.4**. Li|| Li symmetric cell can cycle steady at 0.1mA cm^{-2} with capacity 1mAh cm^{-2} for more than 1700 hours. More than 500 stable cycles can be achieved in Li||Li symmetric cell with 0.5 mA cm^{-2} **(Figure 3.S4).** However, due to the intrinsic high viscosity and low conductivity, the overpotential for symmetric cell is large than usual.

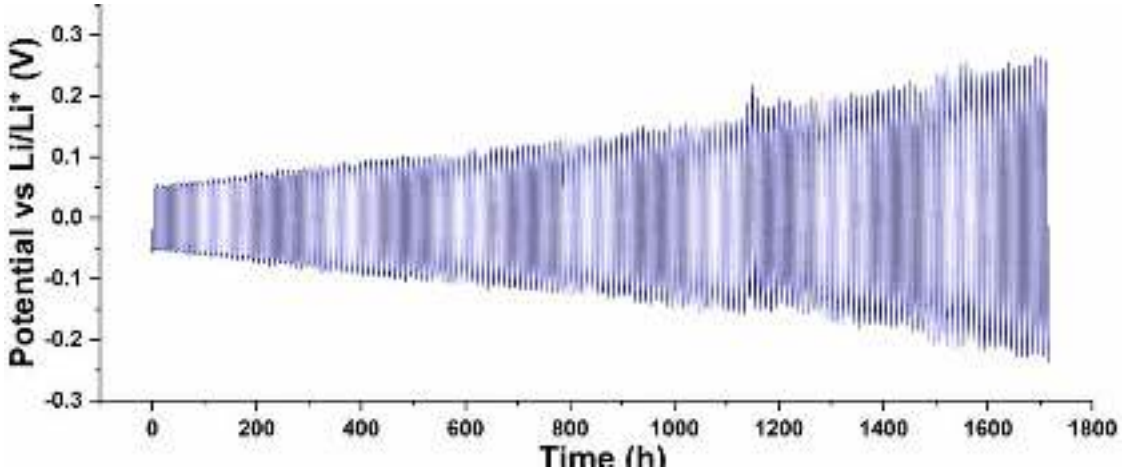

Figure 3.4 Cycling curve of a Li||Li symmetric cell in CIL electrolyte 0.1mA cm^{-2} with capacity 1mAh cm^{-2} .

3.4.3 CIL applied in Li-S batteries

Due to the good chemical stability and proper electrochemical stable window of CIL, it can be applied in Li-S batteries. The widespread deployment of Li||S batteries remains hindered by their low specific energy and short cycle life. CIL might be a good candidate to solve both issues by decoupling the electrolyte volume with sulfur reduction pathway. The solubility of representative polysulfide Li_2S_8 in CIL is less than 0.01M comparing to 0.5M in commonly used DOL/DME binary solvent. [23] The low solubility enables the Li-S operating via sparingly solvating pathway. [10] Comparison of the discharge charge curve between the widely used DOL/DME electrolyte and CIL with different E/S ratio in **Figure 3.5 a and b** can illustrate that CIL decouples the electrolyte volume and sulfur reduction pathway. For the conventional DOL/DME electrolyte, polysulfide species need to dissolve into electrolyte for further reduction. Electrolyte is not only an ion transport mediate, but also the place where polysulfide dissolved. When the E/S ratio is decreased, the overpotential increases due to the higher concentration of polysulfides in the electrolyte as discussed in Chapter 2 in details. The CIL electrolytes provide a quasi-solid state reaction which in the middle of conventional solid-liquid-solid pathway of DOL/DME electrolyte and complete solid-state pathway from solid state electrolyte or sub-nano confined sulfur cathode.[24] Owing to the low but non-zero solubility, the presence of small amount of dissolved high order polysulfide enable self-disproportion reaction to be sulfur and lower order polysulfide at interface. This will lead to a short residence time of polysulfide in solvated state. That is also the reason for only one plateau in the discharge profile of Li-S cell in CIL electrolyte shown in **Figure 3.5b**. All the three E/S ratios show the same discharge-charge profile regardless electrolyte

amount. In the quasi solid state reaction, as long as electrolyte is enough to wet electrodes particle surface, the reaction can proceed normally. More electrolyte amount does not facilitate cell performance.

Therefore, CIL can enable high specific energy by operating Li-S under lean electrolyte condition. **Figure 3.5c** shows discharge-charge curve of Li-S coin cell with different areal sulfur loading operating in 50°C with E/S = 3 and current density of C/100 (16 mA g^{-1}). 1250 mAh g^{-1}specific capacity in first cycle and 1330 mAh g^{-1} specific capacity in second cycle is achieved with 8mg cm^{-2} sulfur areal loading, which indicates that 413 Wh kg^{-1} can be achieved in a 1.5Ah pouch cell based on our calculation. However, more characterizations are need to understand the reaction pathway in detail.

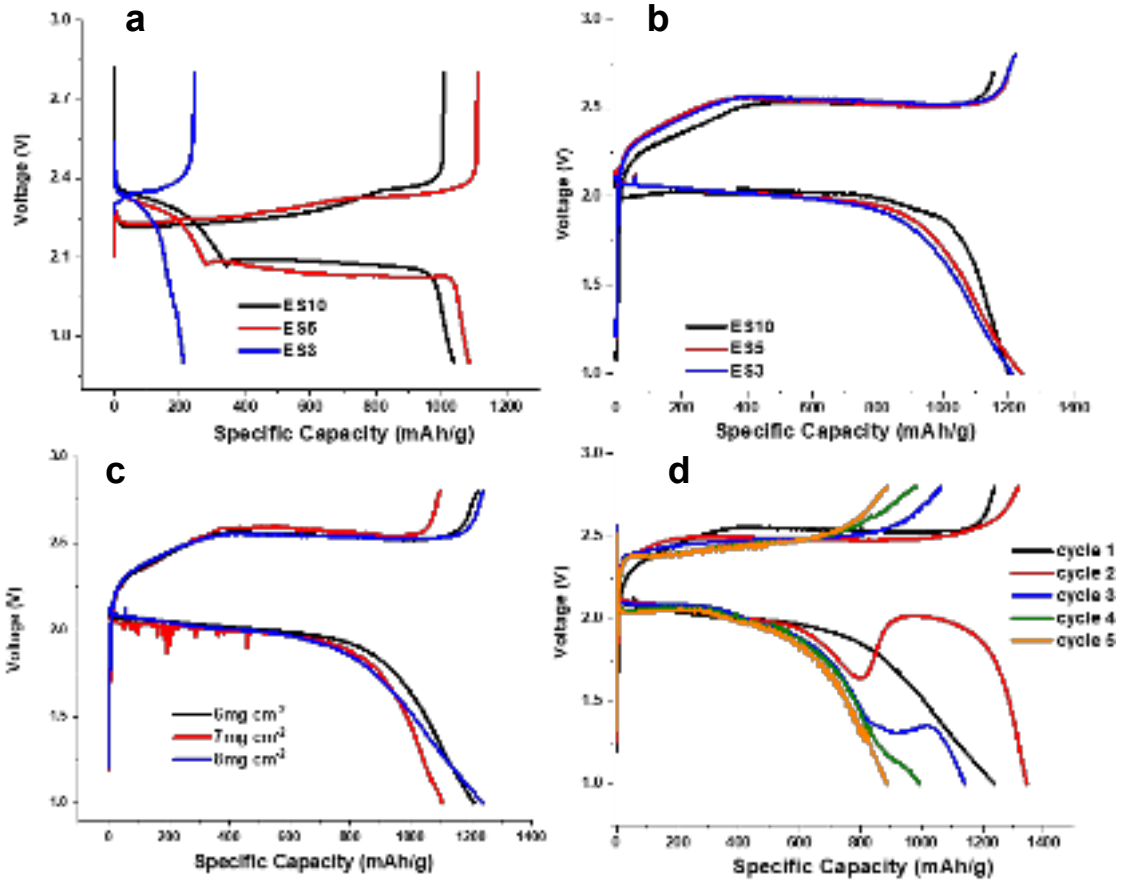

Figure 3.5 Discharge charge profiles of Li-S batteries in (a)1M LiTFSI in DOLDME electrolyte with different representative E/S 3 5 and 10.Cycling between 1.7-2.8V vs Li/Li^+ in room temperature at C/100(b) CIL electrolyte with different representative E/S ratio of 3, 5, and 10. Cycling between 1-2.8V vs Li/Li^+ in 50 °C at C/100 (c) CIL electrolyte in E/S 3 with different sulfur areal loading. (d) cycle data of CIL electrolyte in E/S of 3 with 8 mg cm^{-2} sulfur areal loading.

3.5 Conclusion and Perspective

In this chapter, a class of novel carboranyl ionic liquid was first synthesized and reported. Such CIL is structurally similar but not same to the new emerging solvated ionic liquid. It shows negligible vapor pressure, wide liquid state range and do not combust under direct exposure to flame. Beside these advantages, CIL is also proven to

be chemical and electrochemically stable towards Li metal and sulfur. A two-dimensional Li growth with long cycle life is enabled by CIL. High specific energy Li-S cells is also demonstrated with CIL via a sparingly dissolving quasi solid state reaction pathway.

However, in-depth understanding is needed for Li deposition and Li-S reaction pathway. More effort is needed including computational modeling can explain the dip in Li-S discharge profile. Due to the high viscosity, Li-S batteries so far have to be operated in 50 °C. Proper dilution of electrolyte which can decrease CIL viscosity, increase ionic conductivity is eagerly needed. Due to the exist of THF, CIL will be oxidized above 3.7 V. Other solvent or proper dilution which can widen the electrochemical window will enable CIL applied in Li-ion batteries.

3.6 Supporting information

Figure 3.S1 CIL after purification procedure

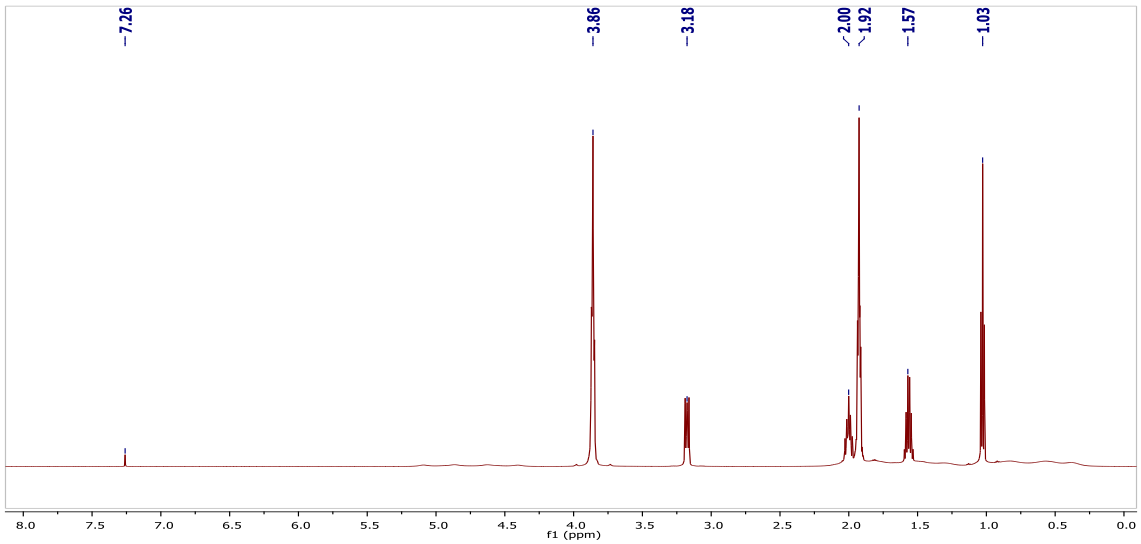
7.26
3.86
3.18
2.00
1.92
1.57
1.03
f1 (ppm)

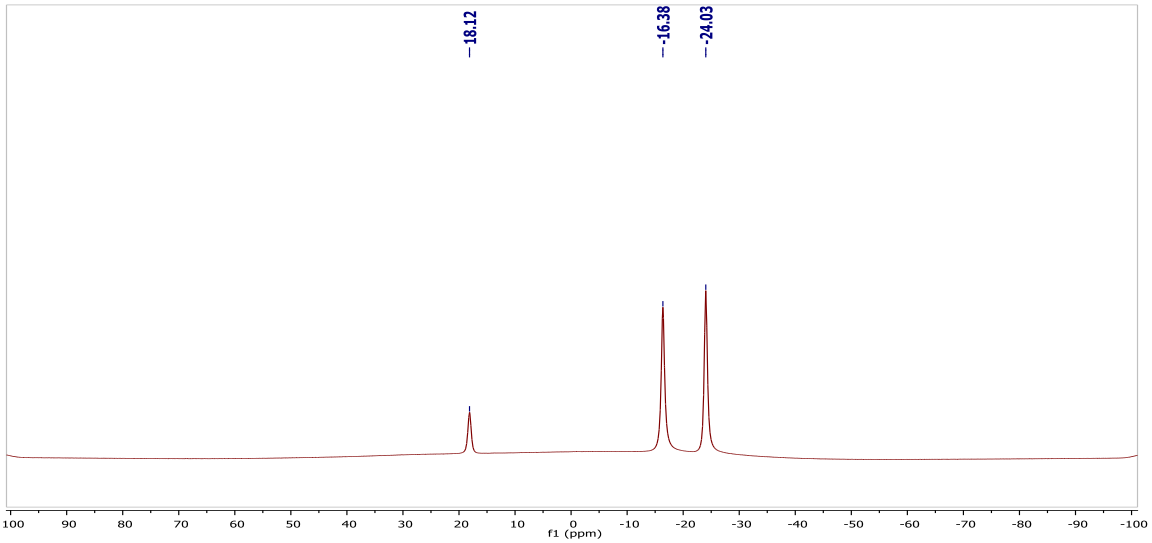
18.12
-16.38
-24.03
f1 (ppm)

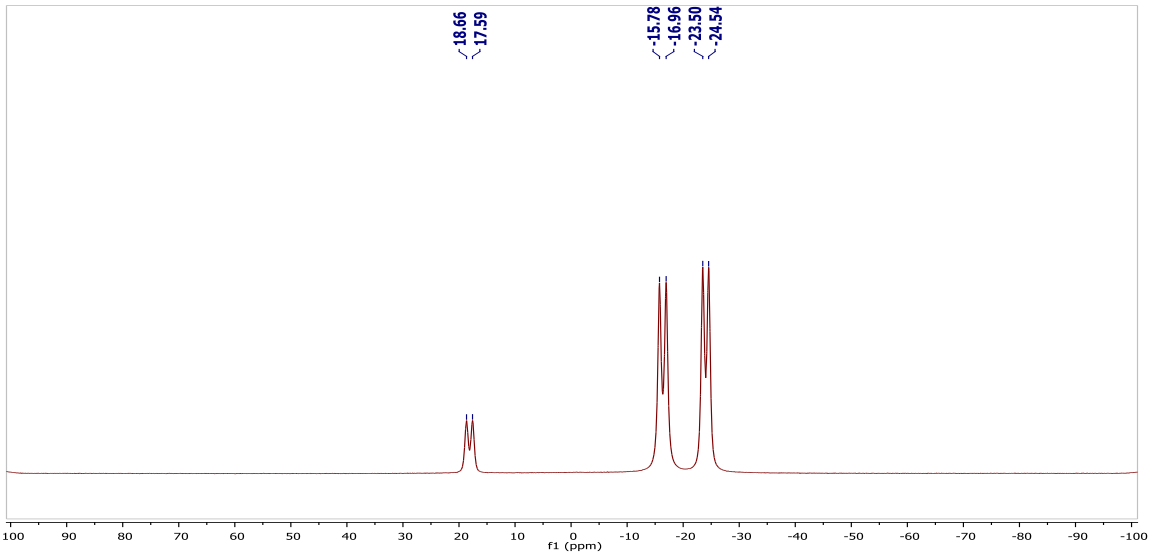
18.66
17.59
-15.78
-16.96
-23.50
-24.54
f1 (ppm)

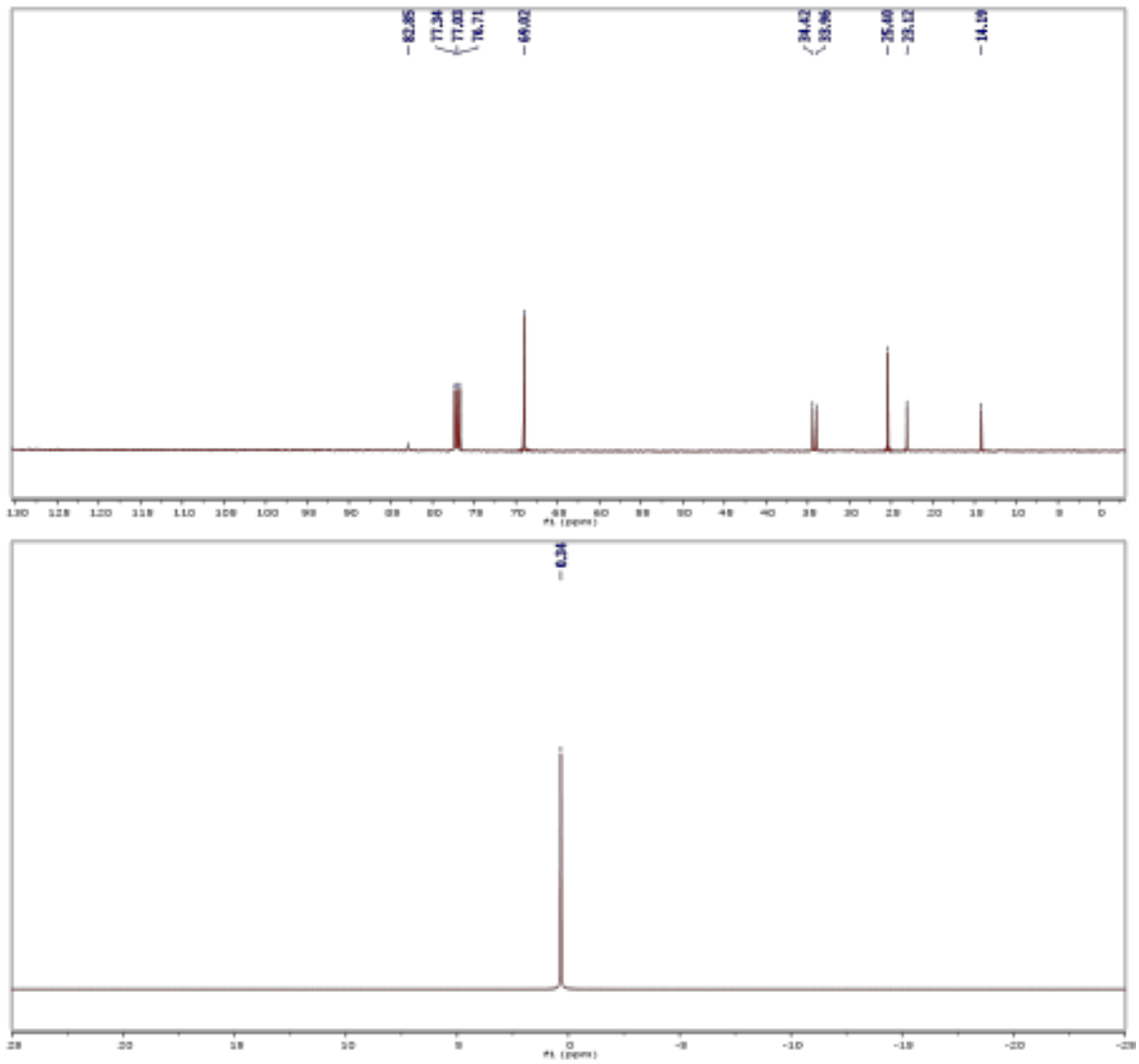

Figure 3.S2 1D ^{1}H, ^{11}B {H},^{11}B,^{13}C and ^{7}Li NMR spectra of Li-THF-carborane

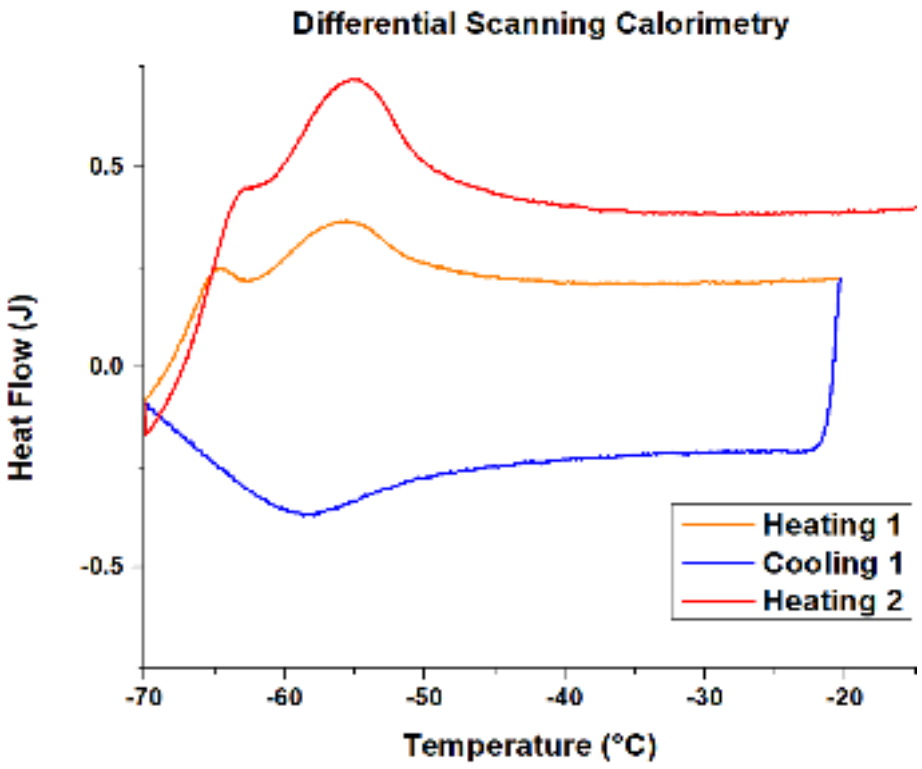

Figure 3.S3 Differential Scanning Calorimetry of CIL.

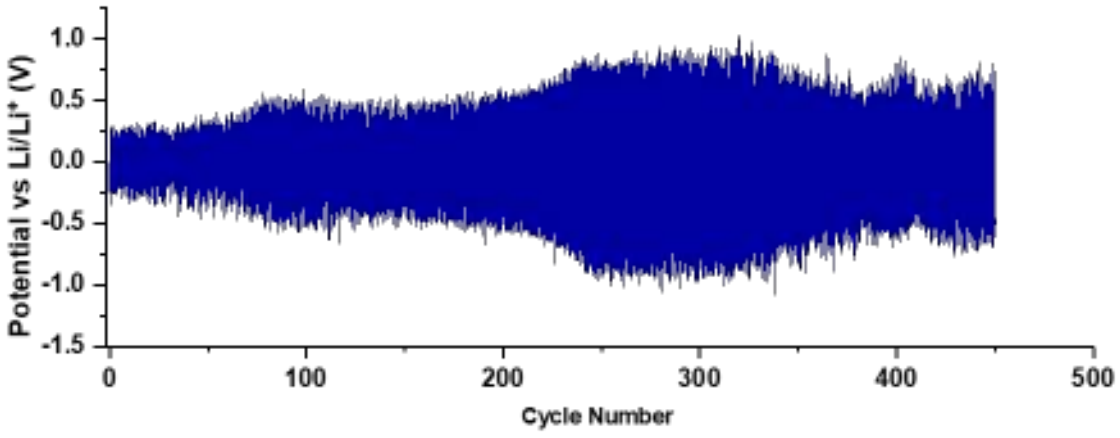

Figure 3.S4 Cycling curve of a Li||Li symmetric cell in CIL electrolyte 0.5mA cm^{-2} with capacity 1mAh cm^{-2}

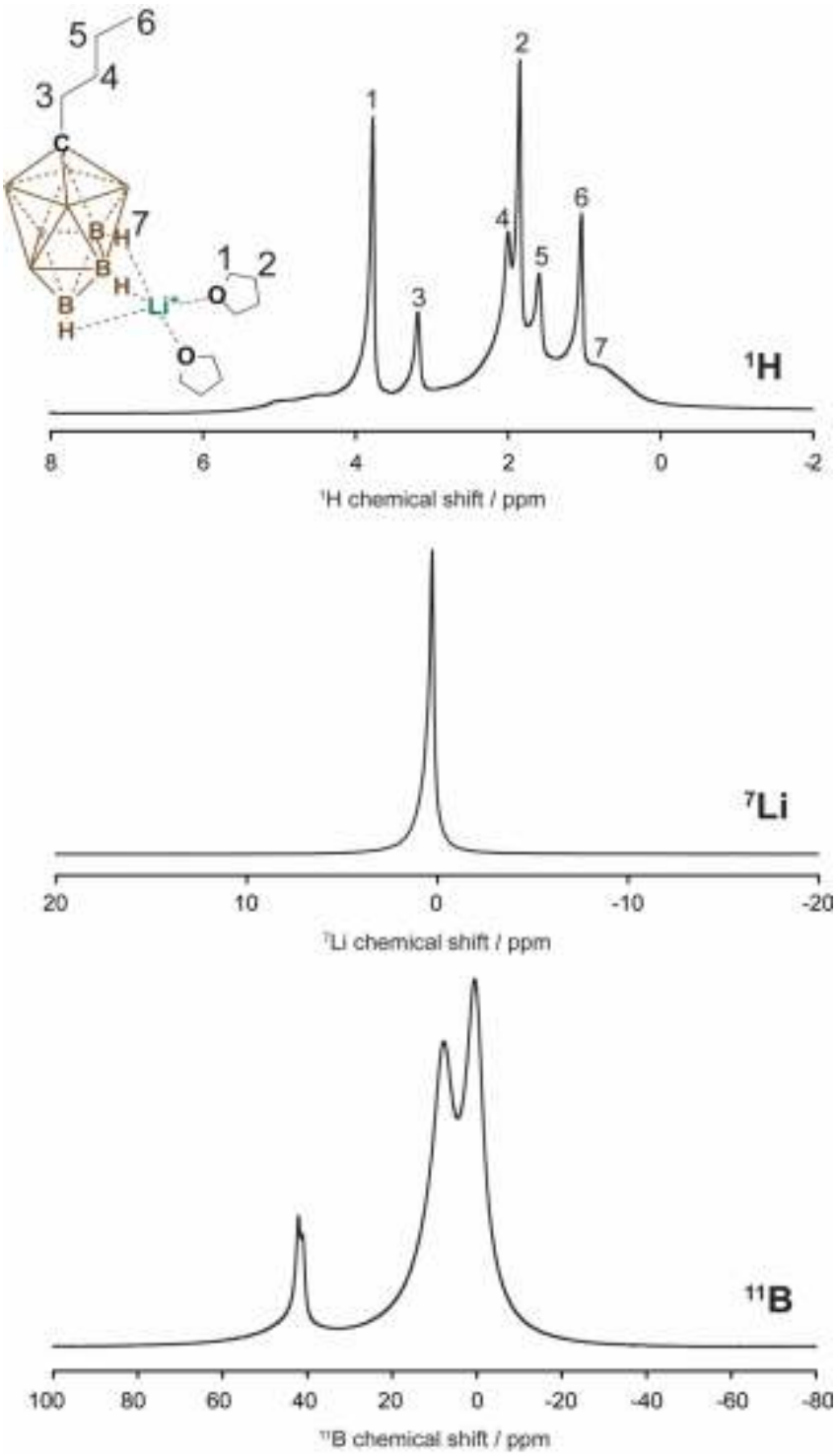

Figure 3.S5 . 1D ^{1}H, ^{7}Li and ^{11}B NMR spectra of Li-THF-carborane collected on Bruker 400 MHz NMR spectrometer at RT

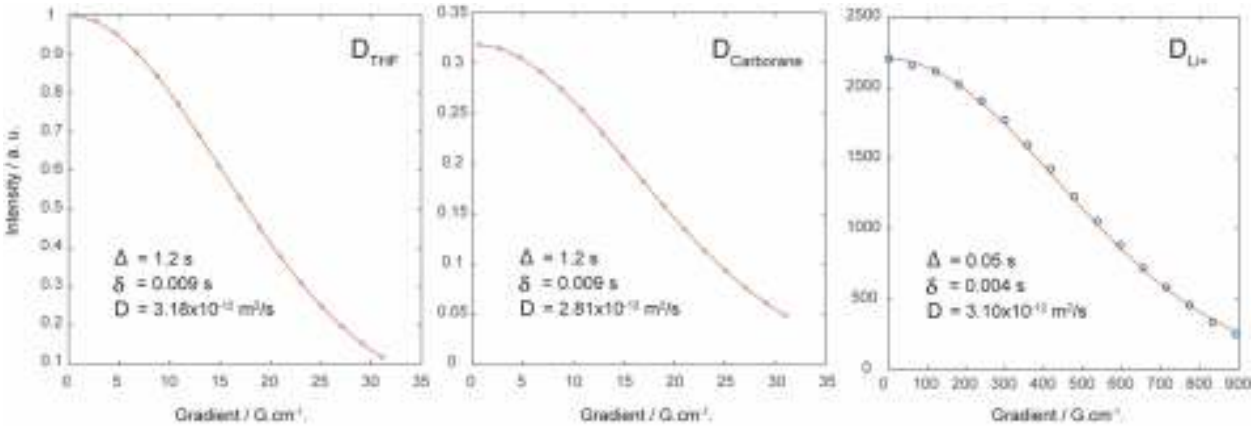

Figure 3.S6. The intensity vs gradient plots measured at 25 ^{o}C calculating the D_{THF}, $D_{carborane}$, D_{Li+}.

Reference

1. Park, J.-W.; Ueno, K.; Tachikawa, N.; Dokko, K.; Watanabe, M., Ionic Liquid Electrolytes for Lithium–Sulfur Batteries. *The Journal of Physical Chemistry C* **2013,** *117* (40), 20531-20541.

2. Xiong, S.; Xie, K.; Blomberg, E.; Jacobsson, P.; Matic, A., Analysis of the solid electrolyte interphase formed with an ionic liquid electrolyte for lithium-sulfur batteries. *Journal of Power Sources* **2014,** *252*, 150-155.

3. Wu, F.; Zhu, Q.; Chen, R.; Chen, N.; Chen, Y.; Ye, Y.; Qian, J.; Li, L., Ionic liquid-based electrolyte with binary lithium salts for high performance lithium–sulfur batteries. *Journal of Power Sources* **2015,** *296*, 10-17.

4. Nair, J. R.; Colò, F.; Kazzazi, A.; Moreno, M.; Bresser, D.; Lin, R.; Bella, F.; Meligrana, G.; Fantini, S.; Simonetti, E.; Appetecchi, G. B.; Passerini, S.; Gerbaldi, C., Room temperature ionic liquid (RTIL)-based electrolyte cocktails for safe, high working potential Li-based polymer batteries. *Journal of Power Sources* **2019,** *412*, 398-407.

5. Lu, H.; Zhu, Y.; Zheng, B.; Du, H.; Zheng, X.; Liu, C.; Yuan, Y.; Fang, J.; Zhang, K., A hybrid ionic liquid-based electrolyte for high-performance lithium–sulfur batteries. *New Journal of Chemistry* **2020,** *44* (2), 361-368.

6. Tamura, T.; Yoshida, K.; Hachida, T.; Tsuchiya, M.; Nakamura, M.; Kazue, Y.; Tachikawa, N.; Dokko, K.; Watanabe, M., Physicochemical Properties of Glyme–Li Salt Complexes as a New Family of Room-temperature Ionic Liquids. *Chemistry Letters* **2010,** *39* (7), 753-755.

7. Yamada, Y.; Furukawa, K.; Sodeyama, K.; Kikuchi, K.; Yaegashi, M.; Tateyama, Y.; Yamada, A., Unusual stability of acetonitrile-based superconcentrated electrolytes for fast-charging lithium-ion batteries. *J Am Chem Soc* **2014,** *136* (13), 5039-46.

8. Dokko, K.; Tachikawa, N.; Yamauchi, K.; Tsuchiya, M.; Yamazaki, A.; Takashima, E.; Park, J.-W.; Ueno, K.; Seki, S.; Serizawa, N.; Watanabe, M., Solvate Ionic Liquid Electrolyte for Li–S Batteries. *Journal of The Electrochemical Society* **2013,** *160* (8), A1304-A1310.

9. Lee, C. W.; Pang, Q.; Ha, S.; Cheng, L.; Han, S. D.; Zavadil, K. R.; Gallagher, K. G.; Nazar, L. F.; Balasubramanian, M., Directing the Lithium-Sulfur Reaction Pathway via Sparingly Solvating Electrolytes for High Energy Density Batteries. *ACS Cent Sci* **2017,** *3* (6), 605-613.

10. Pang, Q.; Shyamsunder, A.; Narayanan, B.; Kwok, C. Y.; Curtiss, L. A.; Nazar, L. F., Tuning the electrolyte network structure to invoke quasi-solid state sulfur conversion and suppress lithium dendrite formation in Li–S batteries. *Nature Energy* **2018,** *3* (9), 783-791.

11. Lv, D.; Zheng, J.; Li, Q.; Xie, X.; Ferrara, S.; Nie, Z.; Mehdi, L. B.; Browning, N. D.; Zhang, J.-G.; Graff, G. L.; Liu, J.; Xiao, J., High Energy Density Lithium-Sulfur Batteries: Challenges of Thick Sulfur Cathodes. *Advanced Energy Materials* **2015,** *5* (16).

12. Zhang, J.; Shi, J.; Wen, X.; Zhao, Y.; Guo, J., Properties of Thin Lithium Metal Electrodes in Carbonate Electrolytes with Realistic Parameters. *ACS Appl Mater Interfaces* **2020,** *12* (29), 32863-32870.

13. Laheäär, A.; Jänes, A.; Lust, E., Cesium carborane as an unconventional non-aqueous electrolyte salt for electrochemical capacitors. *Electrochimica Acta* **2014,** *125*, 482-487.

14. Fisher, S. P.; Tomich, A. W.; Lovera, S. O.; Kleinsasser, J. F.; Guo, J.; Asay, M. J.; Nelson, H. M.; Lavallo, V., Nonclassical Applications of closo-Carborane Anions: From Main Group Chemistry and Catalysis to Energy Storage. *Chem Rev* **2019,** *119* (14), 8262-8290.

15. Tutusaus, O.; Mohtadi, R.; Arthur, T. S.; Mizuno, F.; Nelson, E. G.; Sevryugina, Y. V., An Efficient Halogen-Free Electrolyte for Use in Rechargeable Magnesium Batteries. *Angew Chem Int Ed Engl* **2015,** *54* (27), 7900-4.

16. Xu, K., Nonaqueous Liquid Electrolytes for Lithium-Based Rechargeable Batteries. *Chem Rev* **2004,** *104*, 4303-4417.

17. REED, C. A., H+,CH3+, and R3Si+ Carborane Reagents: When Triflates Fail. *ACCOUNTS OF CHEMICAL RESEARCH* **2010,** *43* (121-128).

18. Douvris, C.; Michl, J., Update 1 of: Chemistry of the carba-closo-dodecaborate(-) anion, CB11H12(-). *Chem Rev* **2013,** *113* (10), PR179-233.

19. Cheng, X. B.; Zhang, R.; Zhao, C. Z.; Zhang, Q., Toward Safe Lithium Metal Anode in Rechargeable Batteries: A Review. *Chem Rev* **2017,** *117* (15), 10403-10473.

20. Yalcin Ozhabes, D. G., and T. A. Arias, Stability and surface diffusion at lithium-electrolyte interphases with connections to dendrite suppression. *arXiv preprint* **2015,** *arXiv:1504.05799*.

21. Ling, C.; Banerjee, D.; Matsui, M., Study of the electrochemical deposition of Mg in the atomic level: Why it prefers the non-dendritic morphology. *Electrochimica Acta* **2012,** *76*, 270-274.

22. Zheng, J.; Kim, M. S.; Tu, Z.; Choudhury, S.; Tang, T.; Archer, L. A., Regulating electrodeposition morphology of lithium: towards commercially relevant secondary Li metal batteries. *Chem Soc Rev* **2020,** *49* (9), 2701-2750.

23. Chen, J.; Han, K. S.; Henderson, W. A.; Lau, K. C.; Vijayakumar, M.; Dzwiniel, T.; Pan, H.; Curtiss, L. A.; Xiao, J.; Mueller, K. T.; Shao, Y.; Liu, J., Restricting the Solubility of Polysulfides in Li-S Batteries Via Electrolyte Salt Selection. *Advanced Energy Materials* **2016,** *6* (11).

24. Fu, C.; Oviedo, M. B.; Zhu, Y.; von Wald Cresce, A.; Xu, K.; Li, G.; Itkis, M. E.; Haddon, R. C.; Chi, M.; Han, Y.; Wong, B. M.; Guo, J., Confined Lithium-Sulfur Reactions in Narrow-Diameter Carbon Nanotubes Reveal Enhanced Electrochemical Reactivity. *ACS Nano* **2018,** *12* (10), 9775-9784.

25. Ringstrand, B.; Bateman, D.; Shoemaker, R. K.; Janoušek, Z., Improved synthesis of [closo-1-CB9H10]– anion and new C-substituted derivatives. *Collection of Czechoslovak Chemical Communications* **2009,** *74* (3), 419-431.

26. Brellochs, B.; Bačkovský, J.; Štíbr, B.; Jelínek, T.; Holub, J.; Bakardjiev, M.; Hnyk, D.; Hofmann, M.; Císarová, I.; Wrackmeyer, B., New Ways to a Series of Parent Representatives of the Eight-, Nine-, and Ten-Vertex Monocarbaborane Family. *European Journal of Inorganic Chemistry* **2004**.

Chapter 4: Sulfur oxidation reaction in Mg-S batteries

4.1 Abstract:

Multivalent nature, high abundance, non-dendrite growth, moderate specific capacity and high volumetric capacity make Mg a promising alternative to Li as the anode material in rechargeable batteries. Sulfur has been proven a good cathode material in Li-S batteries, thus the Mg-S battery is no doubt a promising candidate for next generation rechargeable batteries. However, due to the requirement for non-nucleophilic electrolytes, suitable electrolytes for Mg-S battery system are limited. In our study, two chloride free Mg electrolytes with weakly coordinating anions, magnesium monocarbonrane and magnesium tetrakis(hexafluoroisopropyloxy) borate, were investigated for the electrochemical behavior in Mg-S batteries. We revealed a different mechnism of the voltage plateau in charge voltage profile which usually is interpreted as the polysulfide shuttle effect.

4.2 Introduction:

Mg metal has great potential to become a viable anode material because of its high volumetric capacity. The commercial LIB corresponds to 837 mAh cm^{-3} for graphite or 2061 mAh cm^{-3} for lithium metal. Mg metal has a capacity of 3832 mAh cm^{-3}. The high abundance (2000 times higher than Li) makes the price of the metal only 1/25 times that of Li, and the environmental friendliness of the metal has greatly promoted the research of this material. Magnesium metal cannot compete with lithium metal in terms of specific capacity (magnesium is 2205 mAh g^{-1}, and lithium is 3862 mAh g^{-1}). Li also has a -3.0 V redox potential versus a standard hydrogen electrode (SHE), compared to -2.3V vs SHE

of Mg.[5, 6] However, the commercialization of lithium metal as anode material is hindered due to safety issues attached to lithium metal during the stripping deposition process of the battery. Lithium metal tends to form needle-like dendritic structures during deposition, especially at higher charging rates, which may cause short circuits and thermal runaway. In direct contrast, there is sufficient literature to prove that magnesium anodes are not troubled by dendrite formation, and there is no such safety hazard.[7-9]

Among all conversion cathode materials, sulfur is the most promising cathode material with a high theoretical capacity of 1675 mAh g^{-1}. Sulfur is also very abundant, environmentally friendly, and very cheap, making sulfur an ideal choice for high energy density magnesium metal batteries as cathode materials. Besides, the 24% volume expansion caused by density difference between S and Magnesium sulfide is significantly lower than the 72% volume expansion of the Li-S system. [10] However, the lack of practical chloride-free electrolyte not only makes Mg metal battery not a substitute alternative for LIB, but also far from practical using. In this paper, magnesium monocarbonrane ($Mg(CB_{11}H_{12})_2$) electrolyte as a candidate for Mg-S batteries was investigated. The high oxidation stability close to 4V relative to Mg and the non-reactivity of anions make this electrolyte system an ideal choice for high energy density Mg-S battery systems. [11-13]

4.3 Experiment:

4.3.1 Materials Preparation and Cell Assembly:

Integrated Ketjen Black (IKB) carbon was adopted as sulfur host via synthesis method reported by Lv et al. [14] Briefly, the nano-sized ketjen black was mixed with citric acid at

60°C in an aqueous suspension. Then ethylene glycol was added with temperature raise to 130°C under agitation. The obtained black mixture was dried in vacuum oven overnight and then carbonized under argon at 400°C for 6 hours and 800°C for another 10 hours to produce IKB. 80 wt% of sulfur was thoroughly mixed with 20 wt% of IKB in mortar and pestle. The resulting mixture was then transfer to a sealed Ar filled tube furnace, followed by a heating process at 155°C for 10 hours. The cathode slurry was prepared by mixing 80 wt.% S-C composite, 10 wt.% polyvinylidene fluoride (PVDF, Sigma Aldrich) binder and 10 wt% carbon black (super C65, Timcal) in N-methyl-2pyrrolidone (NMP) solvent. The slurry was coated onto Al foil (Alfa aesar) with sulfur areal loading about 1mg cm^{-2} and the electrode was dried in a vacuum oven at 50°C for 12 hours. Mg metal (99.9% MTI) anode was polished with scalpel in Ar-filled glovebox to remove the outer intrinsic oxide surface before cell assembling. Both Mg foil before and after scalpel polish were both characterized by XPS measurement. Mg 2p data in **Figure 4.S1a** is the pristine Mg which have a large fraction of oxidation layer on Mg surface. **Figure 4.S1b** is the polished one. The fraction of pristine passivation layer on Mg surface is lower. However, due to long time transportation before XPS measurement, the fresh polished Mg surface is cleaner than the one shown in Figure 4.S1b.

0.5M $Mg(TFSI)_2$ (99.5% Solvionic) in Tetraethylene glycol dimethyl ether (G4, Sigma Aldrich), 0.75M $Mg(CB_{11}H_{12})_2$ in G4, and 0.3M magnesium tetrakis(hexafluoroisopropyloxy) borate $Mg[B(hfip)_4]_2$ (hfip = $OC(H)(CF_3)_2$) in Dimethoxy ethane (DME) electrolyte which are the only available electrolyte systems for Mg-S batteries were investigated in this experiment. G4 and DME were dried over

molecular sieves with water content less than 10 ppm, measured through Karl Fischer titration. $Mg(TFSI)_2$ was vacuum dried at 100°C in glovebox for 24 hours before dissolved into G4.

$Mg(CB_{11}H_{12})_2$ was prepared by the method of McArthur et al.[12, 13] Briefly, Cs $(CB_{11}H_{12})$ was first prepared according to the method of Reed et al. [15]After recrystallization, dissolve Cs $(CB_{11}H_{12})$ in hot water and add 1.0 equivalent trimethylamine hydrochloride to obtain white powder. Add $(HNMe_3)^+$ $(HCB_{11}H_{11})^-$ to a suspension of Mg powder in a minimum amount of THF and stir the resulting suspension 1 hour. After 1 hour, additional THF was added, and the suspension was stirred for 24 hours. The THF solution was then filtered through a sintered funnel of medium porosity. Wash the collected white powder with 1,2-dimethoxyethane (DME) and dissolve the collected precipitated white powder. Collect unreacted magnesium powder and reuse it. The DME solvent was removed under vacuum to obtain compound $Mg(CB_{11}H_{12})_2$ as a white powder with a yield of 91%.

Mg[B(hfip)4]2 was synthesized by method of Zhao`s group method.[16, 17] Magnesium tetrahydroborate $(Mg(BH_4)_2)$ was first made by milling magnesium hydride and triethylamine borane and heat at 100°C under reflux for 1 hour and afterwards at 145°C for another six hours in glovebox. [18] After adding hexane, the suspension was stirred for 8 hours at room temperature and subsequently filtered, washed and dried. The obtained $Mg(BH_4)_2$ powder dissolved into DME with 8.2 equivalents of $HOC(H)(CF_3)_2$ adding drop wisely and stir for 1 hour at room temperature. The mixture was further refluxed at

85°C under Ar for 2 more hours. The $Mg[B(hfip)_4]_2$ white powder can be collected after removing the solvent of the obtained mixture.

Coin cell (2032 type) was assembled with Celgard® 2400 separator, ½ inch diameter polished Mg metal anode and ½ inch diameter above mentioned IKB sulfur cathodes with 50 ul electrolyte.

4.3.2 Electrochemical and Material Characterizations:

The galvanostatic discharge-charge of 2032 coin cells were cycled between 0.3-3 V versus Mg/Mg^{2+} at room temperature in Arbin battery test station. The cyclic voltammetry was performed between 0.3-3 V versus Mg/Mg^{2+} at room temperature in Gamry Interface 1000 with 0.05mV/s scan rate. To perform the X-ray photoelectron spectroscopy (XPS), samples were transferred from the glovebox to the XPS facility through a sealed stainless steel transfer jar. The XPS experiment was performed using a Kratos Axis Supra with a dual anode Al/Ag monochromatic X-ray source (280 W). Transfer the sample to the analysis chamber via an integrated glove box filled with Nitrogen gas.

4.4 Result and discussion:

4.4.1 Electrochemical behavior of Mg-S battery in carbonrane electrolyte

As one of the chloride free Mg electrolytes with weakly coordinating anions for Mg metal battery, $Mg(CB_{11}H_{12})_2$ could be the most promising candidate for Mg-S batteries. Such electrolyte system for Mg stripping and deposition has been investigated by our group in 2019.[11] The wide electrochemical potential window and chemically stable nature makes $Mg(CB_{11}H_{12})_2$ electrolyte suitable to pair with sulfur cathode. **Figure 4.1 a** shows

the galvanostatic discharge charge profile of Mg-S cells for $Mg(CB_{11}H_{12})_2$ electrolyte with C rate at C/100 (16mA g_s^{-1}). Typical two plateaus discharge profiles at 1.4 V and 0.6 V reveal the typical sulfur reduction pathway demonstrated in Li-S batteries.[19] Sulfur was first reduced to high order polysulfide and dissolved in electrolyte during the first plateau at 1.5V vs Mg/Mg^{2+}. The high order polysulfide was futher reduced to low order polysulfide or eventually MgS in second plateau at 0.8 V vs. Mg/Mg^{2+}. However, an infinite capacity charge profile which has been interpreted as severe shuttle effect occurs in charge profile. When the current was manully switched to negtive discharge current, the discharge capacity in later cycle is drastically decreased. The polysulfide shuttle effect can be attributed to a similar reaction that is ubiquitous in Li-S batteries. When the high-order polysulfides formed during the charging process diffuse to the Mg electrode. High-order polysulfides chemically and eletrochemically reacted with Mg anode to form low-order polysulfides, a polysulfide shuttle mechanism will occur. Cyclic voltametry (CV) was performed at scan rate of 0.05 mV s^{-1} between 0.3 and 3V starting with negtive scan as shown in **Figure 4.1b**. Due to the sluggish kinetic of Mg-S battery, two reduction peaks were overlapped as one broad peak shown at 1 V vs Mg/Mg^{2+} in the first cycle. However, this reduction peak is significantly diminished in the following cycles. A small oxidation peak is consistently present in the CV scan. The polysulfide shuttle-like behavior observed in the charing curve as well as the missing reduction peak in CV raise questions on the oxidation mechnisms. Based on the knowledge from Li-S batteries, the IKB carbon host is able to sequatrate polysulfides well in the first a few cycles without shuttle behavior. In addtion, the solubility of lithium polysulfide in glyme electrolyte is

much higher than magnesium polysulfide.[20] Therefore, the severe polysulfide shuttle is not suppose to happen in Mg-S battery in first few cycle, and the missing reduciton peak in CV cannot be explained.

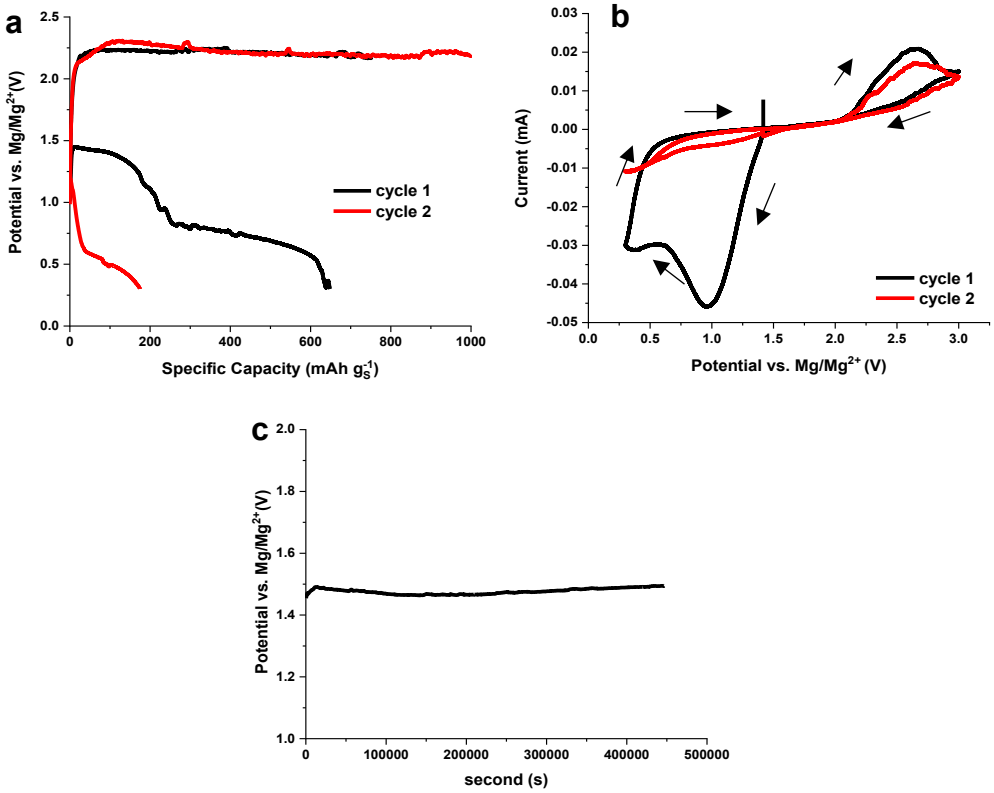

Figure 4.1 Electrochemical behavior of Mg-S battery with IKB-S cathode in $Mg(CB_{11}H_{12})_2$ electrolyte. (a) Galvanostatic discharge-charge curve of Mg-S in C/100. First discharge, then charge. (b) CV curve of Mg-S with scan rate 0.05mA/s between 0.3-3V vs Mg/Mg^{2+}. Starting with negtive scan (c) Open circuit potential of Mg-S battery**.**

If it is not polysulfide shuttle effect causing both charge profile voltage plateau and the missing reduction peak in CV. It might be due to certain side oxidation reaction during

charging. To valididate the hypothesis, the open circuit potential test was first done as shown in **Figure 4.1c** to make sure it is not the self-discharging leading to the "potential plateau" during charing. Commercially obtained mesoporous carbon CMK-3 (ACS material) was also used as carbon host to insure no side reaction caused by carbon hose evident by the discharge-charge profile data shown in **Figure 4.S2**. To understand the oxidation reaction mechanism during charging, the charging mechanism has to be reviewed first. After discharging, the sulfur was not fully reduced to magnesium sulfide (MgS). Due to the complex sulfur reduction pathway, the low solubility and low conductivity of low order polysulfide, sulfur in cathode can not be fully reduced. The insulating low order polysulfide will cover the unreacted avtive material cause high charge transfer impedence. With large amount of polysulfide dissolved in electrolyte, electrolyte will be more viscous and lower ionic conductivity. Both of the reason can terminate the further reduction by increasing the overpotential. Which has been investigated in Chapter 2. So after discharging, there will be lower order polysulfide coverd higher order polusulfide even unreacted or dispropernated sulfur element in IKB cathode. It have been proven in **Figure 4.2b** in XPS experiment. Compare to the XPS data of pristine sulfur cathode in **Figure 4.2a**. Both elemental sulfur, magnesium polysulfide and magnesium sulfide can been seen in S 2p XPS profile. As we known polysulfide can be oxided to element sulfur during charging. Such sulfur should be electrochemical active which can be futher reduced in later cycle. What if sulfur element can be further oxided to some unknow chemisry irreversibly during charging. The charge profile will show a plateau as the unknow oxidation reaction of sulfur happening. The

oxidation product covered the cathode electrode and stop further cycle. It may be eletrochemically inactive or ioniclly insulating. So the voltage plateau in charge profile and the oxidation peak in CV profile may not cause by polysulfide shuttle effect.

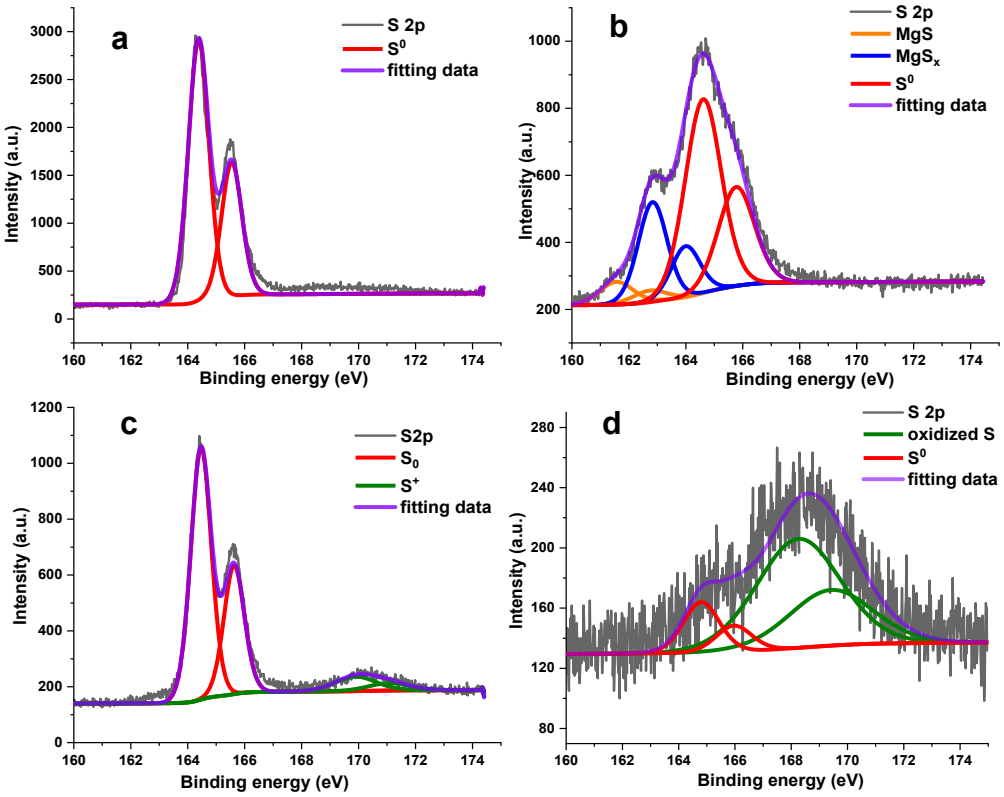

Figure 4.2 Deconvoluted S 2p XPS spectra of (a) Pristine IKB-S cathode; (b) IKB-S cathode after discharging in $Mg(CB_{11}H_{12})_2$ electrolyte; (c) IKB-S cathode after directly charging in $Mg(CB_{11}H_{12})_2$ electrolyte, the electrode is washed with G4; (d) IKB-S cathode after charging $Mg(CB_{11}H_{12})_2$ electrolyte, without G4 washing.

To validate the hypothesis, the prinstine Mg-S battery was charged first at C/200 from open circuits potential to cut-off voltage of 3 V. The charge profile is shown in **Figure 4.3a**. Superingly, the prising sulfur cathode can be charged. A plateau appears at 1.6V vs Mg/Mg^{2+} ,continuing with a slope between 1.8V-2.4V vs Mg/Mg^{2+}. Cyclic voltametry (CV)was tested at scan rate of 0.05mV s^{-1} starting with positive scan direction (starting from open circuits potential to 3V then back to 0.3V) as data shown in **Figure 4.3b.** There is a broad oxidation peak staring at 1.6 V. Such peak can corresponding to the plateau at 1.6V vs Mg/Mg^{2+} in charge profile. Definitly, there is a unknow oxidation reaction happeing.

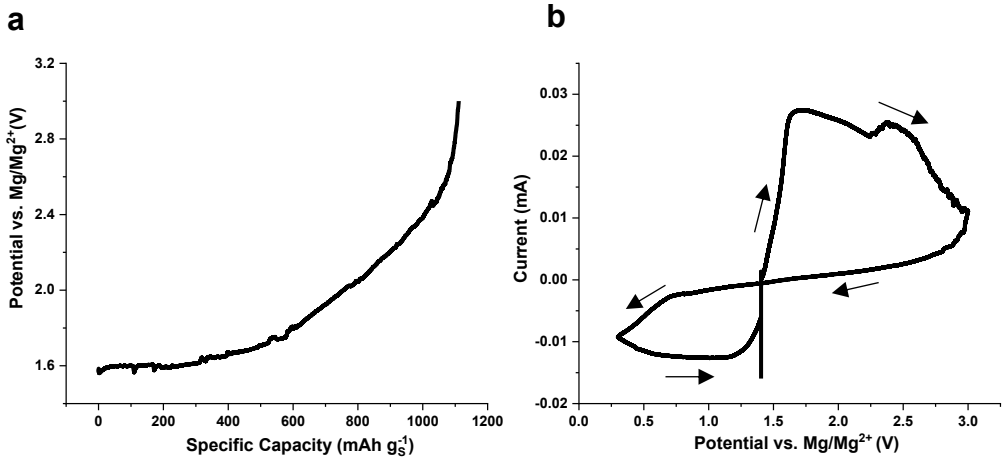

Figure 4.3 (a) Galvanostatic charge profile of IKB-S cathode in $Mg(CB_{11}H_{12})_2$ electrolyte at C/200 (b) CV profile of IKB-S cathode in $Mg(CB_{11}H_{12})_2$ electrolyte starting with positive scan.

After charging, sulfur cathodes were washed carefully with G4 and vaccum dried in room temperature for further XPS (**Figure 4.2c**). **Figure 4.2d** shows the XPS spectrum of cathode after charging without washing with G4.(NMR data of G4 after washing sulfur

cathode is shown in **Figure 4.S3**. It shows that G4 is stable with oxidized sulfur) Due to lower conductivity of electrolyte leftover on cathode surface. S 2p shows much higher noise. From the XPS data, we can cleanly see that, sulfur element is been oxidizied to higher oxidation state with the green line shows in Figure 4.2 c and d. Sulfur oxidation state is complicated, it could be -2 sulfide ,+2 sulfur monoxide, +4 sulfur dioxide or sulfite and +6 sulfate. Or more complicated organic compound. Even though we still don`t know what the oxidation reaction is, we are the first one propose the sulfur element can be oxidized in Mg-S batteries evident by the XPS data and electrochemical data. More vadidation can be done computationally. Thence, the "shuttle phenomenon" could be explained differently. The oxidation product is electrochemically irreversible. It covered cathode surface and stop the sulfur been reduced in later discharge cycles with XPS depth profiling data in **Figure 4.S4**.

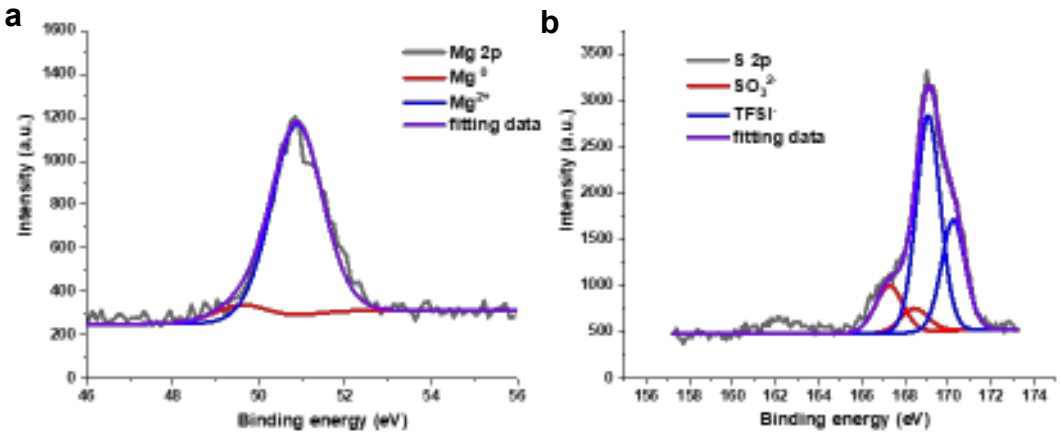

Figure 4.4 XPS spectra of scalpel polished Mg after soaking in 0.5M $Mg(TFSI)_2$ in G4 for 6 days.(a) Mg 2p. (b)S 2p

4.4.2 Electrochemical behavior of Mg-S battery in $Mg[B(hfip)_4]_2$ electrolyte

Electrolytes for Mg-S batteries are reviewed in Chapter 1. 0.5M $Mg(TFSI)_2$ in glyme and 0.3M $Mg[B(hfip)_4]_2$ in DME are the only two chloride-free choices for Mg-S batteries which had been published before. However, surface characterization results show that $Mg(TFSI)_2$ has unstable anions and is prone to cathodic decomposition, which leads to the formation of SEI on Mg metal(**Figure 4.4a**). Theoretical studies on Mg $(TFSI)_2$ show that there is ion pairing between partially reduced Mg^{2+} cations (to Mg^+) and $TFSI^-$ anion, which promotes the decomposition of $TFSI^-$ on the electrode surface. We can clearly see the $TFSI^-$ anion decomposition from XPS data. Because the XPS peak position of sulfur in $TFSI^-$ anion decomposition product is overlap with the sulfur peak we are interested (**Figure 4.4b**). Even though 0.5M $Mg(TFSI)_2$ in glyme can be applied for Mg-S with some additives such as LiTFSI or $MgCl_2$,[22, 23] it is not an ideal candidate to validate the oxidation behavior of elemental sulfur. 0.3M $Mg[B(hfip)_4]_2$ in DME as the only choice was used for validation. The discharge- charge profile is shown in **Figure 4.5**. The polysulfide shuttle is also shown in Figure 4.5a. If we charge the pristine Mg-S battery first, the charge profile is similar with the one in carbonrane electrolyte(Figure 4.5b). Therefore, we might be able to say the oxidation reaction of sulfur element may happening in all chloride-free weakly-coordinated Mg salt Mg-S battery system. Because only in this system, there is Mg^{2+} cation. More work needs to be done to reveal the exact redox reaction.

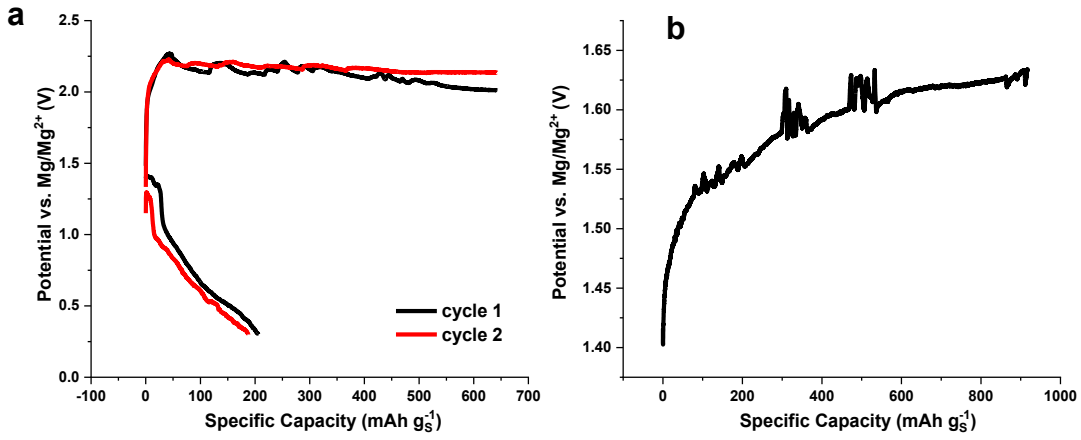

Figure 4.5 (a) Galvanostatic discharge-charge curve of Mg-S in C/100 in 0.3M $Mg[B(hfip)_4]_2$ in DME electrolyte. (b) Galvanostatic charge profile of IKB-S cathode in $Mg[B(hfip)_4]_2$ electrolyte at C/200

4.5 Conclusion and Perspective:

Mg metal as a good alternative for Li metal in energy storage device due to its high abundance and safety. Sulfur can be used to pair with Mg metal in a high specific energy, low safety concern Mg-S battery. $Mg(CB_{11}H_{12})_2$ as a closo cluster ,which have closed shell electronic structures and complete polyhedral shape, can be a promising electrolyte candidate for Mg-S battery with low overpotential for Mg stripping-deposition, good anodic and cathodic stability. We are the first group report the electrochemical behavior of $Mg(CB_{11}H_{12})_2$ electrolyte for Mg-S battery with promising discharge specific capacity. Besides, the sulfur oxidation reaction during charging is also the first been reported by our group in this paper. Which can raise up a new explanation for "shuttle" behavior in Mg-S battery during charging. Such oxidation reaction not only happening in

$Mg(CB_{11}H_{12})_2$ electrolyte but also in $Mg[B(hfip)_4]_2$ electrolyte system. Which are the only two candidates for chloride free weakly coordinated Mg salt Mg-S battery system. Mg^{2+} cation only exist in the chloride free weakly coordinated Mg salt Mg-S battery system among all the Mg metal battery electrolyte. Such cation may cause sulfur oxidation reaction. However, the exact redox reaction of sulfur cannot be proposed in this paper. Computational modeling can facilitate the explanation by giving an exact redox model for sulfur during charging. With deep understanding of sulfur oxidation reaction, additives may apply for future research to eliminate the sulfur oxidation reaction. The $Mg(CB_{11}H_{12})_2$ electrolyte can also be optimized for Mg-S battery by tuning the concentration , applying solvent to reduce the viscosity, adding additives to eliminate side reaction and reduce the overpotential.

4.6 Supporting information

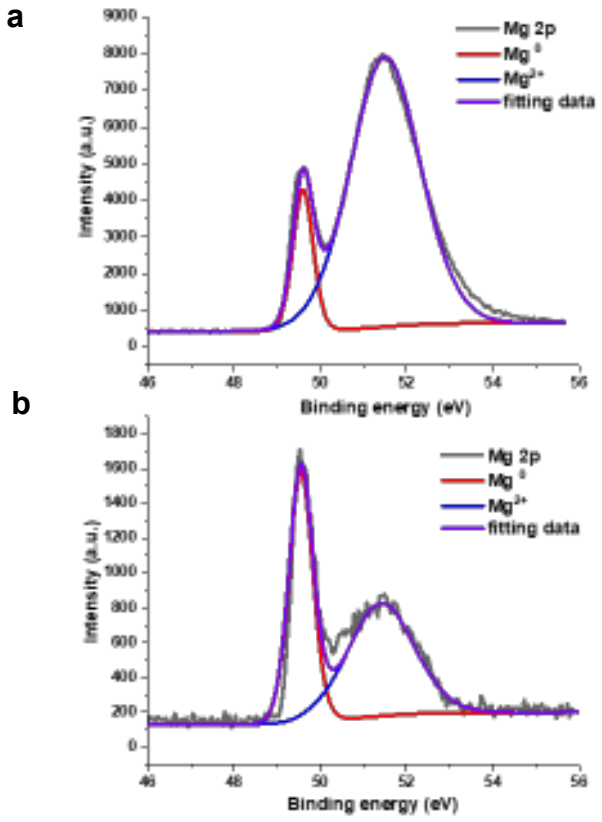

Figure 4.S1 XPS Mg 2p profiles for Mg foil. (a) Pristine Mg as received. (b) Mg foil after scalpel polished

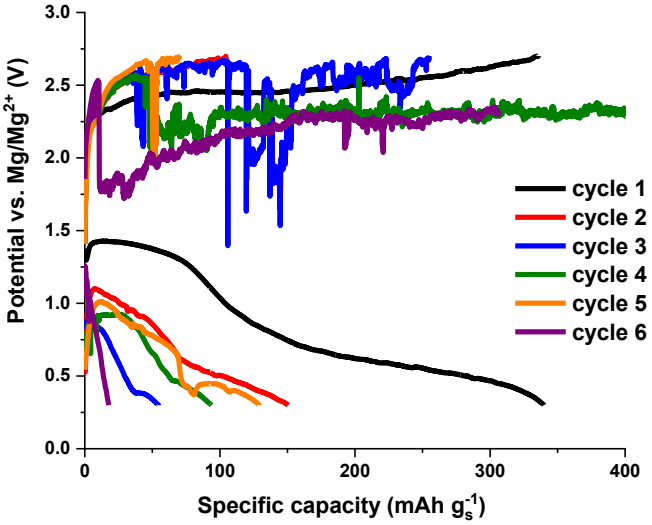

Figure 4.S2 Galvanostatic discharge-charge curve in C/100 with CMK-3-S cathode in $Mg(CB_{11}H_{12})_2$ electrolyte.

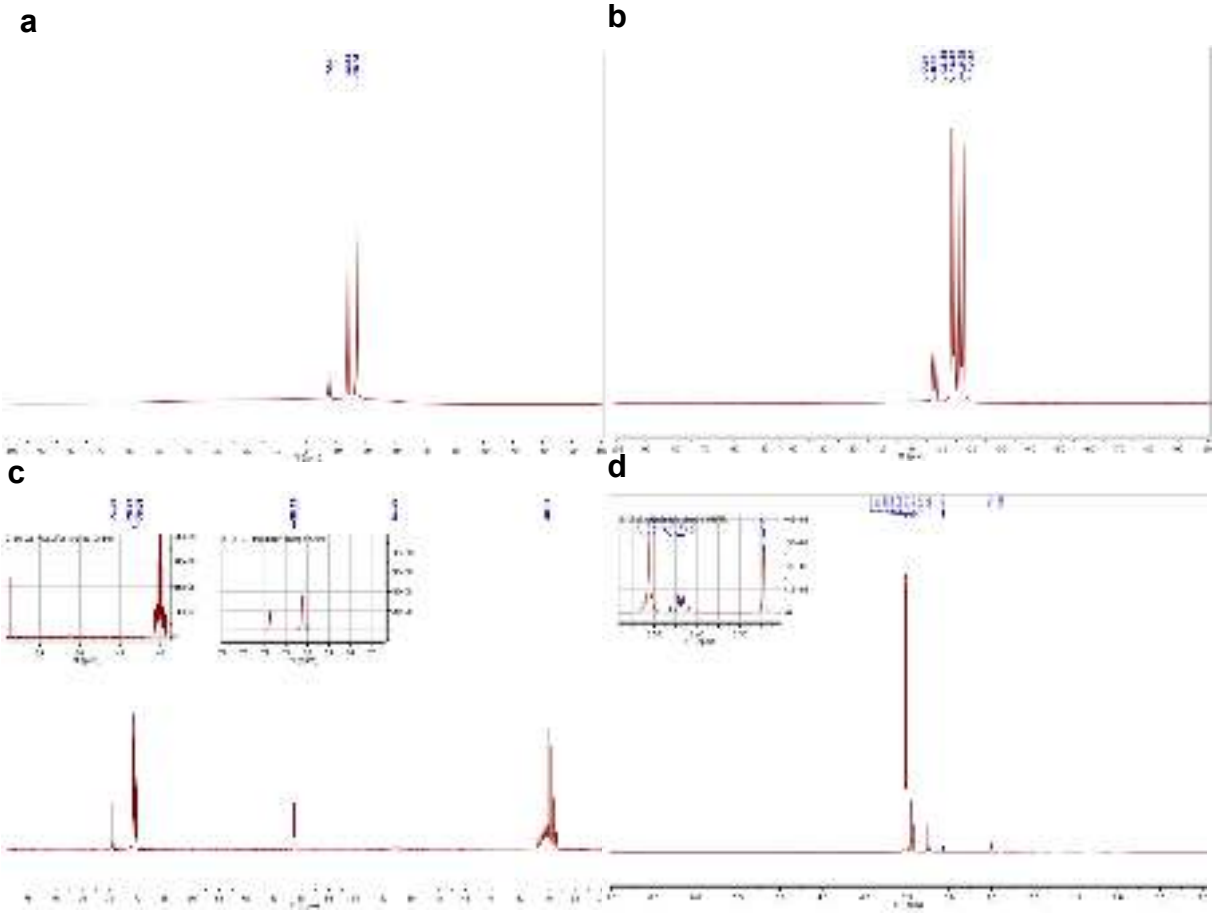

Figure 4.S3 NMR spectra of G4 washed IKB-S cathode for the Mg-S batteries in $Mg(CB_{11}H_{12})_2$ electrolyte. After galvanostatic charing,deassemble cells and wash with G4. (a) Boron proton decoupled NMR (b)B NMR (c) C NMR (d)H NMR. Confirm that the oxidized sulfur species is not soluble in electrolyte.

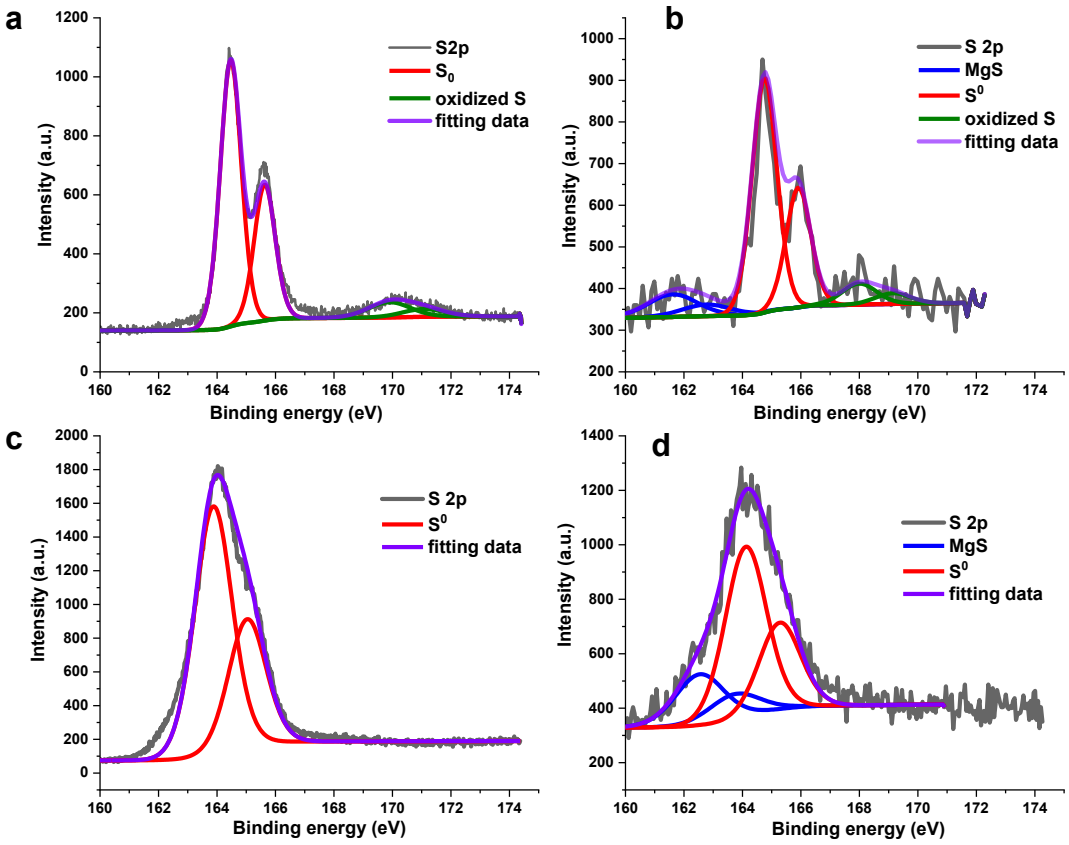

Figure 4.S4 XPS S 2p spectra of Mg-S batteries with IKB-S cathode in $Mg(CB_{11}H_{12})_2$ electrolyte. Oxidized sulfur species occur in G4 washed cathode (a)after charging and (b) after 1cycle of discharging and charging. After ion sputtering, the oxidized sulfur species disappear both in (c)IKB-S cathode after charging and (d) after 1cycle of discharging and charging. Indicating sulfur was oxidized and cover cathode. The oxidized sulfur species will terminate the further electrochemical reaction**.**

Reference:

1. K. Mizushima, P. C. J., P.J. Wiseman and J.B. Goodenough, LixCoO 2 (0<x~l): A NEW CATHODE MATERIAL FOR BATTERIES OF HIGH ENERGY DENSITY. *Materials Research Bulletin* **1980,** *15* (6), 783-789.

2. Nagaura, T. T., K. , Lithium ion rechargeable battery. *Progress in Batteries & Solar Cells* **1990,** *9*, 209-217.

3. Fischer, M.; Werber, M.; Schwartz, P. V., Batteries: Higher energy density than gasoline? *Energy Policy* **2009,** *37* (7), 2639-2641.

4. Li, M.; Lu, J.; Ji, X.; Li, Y.; Shao, Y.; Chen, Z.; Zhong, C.; Amine, K., Design strategies for nonaqueous multivalent-ion and monovalent-ion battery anodes. *Nature Reviews Materials* **2020,** *5* (4), 276-294.

5. Li, D.; Yuan, Y.; Liu, J.; Fichtner, M.; Pan, F., A review on current anode materials for rechargeable Mg batteries. *Journal of Magnesium and Alloys* **2020,** *8* (4), 963-979.

6. Guo, Q.; Zeng, W.; Liu, S.-L.; Li, Y.-Q.; Xu, J.-Y.; Wang, J.-X.; Wang, Y., Recent developments on anode materials for magnesium-ion batteries: a review. *Rare Metals* **2020,** *40* (2), 290-308.

7. Wang, Z.; Sun, Z.; Li, J.; Shi, Y.; Sun, C.; An, B.; Cheng, H. M.; Li, F., Insights into the deposition chemistry of Li ions in nonaqueous electrolyte for stable Li anodes. *Chem Soc Rev* **2021,** *50* (5), 3178-3210.

8. Chen, X. R.; Zhao, B. C.; Yan, C.; Zhang, Q., Review on Li Deposition in Working Batteries: From Nucleation to Early Growth. *Adv Mater* **2021,** *33* (8), e2004128.

9. Cheng, X. B.; Zhang, R.; Zhao, C. Z.; Zhang, Q., Toward Safe Lithium Metal Anode in Rechargeable Batteries: A Review. *Chem Rev* **2017,** *117* (15), 10403-10473.

10. Mao, M.; Gao, T.; Hou, S.; Wang, C., A critical review of cathodes for rechargeable Mg batteries. *Chem Soc Rev* **2018,** *47* (23), 8804-8841.

11. Jay, R.; Tomich, A. W.; Zhang, J.; Zhao, Y.; De Gorostiza, A.; Lavallo, V.; Guo, J., Comparative Study of Mg(CB11H12)2 and Mg(TFSI)2 at the Magnesium/Electrolyte Interface. *ACS Appl Mater Interfaces* **2019,** *11* (12), 11414-11420.

12. McArthur, S. G.; Geng, L.; Guo, J.; Lavallo, V., Cation reduction and comproportionation as novel strategies to produce high voltage, halide free, carborane based electrolytes for rechargeable Mg batteries. *Inorganic Chemistry Frontiers* **2015,** *2* (12), 1101-1104.

13. Fisher, S. P.; Tomich, A. W.; Lovera, S. O.; Kleinsasser, J. F.; Guo, J.; Asay, M. J.; Nelson, H. M.; Lavallo, V., Nonclassical Applications of closo-Carborane Anions: From Main Group Chemistry and Catalysis to Energy Storage. *Chem Rev* **2019,** *119* (14), 8262-8290.

14. Lv, D.; Zheng, J.; Li, Q.; Xie, X.; Ferrara, S.; Nie, Z.; Mehdi, L. B.; Browning, N. D.; Zhang, J.-G.; Graff, G. L.; Liu, J.; Xiao, J., High Energy Density Lithium-Sulfur Batteries: Challenges of Thick Sulfur Cathodes. *Advanced Energy Materials* **2015,** *5* (16).

15. REED, C. A., H+,CH3+, and R3Si+ Carborane Reagents: When Triflates Fail. *ACCOUNTS OF CHEMICAL RESEARCH* **2010,** *43*, 121-128.

16. Zhao-Karger, Z.; Gil Bardaji, M. E.; Fuhr, O.; Fichtner, M., A new class of non-corrosive, highly efficient electrolytes for rechargeable magnesium batteries. *Journal of Materials Chemistry A* **2017,** *5* (22), 10815-10820.

17. Zhao-Karger, Z.; Liu, R.; Dai, W.; Li, Z.; Diemant, T.; Vinayan, B. P.; Bonatto Minella, C.; Yu, X.; Manthiram, A.; Behm, R. J.; Ruben, M.; Fichtner, M., Toward Highly Reversible Magnesium–Sulfur Batteries with Efficient and Practical Mg[B(hfip)4]2Electrolyte. *ACS Energy Letters* **2018,** *3* (8), 2005-2013.

18. Chłopek, K.; Frommen, C.; Léon, A.; Zabara, O.; Fichtner, M., Synthesis and properties of magnesium tetrahydroborate, Mg(BH4)2. *Journal of Materials Chemistry* **2007,** *17* (33).

19. Gao, T.; Ji, X.; Hou, S.; Fan, X.; Li, X.; Yang, C.; Han, F.; Wang, F.; Jiang, J.; Xu, K.; Wang, C., Thermodynamics and Kinetics of Sulfur Cathode during Discharge in MgTFSI2 -DME Electrolyte. *Adv Mater* **2018,** *30* (3).

20. Bieker, G.; Küpers, V.; Kolek, M.; Winter, M., Intrinsic differences and realistic perspectives of lithium-sulfur and magnesium-sulfur batteries. *Communications Materials* **2021,** *2* (1).

21. Fu, C.; Wong, B. M.; Bozhilov, K. N.; Guo, J., Solid state lithiation-delithiation of sulphur in sub-nano confinement: a new concept for designing lithium-sulphur batteries. *Chem Sci* **2016,** *7* (2), 1224-1232.

22. Gao, T.; Hou, S.; Wang, F.; Ma, Z.; Li, X.; Xu, K.; Wang, C., Reversible S(0) /MgSx Redox Chemistry in a MgTFSI2 /MgCl2 /DME Electrolyte for Rechargeable Mg/S Batteries. *Angew Chem Int Ed Engl* **2017,** *56* (43), 13526-13530.

23. Gao, T.; Noked, M.; Pearse, A. J.; Gillette, E.; Fan, X.; Zhu, Y.; Luo, C.; Suo, L.; Schroeder, M. A.; Xu, K.; Lee, S. B.; Rubloff, G. W.; Wang, C., Enhancing the reversibility of Mg/S battery chemistry through Li(+) mediation. *J Am Chem Soc* **2015,** *137* (38), 12388-93.

Chapter 5: Conclusions

Due to the urgent demand of alternative clean energy, energy storage rechargeable with high specific energy are eagerly needed. Rechargeable batteries as energy storage devices have been review firstly in Chapter 1. Owing to the high specific capacity and low density for both lithium (Li) and sulfur(S), high working potential as well as high theoretical specific energy, Li-S batteries have been regarded as one of the most promising candidates for next generation rechargeable batteries. However, wide commercialization of Li-S batteries is still challenged by non-ideal specific energy and poor cycle life due to the interplay of the Li anode, sulfur cathode and electrolyte. The amount of electrolyte in batteries or electrolyte to sulfur ratio (E/S) is the key challenge in achieving high specific energy. Based on our calculation, E/S ratio need to be lower than 3 to achieve a battery with specific energy significantly higher than state of the art Li ion battery. Many strategies have been studied to decrease E/S including using ultra high sulfur loading, applying electrocatalysis in cathode, introducing electrolyte additives, demonstrating novel binders and studying sparingly solvating electrolyte. However, none of them are working perfectly to some degree. Magnesium (Mg) with high theoretical volumetric capacity and higher abundance which has been considered as an alternative anode material to Li. A battery pairing Mg anode and S cathode will definitely have a bright future. However, the availability of Mg-S batteries electrolyte is actually the main obstacle which limit the development of Mg-S system. Mg-S electrolyte research is desperately needed including the in-depth understanding of Mg-S mechanism and studying of novel chloride free Mg-S electrolyte.

As the importance of E/S in achieving high specific energy batteries mentioned above, the failure mechanism of Li-S batteries under lean electrolyte condition is studied in Chapter 2. The interfacial process of cathode under lean electrolyte condition during discharge is probed by operando EIS and GITT experiments. The results indicate that during the transition region from high-order polysulfides to low-order polysulfides, kinetic issues cause the low specific capacity. Once the kinetic bottleneck during the transition region is passed, high specific capacity can achieve even under lean electrolyte condition. Such a bottleneck is induced by high mass transfer limitations due to rapid accumulation of polysulfides at the electrode-electrolyte interface. The dissolved high-order polysulfide can rapidly saturate the electrolyte and limit mass transfer at the interface for the upstream sulfur reduction. Improving the adsorption of high-order polysulfide can promote the reaction by alleviating the charge transfer resistance and decreasing overpotential significantly.

As an important part of the battery, the electrolyte plays a key role in achieving electrochemical performance. Electrolytes are ubiquitous and indispensable in batteries. The role of the electrolyte is to act as a medium for transferring charge in the form of ions between the cathode and the anode. Electrolyte must be stable as an inert component in the battery both electrochemically and chemically. Thus ionic liquid-based electrolytes attract more attention because of their excellent thermal stability, negligible volatility and non-flammability. For the first time, we report a novel Carboranyl Ionic Liquids (CIL) -- $[H_9C_4CB_9H_9]$-$[Li(THF)_{1.0}]$+ in Chapter 3. Such CIL is structurally similar but not same to the new emerging solvated ionic liquid. We demonstrated good chemical and

electrochemical stability of CIL in the presence of lithium metal. Li will electrochemical deposit in two dimensional manner. As CIL`s good stability toward Li metal, SEI layer is different with the one formed in conventional electrolyte . High specific energy Li-S battery is also prospected in applying CIL via a sparingly dissolving pathway. A 1.5Ah pouch cell with 413 Wh kg^{-1} specific energy is calculated based on the Li-S date.

As reviewed above, Mg-S batteries is no doubt a promising candidate for next generation rechargeable batteries. However, there are limited numbers of electrolyte systems which are suitable and chloride free for Mg-S battery system. In Chapter 4, the electrochemical behaviors of two weakly coordinated chloride free magnesium salt electrolytes, magnesium monocarbonate and magnesium tetra(hexafluoroisopropoxy) borate, in Mg-S batteries were studied. In the meanwhile, we propose another explanation for the voltage plateau in the charging voltage curve, which is usually explained as the polysulfide shuttle effect.